POLITECNICO DI MILANO

School of Industrial and Information Engineering
Master of Science in Mechanical Engineering

Numerical investigation on the influence of piston head geometry and injection parameters on HCCI and TCRCI combustion modes

Supervisor: Tommaso LUCCHINI

Master thesis by:

Mattia PELOSIN ID 920352

Accademic year 2019 - 2020

A special thanks goes to Tommaso Lucchini and Qiyan Zhou for their constant help during these troubling times

Contents

List of Tables

List of Figures

Acronyms

aHRR apparent Heat Release rate.

CAD Crank Angle Degree.

CC Combustion Chamber.

CCI Conventional Compression Ignition.

CR Compression Ratio.

DI Direct Injected.

EGR Exhaust Gas Recirculation.

GIE Gross Indicated Efficiency.

GIMEP Gross Indicated Mean Efficiency.

HCCI Homogeneous Charge Compression Ignition.

HRR Heat Release Rate.

ICE Internal Combustion Engine.

ID Ignition Delay.

LTC Low Temperature Combustion.

LTCE Low Temperature Combustion Engine.

MFB Mass Fraction Burned.

PCCI Premixed Charge Compression Ignition.

PFI Port Fuel Injection.

PM Particulate Matter.

PRR Pressure Rise Rate.

RCCI Reaction Controlled Compression Ignition.

SI Spark Ignition.

SOF Soluble Organic Fraction.

SOI Start of Injection.

SOL Solid Fraction.

TCRCI Temperature Controlled Reactivity Compression Ignition.

TWM Tabulated Well Mixed.

uHC unburned Hydrocarbon.

Introduction and thesis objective

Nowadays conventional compression ignition engines are widely used in automotive, heavy-duty, marine and train applications. The reason is the larger efficiency, respect to SI engines, both at steady-state and transient operation thanks to the higher compression ratio and the partialization of the load achieved by the decrease of the global air-fuel ratio. The drawback of this type of engine is the higher emission of NO_x and soots, therefore it requires complex and expensive exhaust gases post-treatment systems. Therefore, it is of great interest to develop a combustion technology that is able to combine the efficiency of CCI engine with low pollutant emissions. Different low-temperature combustion strategies like Homogeneous Charge Compression Ignition (HCCI), Reactivity Controlled Compression Ignition (RCCI) and Temperature Controlled Reactivity Compression Ignition (TCRCI) have been studied over the last few years. The use of numerical model has given a boost to the development of this kind of technology since it allows to have a deeper understanding of the physical phenomena inside the engine. As a consequence a constant effort to improve the models is carried on worldwide. This work is based on 3D simulations performed using a library of OpenFOAM internally developed by the ICE group of Polimi called LibICE and it has the ambitious goal to help the development of HCCI and TCRCI technologies.

Thesis objective

This thesis work is focused on the understanding of the combustion processes of HCCI and TCRCI combustion modes and it aims to lay the basis for further developments. The first objective is to validate the numerical model developed for HCCI and TCRCI combustion modes by the ICE group of Polimi thanks to a set of experimental operating conditions provided by the industrial partner Marmotors s.r.l. . This step is particularly important since it helps the industrial company to understand the evolution of the combustion process inside the engine and allows to rely on the CFD simulations in the development of these combustion modes. A preliminary analysis on the engine parameters of the experimental operating conditions has been conducted to verify their accuracy. This is necessary to correctly set the initial conditions of the simulations. Once the reliability of the experimental parameters has been ascertained, the operating points have been simulated and their results compared with the experimental ones to validate the numerical model.
The influence of the piston head geometry on the combustion processes has been investigated. This study provides the basis to manufacture an optimized piston head for the test bench engine of the industrial company since it has operated with the conventional Diesel piston up to now, which is not optimized for these new combus-

tion modes. Lastly, the influence of the injection strategy on the TCRCI combustion process has been investigated to define an effective engine control parameter and to understand the effects of the supercritical injection.
All the experimental results have been provided by Marmotors s.r.l. and they derive from a test bench based on a retrofit of a 4 cylinder 2.0l MultiJet engine able to operate both in HCCI and TCRCI conditions.

The structure of this work is here summarized:

- An introduction to the basic concepts of combustion is proposed in order to simplify the understanding of the achieved results.
- The CCI combustion is described in order to understand its characteristics.
- A bibliographic research is proposed to investigate the characteristics of LTC engines and to show previously implemented combustion chamber geometries. TCRCI is a pioneering technique which is still in the first stage of development, therefore, since it shows various similarities with the more mature RCCI, the latter is wider treated.
- The results of HCCI combustion simulations are presented.
- The effect of the Combustion Chamber (CC) geometry on HCCI combustion mode is analyzed and a new optimized piston geometry is proposed.
- The results of TCRCI combustion simulations are presented.
- The effect of the different injection strategies on the TCRCI combustion process is discussed.
- The effect of the combustion chamber geometry on TCRCI combustion mode is analyzed.

Chapter 1

Combustion characteristics and performance parameters of Internal Combustion Engines

Different configurations of Internal Combustion Engine (ICE) are mainly referable to differences in combustion characteristics, for this reason the main differences between premixed and diffusive combustion will be discussed in this chapter. Combustion is a chemical globally exothermic chain of reaction between an oxidizer (air) and a fuel, it controls the conversion from chemical energy stored in the fuel to mechanical energy achieved by an increase of in-cylinder pressure and temperature. It has a strong influence on engine performances and pollutant formation. Flame development is a function of the characteristics and kinetics of chemical reactions, the transport of mass and energy in the reaction area and by the heat exchange with the surrounding environment. Combustion occurs when the reactants are in the gaseous state, hence, one of the most relevant parameters for combustion development is the state of fuel and oxidizer before the ignition. Two main categories are defined: Premixed and Diffusive Combustion

1.1 Premixed Combustion

The premixed flame is formed when combustion occurs in a premixed gaseous charge of fuel and oxidizer. Considering that combustion reaction occurs in the gaseous state, combustion velocity is maximized in premixed flame, because all the physical time of vaporization of fuel and mixing with air are excluded. A further distinction can be done between homogeneous premixed mixture, where fuel mass fraction is constant all over the mixture and stratified mixture, where there is the stratification of fuel mass fraction. These different conditions depend on the injection strategy. The fundamental quantity which describes this mode of combustion is the laminar burning velocity[1], defined as flame speed when the mixture is steady (no influence of turbulence). It is important to notice that the mixture in ICE is in turbulent motion, this condition enhances flame speed because it increases the mixing rate between fuel and oxidizer speeding up the intermediate reactions. Furthermore it is worth focusing on laminar flame speed concept to understand the parameters that influence combustion.

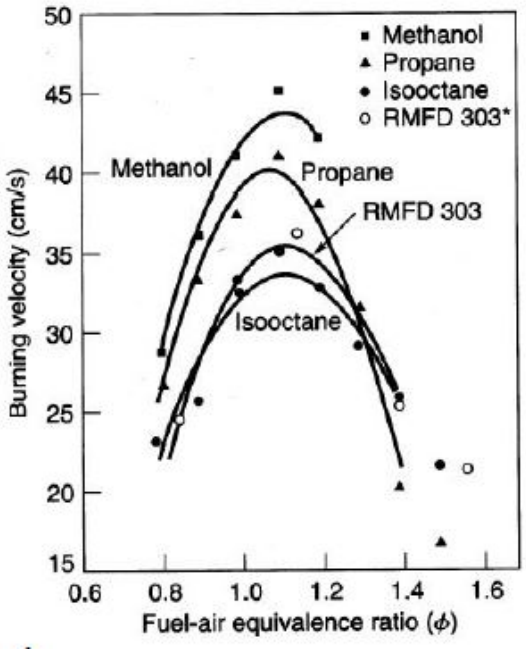

Figure 1.1: Laminar Flame Speed equivalence ratio influence

1.1.1 Laminar Flame Speed

Laminar flame speed is a function of equivalence ratio and the reactants temperature. Equivalence ratio represents the fuel concentration respect to the stoichiometric condition and it is defined as:

$$\phi = \frac{A/F}{A/F_{stoic}} \tag{1.1}$$

The dependence from temperature can be easily explained through the concept of activation energy: the molecules to react must have an energy that overcomes a threshold called activation energy. The higher the temperature is, the higher the fraction of molecules that have the necessary energy and so the faster the reaction is.

The influence of the equivalence ratio is well represented in figure 1.1. The highest laminar speed is reached at a slightly rich mixture. In rich and lean environment laminar speed decreases because the excess of fuel or air absorbs part of the heat released by combustion, decreasing the useful energy exploitable by the reactants. This effect is more relevant for lean mixture, being the air quantity much higher respect to fuel quantity. A limit for the ignition exists both at rich and lean mixture, where the heat capacity of the excess of fuel or air is so high that does not allow the propagation of the flame. The thermodynamic in-cylinder conditions affect laminar flame speed. The flame speed increases with the in-cylinder temperature since chemical kinetic and mixture diffusivity coefficient increases; a pressure rise normally leads to a small decrease of flame speed because chemical kinetics is not affected, but transport of mass and energy is reduced.

1.1.2 Autoignition

In Low Temperature Combustion (LTC) and CCI engines, there is not the presence of an external supplier of energy (like spark plug), which triggers the mixture starting the combustion. For this reason, an important concept is autoignition. Autoignition is the result of a series of pre-combustion reactions, which release energy and a series of unstable products of partial oxidation that allow the start of the combustion process[2]. This condition occurs when the amount of energy released is bigger than the heat exchanged with the environment, allowing a temperature increase that speeds up the further oxidation reactions. Autoignition is well represented by Ignition Delay (ID), defined as the time interval between the moment in which the mixture is brought to fixed thermodynamic conditions and the start of combustion. It can be expressed by the equation:

$$\tau_a = A * p^{-n} * exp(E_a/(RT)) \tag{1.2}$$

Note that the equation (1.2) is reciprocal to the one of laminar flame speed. τ is experimentally obtained in a fast compression machine, which compresses the mixture to the prefixed thermodynamical conditions.

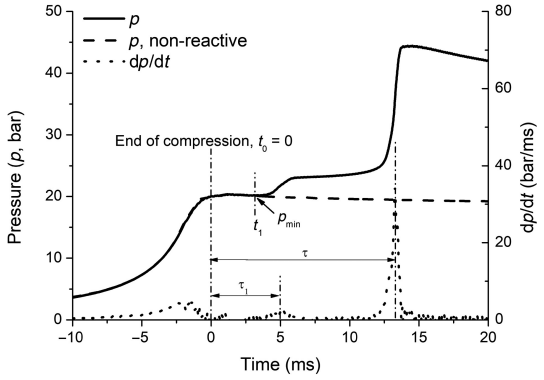

Figure 1.2: Ignition Delay

Normally for hydrocarbons in a range of temperature between 250°C and 400°C, ignition occurs in two stages, as shown in fig 1.2. Low exothermic oxidation reactions cause the first small increase of pressure at 5 ms called cool flames, which are characterized by an increase of temperature in the order of tens degree Kelvin. It is followed by a hot flame that represents the real start of the highly exothermic reactions and so the start of combustion. For higher temperature normally ignition occurs only in one stage. Also ID is influenced by Φ, the minimum ID occurs at the slightly rich mixture and it increases moving far from it.

1.2 Performance Parameters

In the following chapters it has been made an extensive use of some characteristic parameters for the study of ICE. They are described in this section to facilitate their understanding. Thanks to the use of a pressure transducer placed on the combustion chamber wall and a volume transducer, it is possible to experimentally obtain on the test bench an engine pressure diagram (fig 1.3) which is the base for the study of the

engine performance. The first important parameter that is possible to derive is the

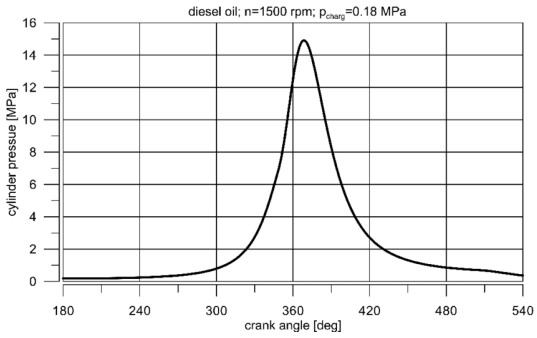

Figure 1.3: Example of pressure trace

work exploitable in the closed cycle (between inlet valve closing and exhaust valve opening). It is called Gross indicated work per cycle and it is defined as:

$$W_g = \int_{IVC}^{EVO} p\,dV \tag{1.3}$$

It is useful to define a new parameter to compare engines with different dimensions since the work is influenced by them. This parameter, Gross Indicated Mean Efficiency (GIMEP), is the pressure integral average over the volume and it is defined as:

$$GIMEP = (1/V) \int_{IVC}^{EVO} p\,dV \tag{1.4}$$

Where V is the cylinder displacement:

$$V = \frac{\pi \cdot b^2 \cdot s}{4} \tag{1.5}$$

Where b is the bore and s the stroke. The last and probably most important parameter is the Gross Indicated Efficiency (GIE), defined as the ratio between the Gross Indicated Work and the energy ideally exploitable from the injected fuel mass per cycle:

$$GIE = \frac{W_g}{m_f \cdot LHV_f} \tag{1.6}$$

It is also possible to derive the Heat Release Rate (HRR) of the combustion process from theoretical elaborations based on the pressure trace . This procedure is based on the first law of thermodynamics applied to the gaseous system inside the combustion chamber. In correspondence of a generic crank angle degree, the heat released by combustion processes ($\frac{dQ_r}{d\theta}$) causes the variation of the system internal energy ($\frac{dE}{d\theta}$), it exchanges mechanical power with the piston ($\frac{dW}{d\theta}$) and heat with the walls ($\frac{dQ_w}{d\theta}$):

$$\frac{dQ_r}{d\theta} = \frac{dE}{d\theta} + \frac{dW}{d\theta} + \frac{dQ_w}{d\theta} \tag{1.7}$$

Since $\frac{dW}{d\theta} = p\frac{dV}{d\theta}$, it is possible to determine the heat release rate through the modeling of the other terms. If the heat exchange with the wall is not considered this is called apparent Heat Release rate (aHRR).

Chapter 2

Overview of Conventional Compression Ignition Combustion and pollutant emission

CCI Engines are highly diffused thanks to their high thermal efficiency. The drawback of this type of engine is linked to the diffusive combustion that intrinsically produces a high value of pollutant emission, particularly NO_x and soots. For these reasons, the combustion mechanism of CCI engine is discussed in this chapter. The basic mechanisms of formation of its characteristic pollutants are analyzed to understand how to cut down on pollutant emissions.

2.1 CCI Combustion Mechanism

Modern CI engines are characterized by compression ratio higher than sixteen to increase the fresh charge temperature of 500-600 °C [2, p. 431]. Fuel injection occurs in the cylinder around -15 Crank Angle Degree (CAD); it evaporates and mixes with the air. Being the in-cylinder pressure and temperature above the auto-ignition conditions, combustion starts where the mixture is stoichiometric after an ignition delay in the order of 1 ms. The consequent temperature rise leads to the combustion of the premixed mixture formed during ignition delay, which rapidly burns bringing gas temperature above 2000 °C and pressure above 15-20 MPa.
As a result, vaporisation and diffusion of spray liquid core are enhanced. Injection continues untill all the required fuel quantity is introduced in the cylinder. During the expansion stroke, the mixing between unburned fuel and residual fresh mixture completes the combustion.

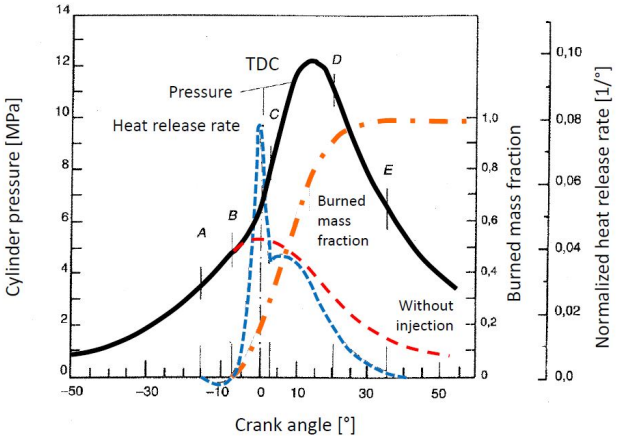

Figure 2.1: CCI HRR and Cylinder P

CCI Injection-Combustion process can be schematized in four different steps :

1. ID, AB in fig 2.1: this is the time between the start of injection and the start of ignition, during this interval atomization and evaporation of the liquid spray (physical delay) and precombustion chemical reaction (chemical delay) occurs;

2. Premixed Combustion, BC in fig 2.1: combustion starts in the inhomogeneous premixed region formed in the ID, and it fastly propagates in this region;

3. Diffusive Combustion, CD in fig 2.1: due to the high temperature reached, diffusive combustion occurs in the core of the spray, governed by the diffusive processes. For this reason, HRR is limited by the characteristic time of vaporisation and diffusion of the spray.

4. End Combustion, DE in fig 2.1: injection is ended and combustion is completed by mixing during expansion stroke of unburned hydrocarbons and residual free oxygen.

All those phases are well represented in the picture 2.2. It represents the Combustion of Jatropha-methyl ester, a second-generation biodiesel, in the optically accessible diesel engine at the Radboud University Nijmegen [3].

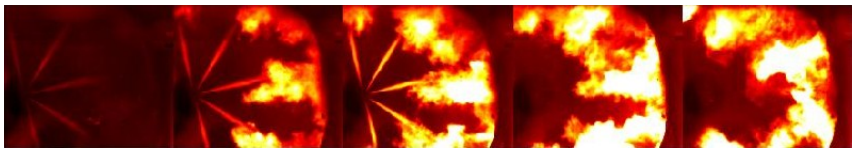

Figure 2.2: CCI Combustion of Diesel Spray

2.2 Pollutant Emissions

Pollutant genesis in Diesel Engine is strongly linked to the charge in-homogeneity, due to the continuous mixing process between fuel and air. The first big distinction can be made between gaseous and solid pollutants. Gaseous Pollutants are unburned Hydrocarbon (uHC), CO,NO_x; solid ones are soots. Pollutant emissions have a rate

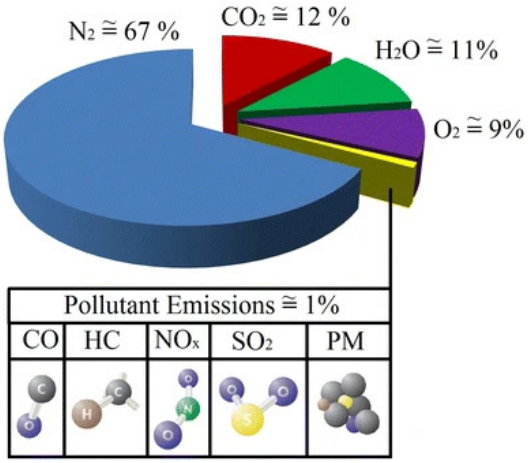

Figure 2.3: Diesel pollutants

of less than 1 % in the diesel exhaust gas. NOx has the highest proportion with a rate of more than 50 %. After NOx emissions, PM has the second highest proportion. The concentration of CO and HC is minimal since the mixture is globally lean. Besides, pollutant emissions include a modicum of SO2 depending on the specifications and quality of fuel (fig 2.3). It is produced by the sulfates contained in diesel fuel [4].

Pollutant	harmful effect	vehicles
CO	cardiac damage, poisoning	$> 80\%$
PM	carcinogenic	$> 80\%$
NO_x	breathing apparatus damage, photo-chemical pollution	$> 40\%$

Table 2.1: Pollutants harmful effects

2.2.1 Nitrogen Oxides Formation

NO_x contributes to acid deposition and eutrophication[1]. NO_2 is associated with adverse effects on human health, when it is present in high concentrations it can cause inflammation of the airways, it also contributes to the formation of secondary particulate aerosols and tropospheric ozone (O3) in the atmosphere [5]. The almost only specie present inside the cylinder is NO, when it enters in contact with the external environment it further oxidizes to NO_2 and NO_3. The main cause of NO_x formation is the oxidation of nitrogen present in the fresh air, following the Zeldovich mechanism:

[1] Eutrophication (from Greek eutrophos, "well-nourished"), distrophication or hypertrophication, is when a water basin becomes overly enriched with minerals and nutrients which induce excessive growth of algae. This process may result in oxygen depletion of the water basin

$$O + N_2 \rightleftharpoons NO + N \tag{2.1}$$
$$N + O_2 \rightleftharpoons NO + O \tag{2.2}$$
$$N + OH \rightleftharpoons NO + H \tag{2.3}$$
$$\tag{2.4}$$

This mechanism requires the dissociation of molecular oxygen and nitrogen in their atomic form, which happens when the temperature is above 2000 K. it occurs in the slightly lean region that surrounds the portion of spray, since it is characterized by the highest temperature and presence of oxygen at partial load. NO_x concentration does not drop at chemical equilibrium values during the expansion stroke because the kinetic of reactions is too slow when the temperature decreases. And that is why their concentration is frozen at higher value respect to chemical equilibrium. This mechanism is particularly favored in CCI combustion firstly because the charge is globally lean, therefore there is always an excess of oxygen, secondly the temperature reached is higher respect to the other form of combustion.

2.2.2 Particulate Matter

Particulate Matter (PM) is a solid pollutant mainly composed of carbon particles deriving from incomplete combustion (fig 2.4) and It is characteristic of Diesel Engine because it is formed from liquid fuel.

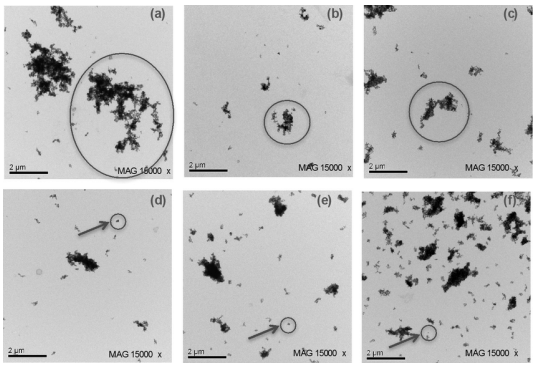

Figure 2.4: TEM images of soot particles [6]

The genesis of PM starts at the beginning of combustion in the core of the spray, where there are a strong heat flux and lack of oxygen. Here hydrocarbon molecules ($H/C \approx 2$) thermally decompose losing hydrogen atoms creating the so-called precursors; new species with $H/C \approx 0.1$. This process is named pyrolysis. Precursors later react with other types of hydrocarbon molecules creating the primary elements of PM. Carbon atoms attach on the surface of primary elements increasing their dimension creating the nuclei ($D_p < 50\ nm$). Some of the nuclei aggregate in particles ($D_p < 2500\ nm$) and others are transported as they are till the external environment. In the meanwhile, oxidation reactions occur in the various stage of the growth process. The composition of the emitted PM is a balance between these two processes. There are also bigger carbon particles that do not directly derive from the described process but are detached deposits from piston walls or valves.

At the exhaust of Diesel Engine, PM is mainly formed by nuclei and agglomerates. Normally those carbon-based solid particles (Solid Fraction (SOL)) are covered by organic species that have been absorbed by their porous surface or that are condensed over them (Soluble Organic Fraction (SOF)).

2.2.3 Carbon Oxides (CO)

Carbon monoxide is a toxic specie. When present in elevate concentration, the human body replaces the oxygen in the red blood cells with carbon monoxide leading to serious tissue damage, or even death. CO is one of the main products of Hydrocarbon oxidation and it is due to thermal decomposition of ketones. It later oxidizes to CO_2 mainly by the following reaction:

$$CO + OH \rightleftharpoons CO_2 + H \tag{2.5}$$

$$\tag{2.6}$$

This reaction is much slower with respect to the one of formation of CO and it quenches during expansion stroke. The air-fuel ratio is the main engine parameter that influences the emission of carbon oxides. The emission of CO is limited for a lean mixture and it grows with the fuel concentration. This is the reason why CCI Engines show CO emissions one order of magnitude smaller respect to SI Engines.

2.2.4 Unburned Hydrocarbon (uHC)

There are many causes of uHC formation, the main ones are presented as follows:

- The charge trapped in the piston crevices during the compression stroke is not able to ignite since the thermal gradient is too high, during the expansion stroke part of this charge goes out from the crevices and partially combusts.
- The flames quenches near the boundary layer of the walls (the thickness is in the order of 0,1 mm) and thereby this region is rich in uHC.
- It can happen that in some region the mixture does not inflame because it is too lean or too rich in EGR.
- A small portion of direct-injected fuel can be trapped in the injection holes.

Chapter 3

Low-Temperature Combustion Engine

As it has been explained in the previous chapter the most harmful pollutants in CCI Engines are caused by the presence of a diffusive flame and by the high temperature reached in the premixed region near the flame front. For this reason, the possibility of running an engine with a CCI like compression ratio and a globally lean in-homogeneous premixed mixture is of interest to achieve a cleaner and efficent combustion [7]. In this way, PM can not be formed since there is no liquid fuel in the combustion chamber and the maximum temperature reached is well below 2000 K avoiding the formation of NO_x. Furthermore, this type of solution shows other benefits that increase engine efficiency. Firstly, the premixed combustion is faster than diffusive one , therefore the cycle is closer to the ideal Otto. Secondly, the average In-cylinder temperature is colder than CCI Engine and, as a consequence, the heat exchange with the chamber wall is smaller.

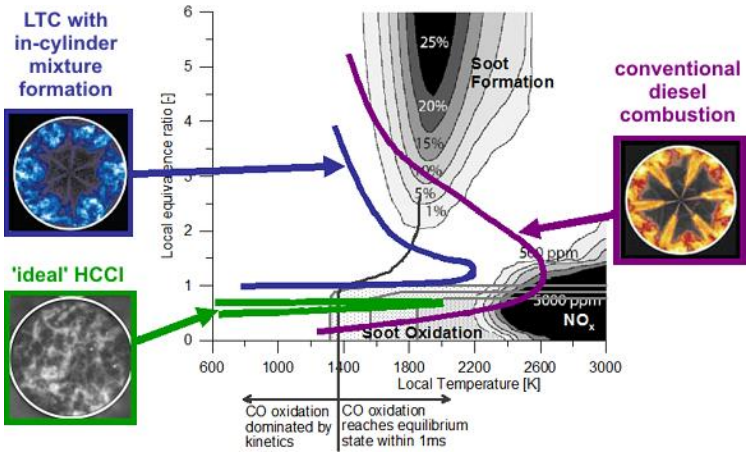

Figure 3.1: Comparison of different engine types

As we can see in the figure 3.1 [8] different types of Low Temperature Combustion Engine (LTCE) have been proposed. In Homogeneous Charge Compression Ignition (HCCI) Engine, the fuel is injected in the intake port or in the cylinder in the first part of the compression; in this way the mixture is almost homogeneous. This type of solution is challenging to control, being the combustion only guided by chemical

kinetic. In other solutions like Reaction Controlled Compression Ignition (RCCI), Temperature Controlled Reactivity Compression Ignition (TCRCI) and Premixed Charge Compression Ignition (PCCI) a portion of the fuel is injected closer to TDC to achieve a charge stratification that helps the control of the combustion.

3.1 Homogeneous Charge Compression Ignition

HCCI technology has been studied for a long time, it was firstly studied to reduce the smoke produced by the first commercial diesel engines, later, with the increase of the environmental responsibility, the possibility of largely decrease the pollutant emissions and the high efficiency linked to this kind of technology have promoted the research. "HCCI diesel combustion using diesel fumigation in the intake port was first described in 1958. Further work in the late 1970s reported stable spontaneous auto-ignition in a two-stroke gasoline engine with port fueling that was attributed to the presence of active radicals. While the focus of many of these early publications was on light fuels (gasoline) in two-stroke engines, later work described the same type of combustion with diesel fuel in four-stroke engines." [8].

Figure 3.2: HCCI cycle

In these engines, the ignition is chemically driven: it occurs spontaneously when the charge reaches the thermodynamic conditions necessary to auto-ignite. Ideally, the combustion starts in all the combustion chamber at the same time, reducing the combustion duration. In this way the cycle is closer to the ideal Otto, increasing the efficiency of the engine.

The typical HRR profile of HCCI combustion is shown in fig 3.3. It is generally called "two-stage ignition" and it is characterized by the presence of cool flames, around -20 CAD; these are low exothermic oxidation reactions, that produce a smaller heat release and they are followed by the main combustion. The presence and intensity of cool flames is a function of the type of fuel. This type of HRR profile is common to other LTC engines that will be discussed in the following chapters.

The drawback is that the Pressure Rise Rate (PRR) is much larger than the one of CCI, leading to high mechanical stresses and vibrations. This problem, and the tendency to show knock-like combustion with pressure oscillation increasing the mixture fraction, limits the application of this type solution at high loads. In the next section, the description of a knock parameter is presented and different strategies to limit the severity of combustion are proposed.

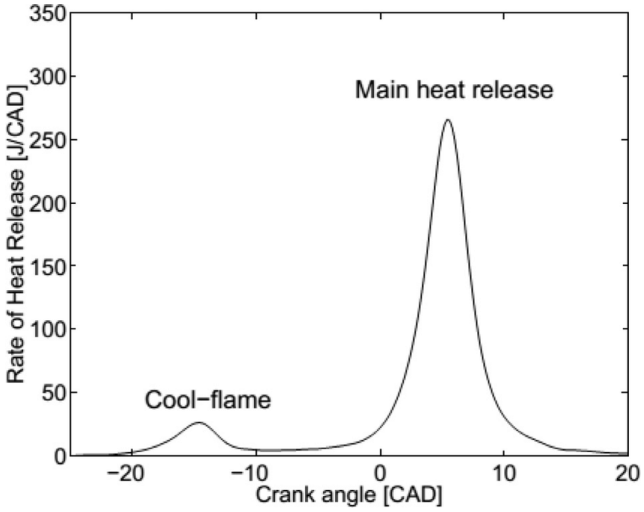

Figure 3.3: HCCI HRR

3.1.1 Knock Parameter

Knock is a particular kind of highly energetic combustion that is called detonation. It produces pressure waves that travel inside the cylinder and are reflected by the walls; these are responsible for the pressure oscillations that are visible in the chart 3.4. Being the knock one of the biggest constrains that limits the high load operations,

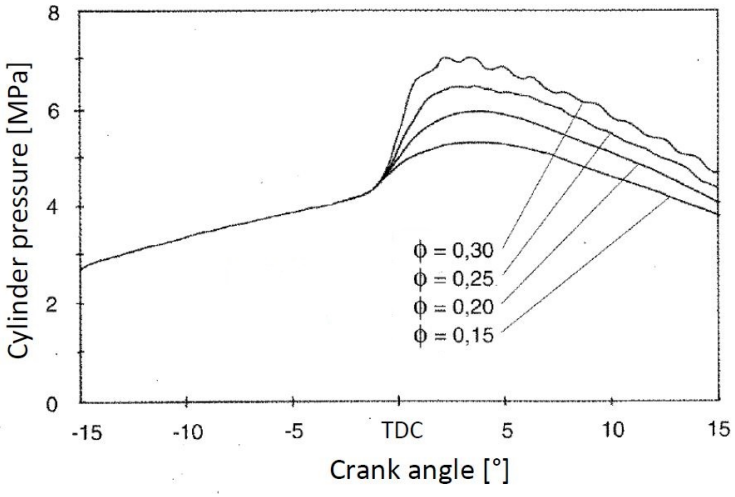

Figure 3.4: Pressure Oscillation HCCI

different studies have been made to define a knock index. Since the excitation of the engine structure is due to the first few waves of the pressure oscillation, the excitation must be proportional to the acoustic energy flux I (watt/m2) associated with these waves, the intensity of the flux is proportional to $\frac{dP}{dt}$ and, as a consequence, the indexes are related to this parameter.

One of the most used is the Ringing Index Proposed by Eng, J.A. [9].

$$RI = \sqrt{\frac{R \cdot T_{max}}{4 \cdot P_{max}^2}} \cdot (\beta \cdot (\frac{dP}{dt})_{max})^2 \tag{3.1}$$

β is a scale factor determined from the experimental data and it has values in order of 0.05 ms, a knock threshold based on this index can be estimated. Some values proposed for different engines by Morgan M. Andreaein [10] are represented in the table 3.1.

	RI Knock Point MW/m^2
GM Data[9]	2
Lund data[9]	6
Ford Data[9]	5.3

Table 3.1: Ring Index Knock thresholds

In the work "On HCCI Engine Knock" [10] directly $\frac{dP}{dt}_{max}$ has been considered as limiting parameter, since the scaling factors T_{max}, P_{max} are used to include engines caracterized by different dimensions and Compression Ratio (CR). If different operating points of the same engine are considered, as in this work, these parameters have a small influence since they follow the same trend. The effectiveness of this Knock parameter can be noticed looking at the fig 3.5, taken from the same article.

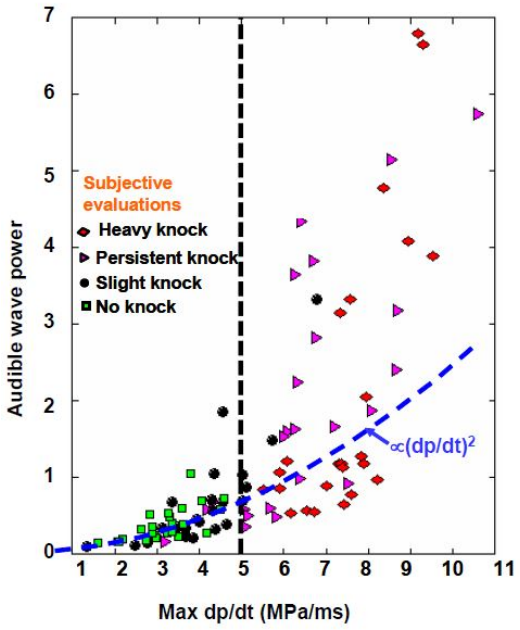

Figure 3.5: Individual cycle audible spectral power from microphone data versus maximum cylinder pressure rise rate

Threshold values are specific for each engine and a summary has been proposed in the cited work with values that range from 3.6 to 7.2 MPa/ms.

3.1.2 Combustion Chamber Geometry

Numerous studies show how geometry generated turbulence affects the combustion of a HCCI engine [11].This is interesting since the combustion chamber geometries that slow down the combustion allow to extend the load range. An interesting analysis regarding this subject has been conducted by the division of combustion engine of Lund University [12] on a Scania D12 engine operating in HCCI conditions with Port Fuel Injection (PFI); two type of pistons, disk shape and square bowl, have ben studied (fig 3.6).

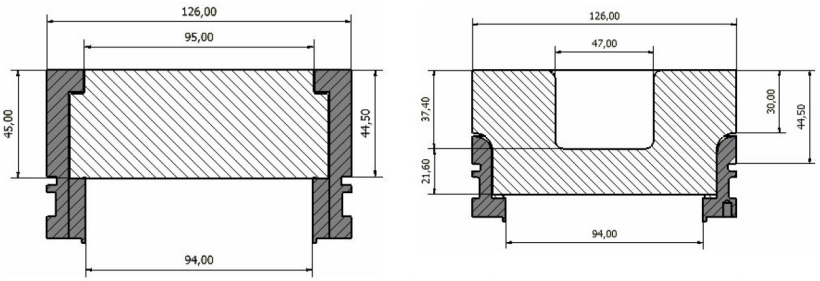

Figure 3.6: Piston shapes

The results, summarized in the table 3.2, show that the square bowl can double the combustion duration and reduce the maximum pressure rate by a third, since combustion starts earlier but last longer (fig 3.7). The reason for this behavior can be understood looking at the High-Speed Cycle-Resolved Chemiluminescence Images.

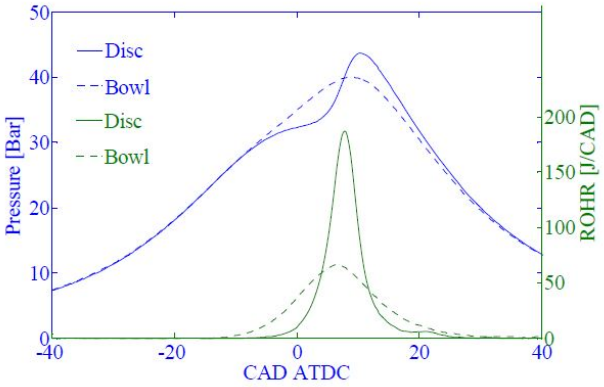

Figure 3.7: Comparison of different piston shapes In-cylinder pressure and ROHR

With regards to the flat piston, the ignition appears near TDC close to the walls and expands slowly in the beginning. At 7 CADs ATDC the combustion speeds up and at 12 CAD ATDC the intensity begins to fade away, and so the heat release decreases (fig 3.8). It is impossible to define an ignition point since combustion starts simultaneously in a large portion of the combustion chamber; the reason is the absence of a relevant temperature and mixture stratification.

With regards to square bowl case, combustion starts in the bowl and propagates trough the squish area (fig 3.9), this leads to an increase of the combustion duration.

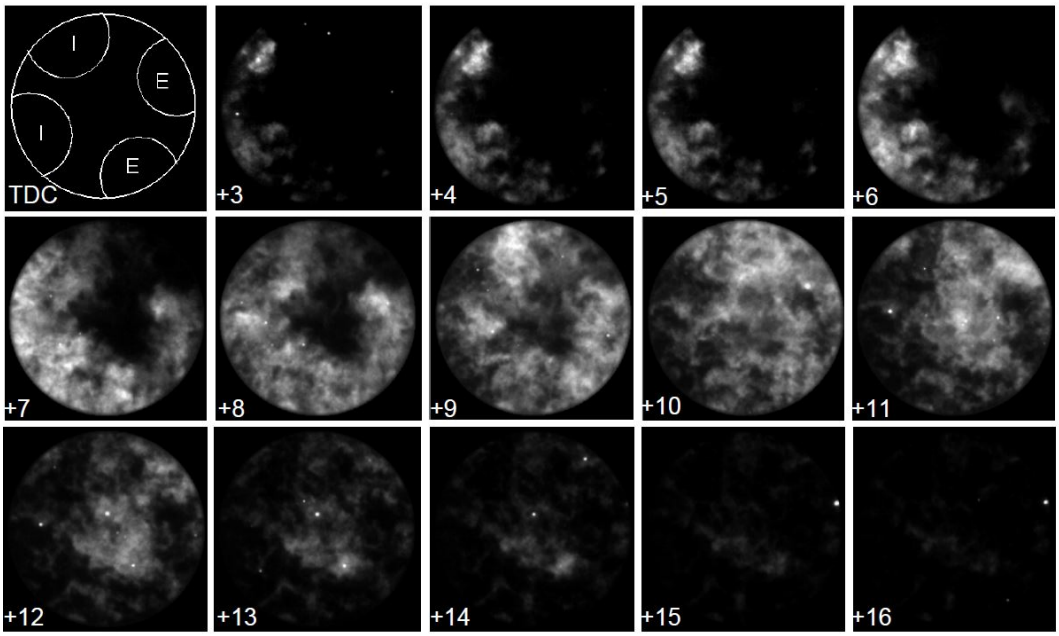

Figure 3.8: single cycle chemiluminescence images Flat piston

The reason has been found in differences in charge temperature instead of the difference in air/fuel ratio because the heat released in the squish area and in the bowl are almost the same and, as a consequence, the assumption of the same amount of fuel in the two regions can be made. This behavior could be explained by the higher percentage of residual gases and by the much smaller heat exchange with the walls as a consequence of much smaller volume surface ratio in the bowl region rather than in the squish region. The reason behind the decrease of combustion speed is the interaction between the geometry generated turbulence and the chemical kinetic. An important evidence that has been found is that for leaner mixture the larger intensity of chemiluminescence images is found in the bowl. This implies that the combustion efficiency in squish area is low, therefore the global efficiency decreases and CO emission increases, limiting the application at low loads of this type of piston bowl.

	Disc	Bowl
λ	3.3	3.3
CA50 [CAD]	8	8
IMEP [bar]	2.81	2.79
CA10-CA90 [CAD]	8.2	17.6
dP [Bar/CAD]	2.73	1

Table 3.2: Operating Conditions and parameters

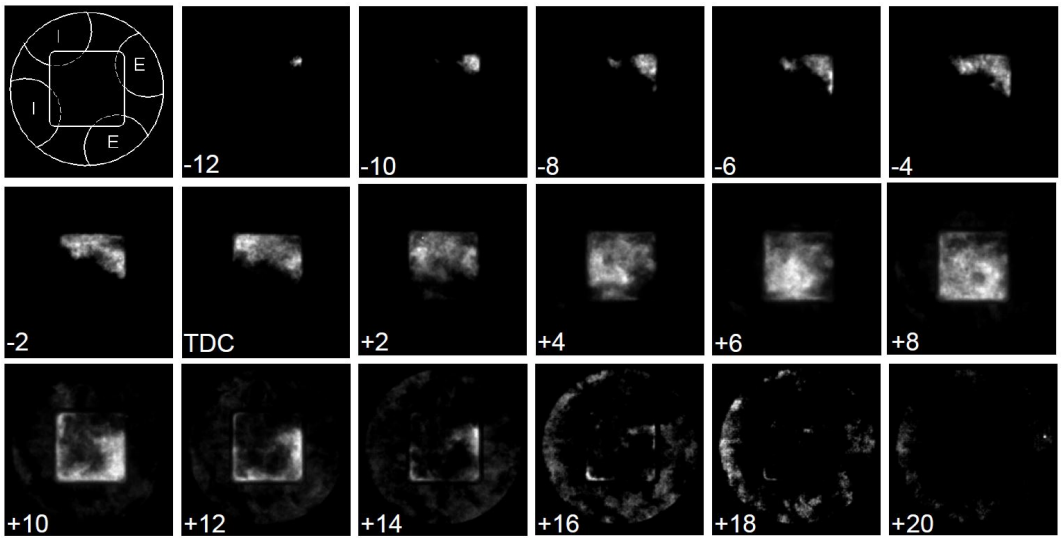

Figure 3.9: single cycle chemiluminescence images square Bowl

In conclusion, the effects of the piston geometry on the combustion are relevant and can be divided into direct and indirect effects [12]:

- Direct effects are the effect of turbulence on the chemical kinetic
- Indirect effects are for example the influence of turbulence on boundary layer, temperature stratification, heat loss and charge homogeneity.

3.1.3 EGR, Compression Ratio

Exhaust Gas Recirculation (EGR) has an important role in the control of the HCCI combustion because it affects the level of inert gases and the thermal level of the mixture [13]. If the exhaust gases are cold (long route EGR), the main effect is of charge dilution with inert species, which delays the ignition and reduces the combustion speed. If the exhaust gases are hot (short route EGR), the in-cylinder temperature increases and the ignition is anticipated.
CR directly affects the thermodynamic condition of the in-cylinder charge . Rate of heat release is only little, or not at all, affected by compression ratio. Peak cylinder pressure is higher for a higher compression ratio but NOX emissions are lower [14]. Applying a control of the effective compression ratio through variable valve timing can help to control the engine.

3.1.4 Stratification

Fuel stratification has the potential to extend the high load limits of homogeneous charge compression ignition (HCCI) combustion by improving the control over the combustion phase as well as reducing the maximum rate of pressure rise [15]. It is the result of injection strategy, an incomplete mix between fuel and air and recirculated exhaust gases. In this way, it is possible to obtain locally richer region, for which the ignition delay is shorter and the stability of the mixture is higher. A similar contribute is played by temperature stratification [16], caused by heat exchange with

combustion chamber walls and mixing with EGR, warmer regions help to ignite the mixture.

3.2 Reactivity controlled Compression Ignition

In HCCI engines the complexity of ignition control leads to emissions of CO and uHC that are in average larger than the ones of conventional CCI engines. This challenge is further enhanced in transient operations, where the continuous changes in engine speed and load are a huge challenge in engine control. A possible solution to these problems has been found in RCCI technology. This engine operates with two fuels with different reactivity. Low Reactivity fuel, typically gasoline, is port injected, a second High reactivity fuel, typically Diesel, is directly injected. The high reactivity fuel reacts with low-temperature reaction, which releases enough energy to ignite the low reactivity fuel in the premixed region. This two-stage combustion helps to increase the combustion duration and to reduce the peak of HRR with respect to HCCI combustion. Furthermore, it introduces two control parameters increasing the overall engine controllability: the percentage of direct-injected fuel and the injection strategy. The drawback of this type of combustion is that it requires two different fuels and hence two different fuel supply systems. This drawback can be partially overcome by the use of an additive for DI fuel to increase the reactivity (fig 3.10).

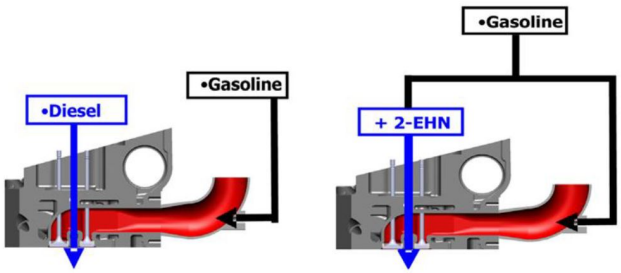

Figure 3.10: RCCI Injection strategy

3.2.1 RCCI Combustion

RCCI combustion (3.11) shows typical Low-Temperature Combustion behavior with two distinct heat releases. At the end of the compression stroke, cold flames are present (around -20 CAD) followed by the main ignition. Cold flames are enhanced by the presence of a rich region of high reactivity fuel, the heat released triggers the premixed mixture of low reactivity fuel that ignites.
The challenge of the LTC Engines controllability is well represented by the cylinder cyclic variability; as it is possible to notice in fig 3.11 the differences between the different cylinders are relevant.

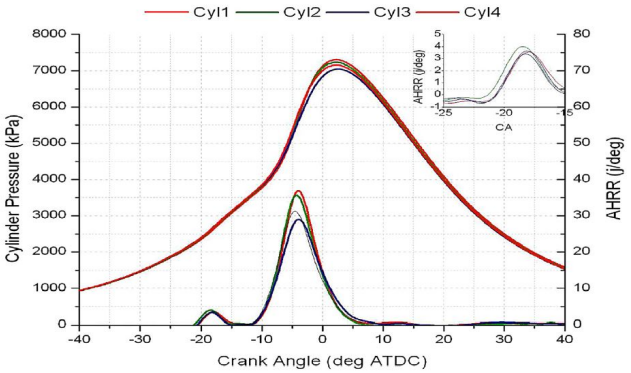

Figure 3.11: Pressure and AHRR for dual-fuel RCCI operating engine

The reason is that chemical controlled combustion is influenced by a large number of parameters that are difficult to fully control[17]:

1. intake pressure and temperature
2. fuel injection strategy (injection duration, Start of Injection (SOI))
3. percentage of Direct Injected (DI) fuel
4. equivalence ratio

3.2.2 Comparison of convention Diesel and RCCI Combustion

To fully understand the advantages and drawbacks of RCCI and in general LTC Engines respect to Diesel ones, the results of the work of S L Kokjohn [18] are presented in this section. The work is based on a direct comparison between the two typologies with the same IMEP of 9 bar.

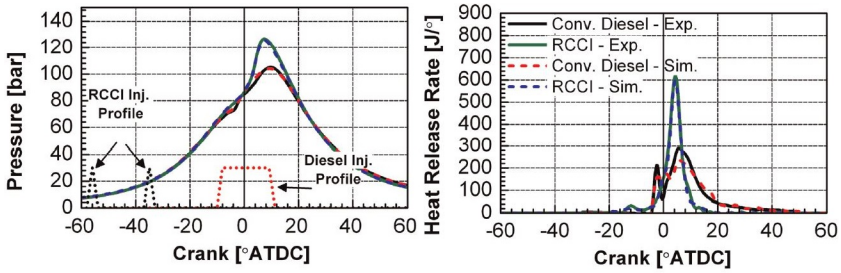

Figure 3.12: Measured and predicted cylinder pressure and AHRRs for conventional diesel and RCCI combustion at 9 bar IMEP

The first parameter to notice is the complete different injection strategy between the two cases, since in RCCI combustion the DI fuel must have the time to evaporate and to mix before the ignition (fig 3.12). The result of the study of this operating condition in terms of emissions and performance parameters are shown in the table 3.3. The emissions of NO_x and soots are different orders of magnitude smaller in RCCI case than Diesel because the combustion is premixed and the mixture lean (tab 3.3). The intensity of the combustion is much larger in the RCCI case, the peak

of HRR is double than CCI case (fig 3.12), however, the RI is well below 5 MW/m^2 (that is the knock threshold fixed for this engine). The increase of combustion losses is the consequence of the fact that the engine has a large ring-pack crevice volume where the premixed charge does not react.

	RCCI	Diesel
IS_{NOx}(g/kW-h)	0.006	9.2
IS_{soot} (g/kW-h)	0.0019	0.133
RI	3.8	1
GIE %	54.3	47.6
Heat Transfer %	10.9	19.1
combustion losses %	1.3	0.3

Table 3.3: Emissions and performance of RCCI and conventional diesel combustion

The increase in efficiency is mainly the consequence of reduced heat transfer. It is the effect of the smaller average in-cylinder temperature and it is also enhanced by the fact that the hot regions in Diesel flames are located on or near the piston bowl, due to the penetration of the fuel spray (fig 3.13). As a consequence, the RCCI combustion process converts 8% more of the fuel energy to useful work than the conventional diesel.

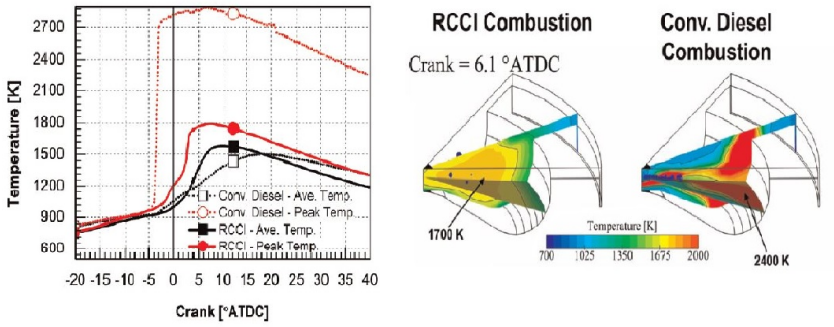

Figure 3.13: Comparison of model-predicted average (global) and peak (local) temperatures for RCCI and conventional diesel combustion

3.2.3 Combustion Chamber Geometry

Being the mixing requirements for RCCI much different from those of conventional diesel combustion, it is interesting to study the effect of the combustion chamber geometry on this type of engine. Derek Splitter has made a comprehensive analysis on this topic that is reported in this section [19]. A flat (pancake-type) piston geometry was used to evaluate the effects of piston bowl depth and squish height. The piston bowl width was held fixed at 2.57 cm and the piston bowl depth was swept from 0.25 cm to 1.50 cm. As the piston bowl depth was changed, the squish height was also changed to hold the compression ratio constant at 15.24:1; the extremes of the analyzed combustion chamber are shown in fig 3.14.

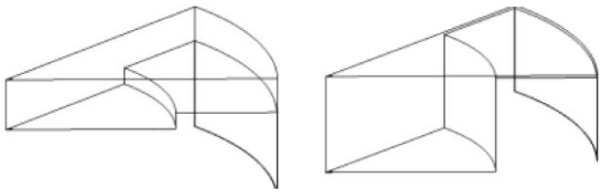

Figure 3.14: Extremes of Combustion Chamber Geometries

Comparisons are also made to an open crater-type piston bowl.
The simulations results show that combustion phasing is weakly dependent on changes in piston geometry, also NO_x and soot emissions are not affected. Thermal efficiency is highly influenced by the geometry, it reaches the maximum at the minimum bowl depth and it decreases until bowl depth equal to 1 cm. For bowl depth bigger than 1 cm, the efficiency increases and remains almost constant for further increases (fig 3.15).

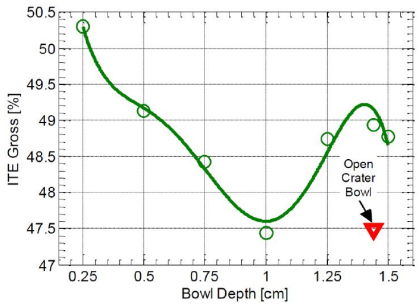

Figure 3.15: Predicted gross indicated efficiency as a function of piston bowl depth

This trend is the consequence of the sum of the heat losses and combustion losses. Heat losses increase with the bowl depth, which affects also the surface/volume ratio. Combustion losses peak for bowl depth equal to 1 cm and they have similar value for minimum and maximum bowl depth, as it is possible to notice in fig 3.16.

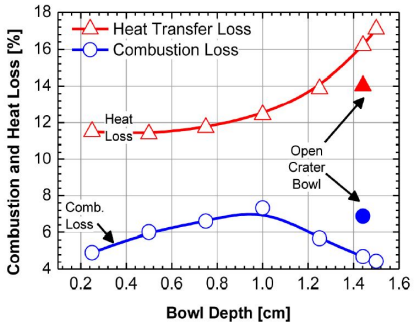

Figure 3.16: Combustion and heat transfer losses as a function of bowl depth

The reason for this trend of combustion losses is directly linked to the emission of uHC that reaches the maximum for Bowl depth equal to 1 cm (fig 3.17).

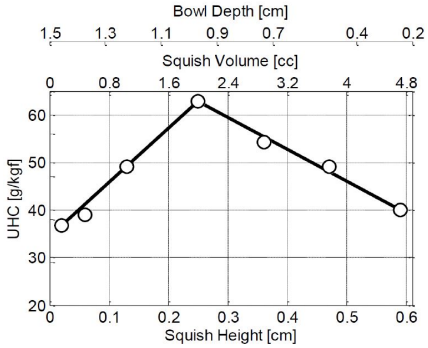

Figure 3.17: uHC as a function of piston bowl depth/squish volume

This behaviour is the consequence of the squish motion induced by the geometry and the penetration of the hot burned gases in the squish region that promotes the combustion of the mixture in that area.
The position of the uHC changes with the bowl depth and the squish height , this is related to the strength of the reverse squish flow during the expansion stroke. That is, as the piston moves downward, the charge is drawn into the squish region. Since a sharp edge exists, the flow tends to move upward towards the firedeck as it is drawn into the squish. As the bowl depth is increased and the squish height is decreased, the momentum of the reverse squish flow increases, causing the bowl fluid to be drawn deeper into the squish region. For the case with a bowl depth of 1.50 cm, the reverse squish flow is strong enough that the fluid moves all the way to the liner and, as it encounters the liner, draws uHC away from it, along the piston top land. This contribution and the penetration of high-temperature gases in the squish region helps to oxidize the remaining uHC (fig 3.18).

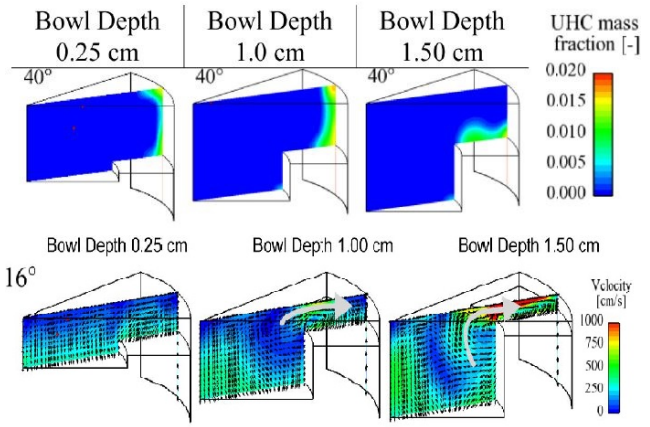

Figure 3.18: Cut-planes in the plane of the spray shown at 40° ATDC colored by uHC mass fraction and velocity projected onto the plane

In conclusion, the piston bowl can be optimized for premixed autoignition combustion and the optimal geometry for minimizing the losses was found to be a piston with a shallow bowl depth and a large squish height.
Starting from this analysis, a piston optimized for RCCI operation has been studied

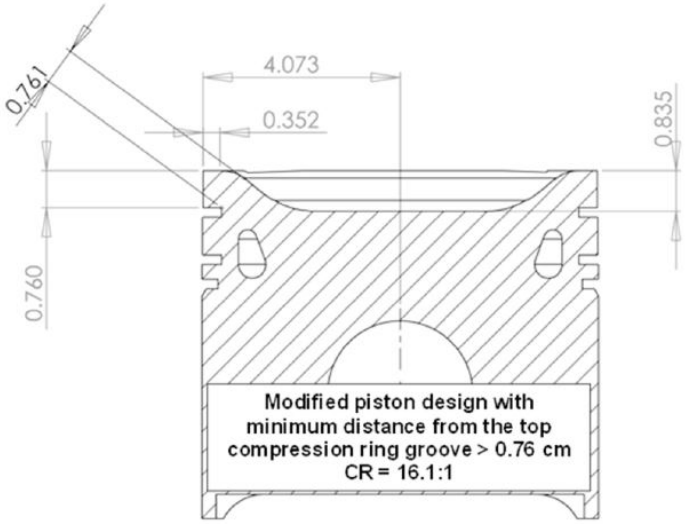

Figure 3.19: RCCI piston final version with increased bowl to ringland thickness

by Reed Hanson (fig 3.19), Scott Curran [20]. The bowl diameter and compression ratio were the parameters that varied in the piston design. Piston bowl diameter is increased from 2 to 4 cm, this leads to an increase of GIE due to decrease of heat exchange with the wall (fig 3.20). The geometric compression ratio of 16.1:1 was chosen to improve low load operations with acceptable high load potentiality. However, the final compression ratio due to machining tolerance has been measured in 15.1:1.

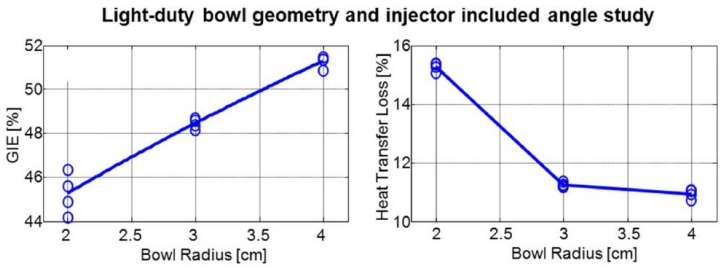

Figure 3.20: Simulated RCCI piston bowl radius vs. GIE

The experimental campaign has been conducted on three different operating conditions. The RCCI technology has been conducted with Diesel OEM piston and optimized RCCI piston. Furthermore, a single injection strategy has been used for RCCI OEM piston while the double strategy has been used for RCCI piston bowl. The result shows that RCCI piston bowl is not able to significantly reduce a the uHC emission, suggesting that the main sources are the crevices. CO emissions increase since the reduced CR of RCCI piston decreases the in-cylinder temperature. Furthermore, the double-injection strategy along with the use of the specially designed RCCI piston offered a reduction of the maximum pressure rise rate and maximum heat release rate and a larger brake thermal efficiency with respect to OEM piston (fig 3.21).

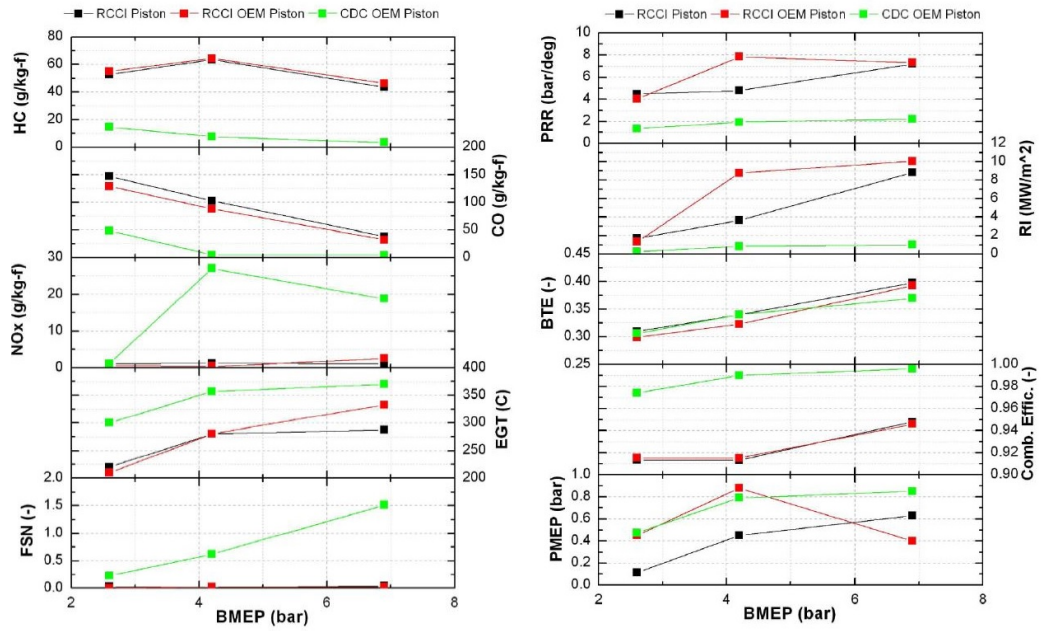

Figure 3.21: Engine out emissions, combustion and performance for the considered cases

3.2.4 Injection Strategy

Since this technology has the advantage to have the presence of a direct injection, it is worth understanding how the injection strategy influences the engine behavior. The most influent parameters are the fraction of DI/PFI fuel and the injection timing. An interesting work regarding this topic has been conducted by Reed M. Hanson and Sage L. Kokjohn on a heavy-duty 2.44 L Caterpillar 3401 Single Cylinder Oil Test Engine (SCOTE) ([21],[22]) and the results are reported in this section (fig 3.22). Engine experiments were performed using an engine load of 9 bar net IMEP and an engine speed of 1300 rev/min; in all the operating conditions a split injection has been used.

The first parameter studied is the Start of the second Injection and a sweep from

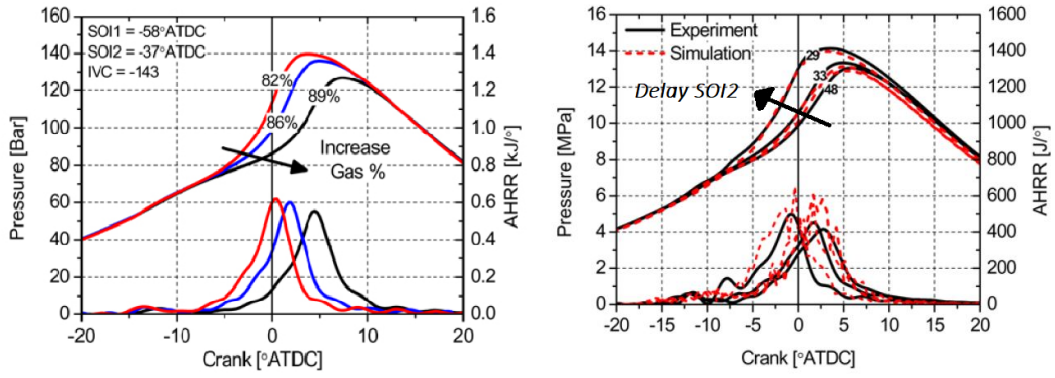

Figure 3.22: SOI2 sweep and PFI fraction effect in RCCI combustion

-48 CAD to -29 CAD has been considered. The earlier the injection is the higher the

time available for the mixing processes to homogenize the mixture is and the later the combustion phasing will be. There is a limit to delay the SOI, otherwise the local temperature reached in the rich mixture is high enough for NOx formation and a portion of the direct injected diesel does not have time to evaporate leading to an increase of soot emissions. If the SOI is anticipated too much, the local mixture at the start of combustion is leaner and, as a consequence, the combustion efficiency decreases with the increase of emissions of CO and uHC. The effect of the PFI/DI fuel fraction is similar since the mixture stratification and the global reactivity increase with the Direct Injected fuel percentage, as consequence combustion timing is anticipated. The considerations regarding the pollutants are the same as the SOI sweep.

3.3 Temperature Controlled Reactivity Compression Ignition

One of the main drawbacks of RCCI technology is that it requires two fuels with different properties and two different fuel supply systems. This leads both to an overall complication of the global system and a complication for the customer in the refueling operation. This problem can be mitigated by the use of addictive to increase directly the reactivity of the low reactivity fuel. A new solution that has been proposed to overcome this limit is the so-called TCRCI; in this case, the direct-injected fuel is the same fuel that is port injected but heated up (fig 3.23). The idea is that the reactivity increase as a consequence of the elevate injection temperature of the directly injected fuel is high enough to promote a combustion similar to RCCI. This technology allows to add the directly injected fuel temperature to the control parameters. Depending on the injection temperature and corresponding vapor pressure, fuel evaporation can take place under standard or flash boiling conditions. Supercritical injectors can be used to avoid high-pressure injectors, in this case the fuel is heated in the supercritical region.

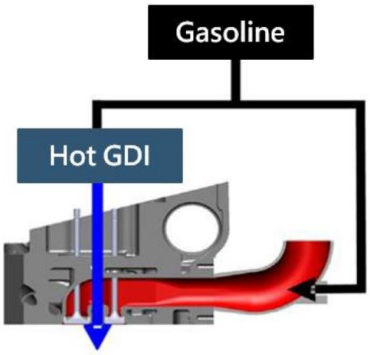

Figure 3.23: TCRCI fuelling strategy

The combustion mode is the same as RCCI combustion: DI fuel reacts with low T reaction releasing enough energy to ignite the premixed mixture. DI fuel temperature ranges from 100° to 500°. Depending on the technology, fuel heating can occur before the injector or within the injector itself.

The cold injection can take place both in the intake port or during the compression stroke if cold DI is present. The cold fuel DI could help to create a further stratification improving combustion stability and controllability. Hot Injection normally is performed with limited fuel mass (up to 20 % of the total injected fuel) later than -60° CAD. The main exploitable advantages of this kind of LTC are:

1. It can be applied using GDI and PFI technology with commercial pump gasoline and biofuels (like E85 and E95)
2. Lower DI injection pressure respect to RCCI, due to higher volatility of fuel enhanced by high temperature
3. Lower pollutant emission (HC and CO) and so higher combustion efficiency, due to higher exhaust gas T due to later combustion phasing.

As shown in a previous Thesis made by Filippo Gazzola [23], simulation results show that in similar condition with the same percentage of DI and PFI the heat release rate of TCRCI is similar to RCCI but combustion phasing is delayed due to smaller difference in reactivity between the two fuels. In the best efficiency point, they also show a very close Gross Internal Efficiency (fig 3.24).

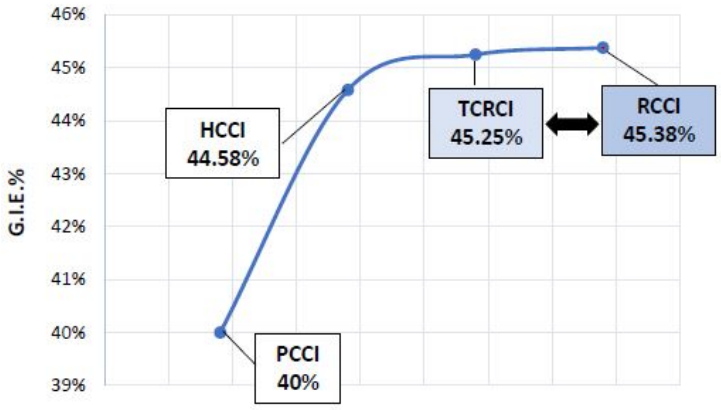

Figure 3.24: LTC Gross Internal Efficiency Comparison

Chapter 4

CFD modeling of combustion

This chapter presents the methodology used for the simulations. The modelling of the ICE combustion process is a challenging task, since it is the result of interaction between the thermochemical and fluid-dynamic process. As a consequence, the numerical model has to solve both the fluid dynamic and chemical equations and it is necessary to define both a model for combustion and a model for the turbulence. In this thesis work, the combustion model used is the so-called Tabulated Well-Mixed Model and the turbulence model is the well-know $k-\varepsilon$ model. In the next sections, the models are described and the governing equation explained.

4.1 Transport Equations

CFD is based on the definition of models that allow to solve the equations that govern the thermo-fluido-dynamic process. The governing equations are here presented.

4.1.1 Mass Conservation

Inside the engine the mass is conserved, mass conservation can be expressed by continuity equation:

$$\frac{\partial \rho}{\partial t} + \vec{\nabla} \cdot (\rho \vec{U}) = \rho \dot{S}_s \tag{4.1}$$

The flow of the fluid inside the infinitesimal volume is balanced by the accumulation term; the source term accounts for the injection. The charge is a mixture of different chemical species, which mass is not conserved as a consequence of the chemical reactions. The evolution of the species mass fractions is taken into account by the combustion tabulated well mixed model.

4.1.2 Momentum transport Equation

Momentum equation is strictly correlated to the Newton second law and can be expressed as follows:

$$\frac{\partial \rho \vec{U}}{\partial t} + \vec{\nabla} \cdot (\rho \vec{U} \otimes \vec{U} + p \bar{\bar{I}} - \bar{\bar{\tau}}) = \rho \bar{f}_e \tag{4.2}$$

The viscous stress tensor $\bar{\bar{\tau}}$ for a Newtonian fluid mimics the mechanical behaviour of the fluid and can be expressed as a function of velocity gradient, the molecular

viscosity µ and the Kronecker delta δ_{ij} ($\delta_{ij} = 1$ if i=j, $\delta_{ij} = 0$ if $i \neq j$) :

$$\tau_{ij} = \mu(\frac{\partial u_i}{\partial x_j} + \frac{\partial u_j}{\partial x_i}) - \delta_{ij}\frac{2}{3}\mu\frac{\partial u_i}{\partial x_i} \tag{4.3}$$

4.1.3 Energy Equation

Energy conservation equation is usually expressed in form of enthalpy transport equation:

$$\frac{\partial \rho h}{\partial t} + \vec{\nabla} \cdot (\rho \vec{U} h) = \frac{dP}{dt} - \nabla \cdot q + \dot{Q} \tag{4.4}$$

The term $\dot{Q}$ takes account of the heat exchanges with the liquid spray and the radiative heat losses that are relevant due to the high temperature reached during the combustion. The heat flux can be expressed as follows:

$$q = -k\nabla T + \sum_{i=1}^{N_s} h_i Y_i \vec{U}_i \rho \tag{4.5}$$

4.1.4 Transports equations necessary for Tabulated Well Mixed Model

The Tabulated Well Mixed Model has been used for the combustion process; therefore the chemical equations are solved separately and the results are stored in a table. To access the table the transport equations for mixture fraction, enthalpy, unburned gas temperature and progress variable are solved in the CFD domain.
Mixture Fraction equation includes fuel evaporation:

$$\frac{\partial \rho Z}{\partial t} = \nabla(\rho U Z) - \nabla(\mu_t \nabla Z) = \dot{S}_Z \tag{4.6}$$

Where μ_t is the turbulent viscosity and the source term is function of the fuel evaporation.
The source term in the progress variable transport equation is derived from the table:

$$\begin{aligned} \frac{\partial \rho C}{\partial t} = \nabla(\rho U C) - \nabla(\frac{\mu_t}{S \cdot c_t}\nabla C) = \rho \dot{C} \\ \dot{C} = (C_{max} - C_{min}) \cdot \dot{c} \end{aligned} \tag{4.7}$$

To consistently access the table data, it is necessary to solve an additional equation for the unburned gas enthalpy, which is then used to compute the unburned gas temperature T_u.

$$\frac{\partial \rho h_u}{\partial t} = \nabla(\rho U h_u) - \nabla(\alpha_t \nabla h_u) = \dot{Q}_s + \frac{\rho}{\rho_u}\frac{Dp}{Dt} \tag{4.8}$$

Where α_t is the turbulent thermal diffusivity and ρ_u the density of the unburned gasses. $\dot{Q}_s$ takes account of spray evaporation.

4.2 Tabulated Well Mixed Model

Since the interest of the simulations is not only the engine performance but emission as well the combustion model have to incorporate detailed chemistry and also the effect of the interaction with turbulence. Chemical kinetics can be handled in two different approaches [24]:

- **Direct Integration**: in this case reaction-diffusion equations are solved online during the simulation for each specie included in the mechanism. Computation of reactions rates requires to solve ODE stiff equation being chemical time scale smaller with respect to flow one.
- **Tabulated Kinetics**: chemical reaction rate are stored in a previously generated table according to a specified mechanism and flame structure; Then they are retrieved as a function of the state of the system.

The necessity to use ODE stiff solver for direct integration leads to a significant increase of the computational time, limiting the maximum number of the species of the mechanism around 100. The advantage to achieve results within an acceptable amount of time leads to the large use of the tabulated method. Tabulated methods differ for the chemical mechanism used and for the flame structure. The chemical mechanism models the species involved in the combustion reaction and the various partial combustion reactions. In the tabulated method the quantities are stored as a function of the state variables of the system and the combustion progress variable. The table includes data of the progress variable reaction rate and chemical composition that is represented by a set of virtual species representing the most important thermodynamic proprieties of the full set of the used mechanism. The idea behind the well-mixed model is that each computational cell of the reactive mixture is treated as a closed homogeneous system, neglecting turbulence-chemistry interaction for the local flow conditions.

4.2.1 Chemistry Table

This section describes the way the tabulation is handled. At first, the user must specify a chemical mechanism and a set of initial conditions for homogeneous constant pressure reactor calculation (that are handled by a python module made to perform chemical calculation called Cantera) in terms of:

- Initial reactor Pressure p
- Initial reactor Temperature T_u
- Mixture Fraction $Z = m_{fuel}/(m_{fuel} + m_{oxidizer})$ [1]
- Oxidizer Composition $(X_{H_2O}, X_{O_2}, X_{N_2}, X_{CO_2})$

This set must cover all the conditions reached by the unburned mixture during the engine cycle. For each combination of the initial conditions, the initial composition of the reactor is computed and the calculation starts. Initial reactor temperature can be set independently from Z or it can vary from two extreme value set from Z=0 to Z=1, including eventually fuel evaporation.

$$h(Z) = (1 - Z)h(T_{Z=0}) + Zh(T_{Z=1}) - Zh_l(T_{Z=1}) \tag{4.9}$$

Both approaches are equivalent and give the same results, since all the possible expected thermodynamic conditions are covered in both the cases. For any specified condition, chemical species equation are solved:

$$\frac{dY_i}{dt} = \dot{w}(T, p, Y_1, ..., Y_n) \tag{4.10}$$

At each time step two different operations are performed:

1. evaluation of the progress variable C
2. computation of the chemical composition by the use of virtual species approach

The progress variable is fundamental in the description of the combustion process since it connects the fluid dynamic and the progress of the chemical reactions. In this model, it is defined as the global heat released by combustion, computed as the difference between the value of the reactor formation enthalpy at the current time step and the initial one.

$$C = \sum_{k=1}^{N_s} h_{298,i} Y_i(t) - \sum_{k=1}^{N_s} h_{298,i} Y_i(0) \tag{4.11}$$

Where N_s is the total number of species used in the mechanism. This variable uniquely characterizes each point of the thermodynamic state space and it is appropriate for a transport equation. At the end of each reactor calculation, progress variable reaction rates and chemical composition are stored as function of the discrete values of the normalized progress variable c:

$$c = \frac{C - C_{min}}{C_{max} - C_{min}} \tag{4.12}$$

C_{min} and C_{max} are found at initial time step and after auto ignition and they are stored in the table as a function of the initial conditions.
The reaction rate of the progress variable is set using the forwarding differencing scheme:

$$\dot{c}_i = \frac{c_{i+1} - c_i}{t_{i+1} - t_i} \tag{4.13}$$

This value is after multiplied for the normalizing term $(C_{max} - C_{min})$ to achieve the proper value of $\dot{C}$ to use in the transport equation. For the chemical composition only seven species are stored at each time step and their mass fractions are computed in order to preserve the main thermodynamic properties of the full set of chemical species used in the mechanism. This is done to have tables with an acceptable dimension and the virtual species are $(H_2, CO_2, CO, fuel, H_2O, N_2, O_2)$, their

composition is computed as:

$$
\begin{aligned}
\sigma_H &= \sum_{i=1}^{N_s} N_{H,i} \cdot x_i = \sum_{k=1}^{N_v} N_{H,k} \cdot x_{v,k} \\
\sigma_C &= \sum_{i=1}^{N_s} N_{C,i} \cdot x_i = \sum_{k=1}^{N_v} N_{C,k} \cdot x_{v,k} \\
\sigma_O &= \sum_{i=1}^{N_s} N_{O,i} \cdot x_i = \sum_{k=1}^{N_v} N_{O,k} \cdot x_{v,k} \\
\sigma_N &= \sum_{i=1}^{N_s} N_{N,i} \cdot x_i = \sum_{k=1}^{N_v} N_{N,k} \cdot x_{v,k} \\
h &= \sum_{i=1}^{N_s} Y_i \cdot h_i(T) = \sum_{k=1}^{N_v} Y_{i,v} \cdot h_i(T) \\
c_p &= \sum_{i=1}^{N_s} Y_i \cdot c_{p,i}(T) = \sum_{k=1}^{N_v} Y_{i,v} \cdot c_{p,k}(T) \\
&\sum_{k=1}^{N_v} Y_{i,v} = 1
\end{aligned}
\tag{4.14}
$$

σ is the total number of elements in the reactor, N_v is the number of virtual species, N is the number of elements in the chemical mechanism, Y is the mass fraction, x the molar fraction , h is the mass-specific enthalpy and c_p is the mass-specific heat. It is possible to add to the table the mass fraction of some species of interest for the user that are present in the mechanism but not in the set of virtual species. The procedure of the table generation is schematized in the figure 4.1.

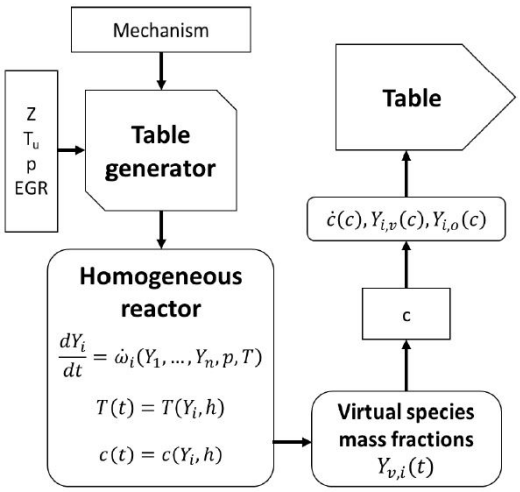

Figure 4.1: Scheme of steps of table generation

4.2.2 Tabulated well-mixed model (TWM)

Once the table is done, the next step is to integrate into the CFD simulation (fig 4.2). In the CFD domain transport equations for mixture fraction, enthalpy, unburned gas temperature and progress variable are solved to define the initial conditions necessary to access the table for each cell. Interpolation of table values at cell conditions is performed by means of an inverse, distance weighted technique. The table outputs are the mass fractions of the virtual species and of the species defined by the user and the reaction rate of the progress variable. Using tabulated Kinetic a $N_s + 2$ problem is simplified to four dimensional problem (T_u, Z, C, p). The result of this simplification is that the regions with rich mixture are characterized by a long ignition delay and a fast one stage ignition. As a consequence, rich regions will ignite almost instantaneously and high value of C will be diffuse through leaner regions leading to a very anticipate auto-ignition. To avoid this problem, reaction rate of regions with equivalence ratio larger than three are normally set to zero.

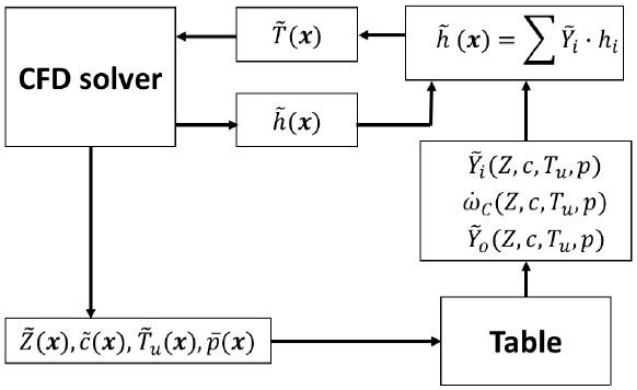

Figure 4.2: Interaction between CFD and table

4.3 Turbulence Model

Turbulence plays an important role in I.C.E. both in the gas exchange process and in the combustion one. "Turbulence causes the appearance in the flow of eddies (vortexes) with a wide range of length and time scales that interact in a dynamically complex way [25]"; different modeling approaches for turbulence have been implemented and they differ for the vortex scale at which the flow is no more solved but modeled:

- **Turbulence models for Reynolds-averaged Navier–Stokes (RANS) equations**: the attention is focused on the main proprieties of the flow (Reynolds average Equations) and the effect of turbulence on these proprieties. Extra terms present in the Reynolds equations due to the influence of turbulence are modeled by classical turbulence model as $k - \varepsilon$ and $k - \omega$ and the Reynolds stress model.
- **Large Eddies Simulation (LES)**: this approach can solve large eddies thanks to space filtering of the unsteady Navier–Stokes equations before the computations, which passes the larger eddies and rejects the smaller ones.

- **Direct numerical simulation (DNS)**: this approach can solve all the scale of turbulence till Kolmogorov. The unsteady Navier–Stokes equations are solved on spatial grids that are sufficiently fine to resolve the Kolmogorov length scales and with time steps sufficiently small to resolve the period of the fastest fluctuations.

The more the vortex are modeled, the faster the computational time required for the simulation is. In the industrial field and the majority of engineering applications the RANS model is used since the interest is focused on the main flow. Also in this thesis work RANS approach is used.

4.3.1 RANS Equations

RANS equations are obtained defining each flow propriety (ϕ) as the sum of an average quantity plus a fluctuation term:

$$\phi = \bar{\phi} + \phi' \tag{4.15}$$

The average quantity is defined as:

$$\bar{\phi(x)} = \frac{1}{\Delta T} \int_{t-\Delta T/2}^{t+\Delta T/2} \phi(x,t)\, dt \tag{4.16}$$

The main proprieties of this operator are (given ϕ and Φ two different flow quantities):

$$\overline{\phi'\bar{\Phi}} = 0 \quad \bar{\phi + \Phi} = \bar{\phi} + \bar{\Phi} \quad \overline{\phi\Phi} = \overline{\phi}\,\overline{\Phi} + \overline{\phi'\Phi'} \tag{4.17}$$

Since $\overline{\phi'\Phi'} \neq 0$ a new term in the Reynolds averaged momentum equation is present that takes the name of Reynold stress tensor, since it acts like a stress added to the viscous molecular one. It must be modeled by a turbulence model. The term is $\vec{\nabla} \cdot (\rho\overline{\vec{U}}' \otimes \overline{\vec{U}}')$ and it derives from the averaging process of $\vec{\nabla} \cdot (\rho\vec{U} \otimes \vec{U})$:

$$\overline{\vec{\nabla} \cdot (\rho\vec{U} \otimes \vec{U})} = \vec{\nabla} \cdot (\rho\bar{\vec{U}} \otimes \bar{\vec{U}}) + \vec{\nabla} \cdot (\rho\overline{\vec{U}}' \otimes \overline{\vec{U}}') \tag{4.18}$$

Since from different experimental investigations it was noted that turbulent stresses increase as the mean rate of deformation increases Boussinesq proposed that Reynolds stress tensor might be proportional to mean rates of deformation (Boussinesq hypothesis).

$$\tau_{ij,t} = \rho u_i' u_j' = \mu_t \left(\frac{\partial \bar{U}_i}{\partial x_j} + \frac{\partial \bar{U}_j}{\partial x_i}\right) - \delta_{ij}\frac{2}{3}\rho k \tag{4.19}$$

μ_t is the turbulence viscosity and k is the Turbulent Kinetic Energy and it is the trace of the Reynolds tensor $k = \frac{1}{2}(u'^2 + v'^2 + w'^2)$; these terms have to be modelled.

4.3.2 $k-\varepsilon$ Model

The so-called $k-\varepsilon$ mode is the most common turbulence model and it can provide a stable and accurate description of the effects of turbulence on the average fluid motion. This model is used in this thesis.
The turbulent viscosity is defined as:

$$\mu_t = C_\mu \rho \frac{k^2}{\varepsilon} \tag{4.20}$$

Where ε is the turbulent kinetic energy dissipation and it derives from the modeling. Therefore the equations are closed by the addition of two new scalar transport equations, one for the turbulent kinetic energy and the other for the turbulent kinetic energy dissipation rate.

$$\begin{aligned} \frac{\partial \rho \vec{k}}{\partial t} + \vec{\nabla} \cdot (\rho \vec{U} \otimes \vec{U} k) &= \vec{\nabla} \cdot [(\mu + \frac{\mu_t}{\sigma_k}) \nabla k] + P_k + p\varepsilon \\ \frac{\partial \rho \vec{\epsilon}}{\partial t} + \vec{\nabla} \cdot (\rho \vec{U} \otimes \vec{U} \varepsilon) &= \vec{\nabla} \cdot [(\mu + \frac{\mu_t}{\sigma_k}) \nabla \varepsilon] + \frac{\varepsilon}{k}(C_{\epsilon 1} P_k - C_{\epsilon 2} \rho \epsilon) \end{aligned} \tag{4.21}$$

Where P_k derives from the Reynolds stress tensor and $(\sigma_k, C_{\epsilon 1}, C_{\epsilon 2}, \sigma_\epsilon, C_\mu)$ are five constants that can be adapted to the specific case. The problem of this model is that the ε equation becomes singular in the close wall region and hence it requires wall functions to model the boundary layer region. kqRWallFunction is used for k and epsilonWallFunction, it provides a simple wrapper around the zero-gradient boundary condition; epsilonWallFunction is used for ε, it provides a wall constraint on the turbulent kinetic energy dissipation rate [26].

4.4 Virtual Injection model

The virtual gaseous injection model has been implemented by the ICE group of Polimi to correctly simulate supercritical injection in TCRCI combustion. This model directly injects inside the cylinder gaseous fuel without considering the physics inside the injector (figure 4.3). This is important since it allows to eliminate from the computational domain the injector duct where complex phenomena happens, as the phase change from liquid to supercritical as a consequence of the heat exchange with the hot walls.

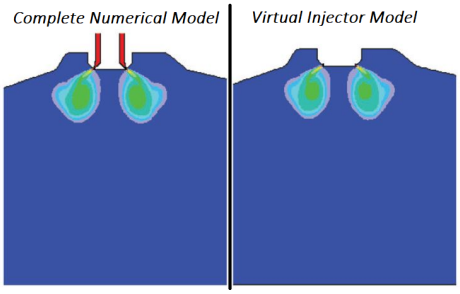

Figure 4.3: Comparison between complete model and virtual injector domain

The basis of virtual Injector model is to define a set of source cells in correspondence of the injector hole. For these an additional source term is added for each of the finite-volume equations to take account of the gaseous injection:

$$S_\Phi = \dot{m}\Phi \tag{4.22}$$

where $\dot{m}$ is the mass flow rate of the injected stream and Φ is the value of a generic flux property attributed to the stream [27].
The grid sizes of the injector cell set and the near-nozzle region have a great influence on the fuel jet evolution and fuel–air mixing [28]; moreover the mesh should be angled as the injection direction to correctly predict the jet penetration. Otherwise the injection velocity tends to be underestimated and a portion of the mass is injected in the wrong direction (fig 4.4).

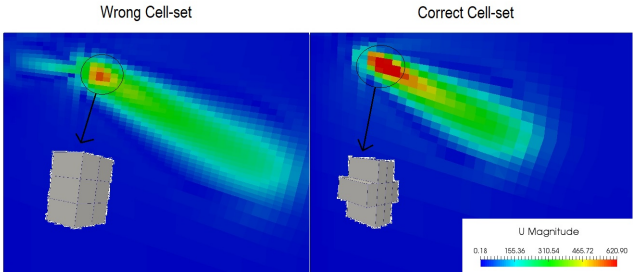

Figure 4.4: Comparison between injection velocity of different types of cell-sets

4.5 OpenFOAM code and Lib-ICE library

OpenFOAM is an opensource C++ code able to carry out CFD internal combustion engine simulation in continuum mechanics. Its distribution contains detailed solvers that can solve specific problems like turbulent flows or stress analysis and utilities in order to manipulate data in pre-processing and post-processing phases.
Associated with OF, the ICE group of Politecnico di Milano developed a set of applications and libraries for internal combustion engine simulation, pre-processing and post-processing called Lib-ICE. The library is based on the OF technology and provide tools and solvers to model physical and chemical phenomena, like liquid spray dynamics and evolution, combustion processes and exhaust gases after treatment. Diesel based combustion solvers are adopted in this work.
The advantage of OpenFOAM and Lib-ICE interconnection consists in the possibility of a continuous evolution by improving the always up-to-date applications and by making new ones.

Chapter 5

HCCI combustion simulations

In this chapter the methodologies used for HCCI simulations and for the comparison of the results with a set of experimental data provided by Marmotors s.r.l. are presented. Firstly a preliminary analysis on the provided operating points has been conducted since some uncertainty regarding the values of the experimental equivalence ratios are present. Secondly the simulation results are presented and a deeper analysis of the combustion process has been performed.

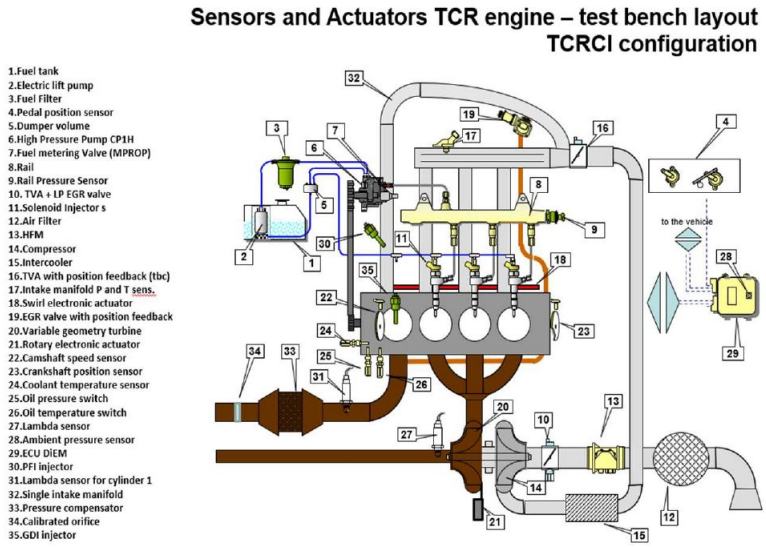

Figure 5.1: Test Bench Layout TCRCI Configuration

5.1 Preliminary analysis of experimental data

The Experimental data come from a 3 + 1 retrofit of a commercial 2.0 lt. JTD FCA engine. As it is possible to see in the fig. 5.1, the engine is an in-line 4 cylinder where three cylinders always operate with the commercial common rail injector system through CCI combustion to stabilize the engine; the last one can perform both HCCI and TCRCI combustion being equipped with a port fuel and a heated direct injector. Since the TCRCI cylinder exhaust manifold is not connected to the turbocharger, a pressure compensator has been installed to simulate the back pressure (item 33 in fig 5.1). The engine is equipped with a Horiba exhaust gas analyzer that is able to provide the relative excess index (λ) from the composition of the exhaust gases.
The main engine characteristics are presented in the table 5.1:

Bore [mm]	83
Stroke [mm]	90.4
IVC [CAD]	-153
EVO [CAD]	124
Number of injector holes (TCRCI)	6
Injector Holes Diameter (μm)	219

Table 5.1: Main Engine Data

Experimental data from twelve operating conditions characterized by different levels of back-pressure, fuel mass and external EGR are available. The first nine points do not have external EGR while the last three have different levels of external EGR. The points without EGR are three sets of 3 points with different values of back pressure. The points with similar back pressures have three different mass of port injected fuel. The main operating parameters of the analyzed points are summarized in the table 5.2.
To have a first validation of the equivalence ratios provided by the Horiba, the filling coefficient is calculated. This coefficient represents the efficiency of the engine filling process, defined as the ratio between the mass of air trapped inside the cylinder and an ideal mass defined as the product between a density and the Cylinder volume.

$$\lambda_v = \frac{m_{tot}}{\rho \cdot V_{Cyl}} \tag{5.1}$$

The density in the definition of λ_v can be the ambient density or the one in the intake port. Since the aim of this analysis is to understand if the equivalence ratio is plausible, it is useless and confusing to add the influence of the air compression. For this reason the density in the intake port is calculated thanks to the temperature and pressure sensors (item 17 in fig 5.1) applying the ideal gases equation.

$$\rho_{boost} = \frac{P_{boost}}{RT_{boost}} \tag{5.2}$$

It is possible to calculate the air mass trapped in the cylinder assuming that the fuel mass is correct (there is no reason to think differently).

$$A = F \cdot \lambda \cdot (\frac{A}{F})_{stoich} \tag{5.3}$$

Operating point	λ_h	IMEP [bar]	Scal. BP [bar]	$m_{PFI}[mg]$	% EGR	$CO_2\%$	$CO\%$	$O_2\%$	$uHC[ppm]$	$NO_x[ppm]$
1	5.048	5.17	0.41	18	0	1.506	0.806	17.72	4027	1.02
2	4.364	7.35	0.43	20	0	2.72	0.28	16.71	2627	0.59
3	4.117	7.94	0.44	21	0	3.04	0.187	16.37	2370	0.5
4	4.118	5.335	0.83	18	0	1.94	1.036	17.06	4456	0.97
5	3.623	7.376	0.88	20	0	3.3	0.35	15.96	3067	0.49
6	3.432	7.961	0.9	21	0	3.69	0.226	15.57	2783	0.63
7	3.922	5.7	1.76	18	0	2.3	0.884	16.71	4213	0.48
8	3.495	7.55	1.82	20	0	3.52	0.294	15.68	2866	0.68
9	3.348	8.058	1.85	21	0	3.84	0.193	15.35	2580	0.78
10	2.836	8.061	1.49	21	0	4.51	0.289	14.36	2875	0.68
11	2.834	8.078	1.48	21	0	4.52	0.288	14.35	2821	0.5
12	2.81	8.097	1.48	21	0	4.58	0.28	14.28	2772	0.46

Table 5.2: Main parameters of experimental operating points

λ is the reciprocal of the equivalence ratio. From the indication of the % of EGR, it is possible to finally calculate the total mass of gas.

$$m_{tot} = \frac{m_{air}}{1 - \%EGR} \tag{5.4}$$

Op. Point	$m_{tot}[mg]$	$\rho_{boost}[kg/m^3]$	λ_v
1	1331	2.098	1.3
2	1278	2.103	1.24
3	1266	2.101	1.23
4	1085	2.137	1.04
5	1061	2.133	1.02
6	1055	2.138	1.01
7	1034	2.129	0.99
8	1024	2.143	0.98
9	1030	2.156	0.98
10	969	2.216	0.89
11	997	2.219	0.92
12	1059	2.241	0.97

Table 5.3: Filling Coefficients

As it is possible to notice from the table 5.3, the points corresponding to the smallest back pressure have values of the filling coefficient too much larger than one and too different from the other ones. This coefficient is not a thermodynamic efficiency and so values bigger than one are not directly a problem and they could be achieved due to dynamic effects.Nevertheless there are no reasons that justify this discrepancy since the engine speed is 2000 rpm and valve timings are equal for all the points. In conclusion the relative air excess indexes of the first three operating conditions are probably overestimated. The next step is to understand if the model used to estimate λ is responsible for this result. The equation used in the exhaust gas analyzer to determine the actual AF ratio derives from the Spindt Equation and it is represented here.

$$\begin{aligned}
\alpha &= CO_2/(CO + CO_2) \\
\beta &= (1.75 * \alpha \cdot HC_{Ratio})/(1 + (2.5 \cdot \alpha)) \\
\chi &= O_2/(CO + CO_2) \\
\delta &= (1 + \alpha + \beta)/2 + \chi \\
\epsilon &= (THC/1000)/4.5/(CO + CO_2) \\
AFR &= \frac{28.97 \cdot 4.77 \cdot \delta}{(1 + 4.5 \cdot \epsilon)(12.011 + 1.008 * HC_{Ratio})}
\end{aligned} \tag{5.5}$$

To understand the terms of this equation it has been analytically determined from the exhaust gases composition following the procedure proposed by N.Coliings [29].

5.1.1 Spindt Equation

The starting point to determine the value of λ is the global chemical equation of combustion normalized with respect to one fuel mole:

$$C_nH_mO_xN_y + \lambda t(O_2 + uCO_2 + vH_2O + wN_2) \rightarrow \\ n_p(X_{CO_2} + X_{CO} + X_{O_2} + X_{H_2} + X_{H_2O} + X_{uHC} + X_{N_rO_z} + X_{N_2}) \quad (5.6)$$

Where t is the number of moles of O_2 required for the complete combustion of 1 mole of fuel ($t = 1 + m/4 - x/2$), n_p is the sum of the exhaust products per fuel mol. Since the actual composition of unburned hydrocarbons is unknown it has been assumed equal to the fuel one, which is iso-octane (IC_8H_{18}) in the considered case. The same consideration is valid for the composition of N_rO_z,which is considered only NO. Being the mass fraction of unburned hydrocarbons much larger respect to the one of NO_x the first assumption is much stronger than the second. The following atom balances for the combustion reaction can be made:

1. Carbon Balance

$$1 + u\lambda\bar{t} = \bar{n_p}(X_{CO_2} + X_{CO} + n'X_{uHC}) \quad (5.7)$$

2. Hydrogen Balance

$$\bar{m} + 2v\lambda\bar{t} = \bar{n_p}(2X_{H_2} + 2X_{H_2O} + \bar{m'}n'X_{uHC}) \quad (5.8)$$

3. Oxygen Balance

$$\bar{x} + \lambda\bar{t}(2 + 2u + v) = \\ \bar{n_p}(2X_{CO_2} + X_{CO} + 2X_{O_2} + X_{H_2O} + \bar{x}'n'X_{uHC} + zX_{N_rO_z}) \quad (5.9)$$

4. Nitrogen Balance

$$\bar{y} + \lambda\bar{t}2w = \bar{n_p}(2X_{N_2} + rX_{N_rO_z}) \quad (5.10)$$

5. The sum of exhaust gases mole fractions must be equal to one

$$\sum X_i = 1 \quad (5.11)$$

6. The reaction equilibrium constant can be considered the water gas shift reaction (WGSR) when the fuel is a hydrocarbon

$$K = \frac{X_{CO}X_{H_2O}}{X_{CO_2}X_{H_2}} \quad (5.12)$$

The barred symbols are normalized respect to the fuel number of carbon atoms (e.g. $\bar{t} = t/n$) and m', n' are the number of hydrogen and carbon atoms in the unburned Hydrocarbon that, for the assumption made, are equal to the one of the fuel.
This system is under-constrained since the set of six equations has five unknowns ($\lambda, X_{N_2}, X_{H_2}, \overline{n_p}, H_{H_2O}$). From this point, different approaches have been developed according to the choice of the equation to neglect. To be consistent with the Horiba

exhaust gas analyzer, the Spindt approach has been followed. The Nitrogen Balance is neglected and proceeding by Gaussian elimination the final algebraic system is obtained:

$$\begin{bmatrix} u & 1 \\ (2+2u+v(1-2\alpha)) & (\bar{x}-\alpha\bar{m}) \end{bmatrix} \begin{bmatrix} \lambda\bar{t}/\bar{n}_p \\ 1/\bar{n}_p \end{bmatrix} = \begin{bmatrix} (X_{CO_2}+X_{CO}+n'X_{uHC}) \\ (2X_{CO_2}+X_{CO}+2X_{O_2}+zX_{N_rO_z}+(\bar{x}'-\alpha\bar{m}')n'X_{uHC} \end{bmatrix} \tag{5.13}$$

where α is:

$$\alpha = \frac{1}{2(1+X_{CO}/KX_{CO_2})} \tag{5.14}$$

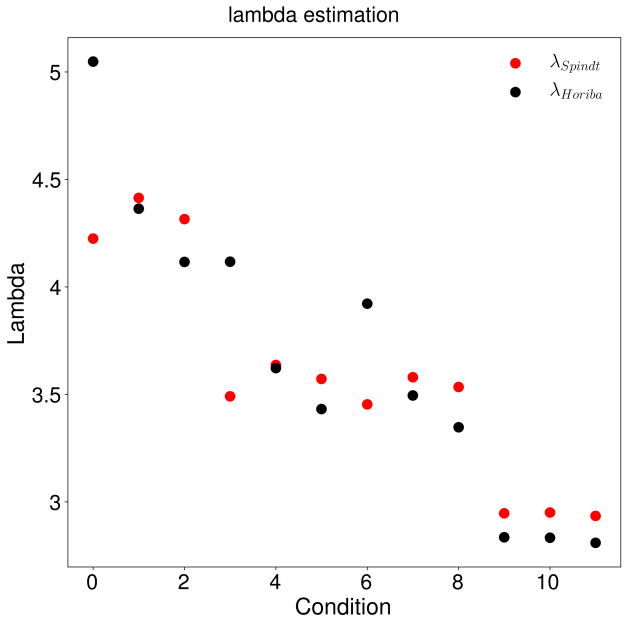

Figure 5.2: Result of study on Lambda

The results of this analysis are shown in the figure 5.2.
There is a good correspondence between Horiba and Spindt values of lambda except for the points with the smaller amount of injected fuel. The discrepancy can be traced back to the strong approximation on the composition of uHC, since these points are characterized by the higher uHC emissions a front of the smaller level of fuel mass. Except for those points, there is a good correlation. In conclusion for the CFD simulations it has been chosen to use the Horiba relative excess of air indexes as starting point and to neglect the operating conditions with the smallest back-pressure, also following the suggestion of the engineer that has worked on the test bench. He suggests that for these points during the overlapping period (when both the intake and exhaust valves are open) a relevant portion of fresh charge can directly flow through the exhaust valve distorting the composition of exhaust gases and therefore the evaluation of lambda.

5.2 Simulations pre-processing

To perform 3D simulations of HCCI combustion is necessary to define the simulation domain, initial conditions and generate the mesh. Being this analysis finalized on the combustion process, only the portion of the cycle when the valves are closed is simulated (closed-cycle simulations). This allows to achieve an evaluation of the gross performances of the engine without the complication of the process of gas exchange. The mixture is considered homogeneous being the fuel port injected; also the temperature is considered constant and so the effects of temperature and mixture stratification between the internal EGR (in order of 7% on the global charge mass) and the fresh charge are neglected.

5.2.1 Mesh

The cylinder geometry has a polar symmetry, therefore only a sector of the cylinder has been simulated using an axi-symmetric mesh and imposing a cyclic boundary conditions to the two symmetrical faces. The mesh has been generated by an au-

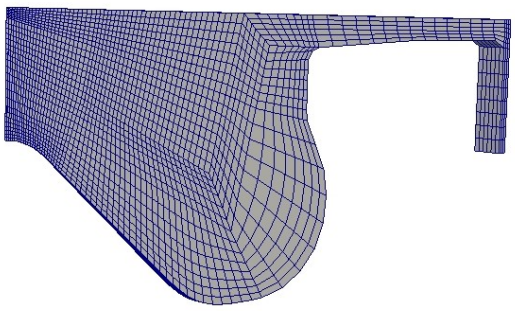

Figure 5.3: HCCI mesh

tomatic Python mesh generator and the cell inclination is suitable to simulate the fuel injection. The injection orientatied mesh shows improvement respect to perfect Cartesian mesh in terms of better prediction of spray distribution and flame structure [30]. This has been done to simulate also the TCRCI case with the same mesh configuration. The sector angle considered is 3° and the mesh is composed of 12324 cells (fig 5.3).An automatic mesh motion technique is used to accommodate the displacement of internal grid points according to the prescribed boundary motion.

5.2.2 Initial Conditions

The first step is the definition of the initial conditions at Inlet Valve Closing (IVC) in terms of pressure, temperature, equivalence ration and flow field. The pressure at IVC is known being available the experimental pressure trace; at first the λ value is set equal to the one of Horiba.

Following the same procedure previously explained in this chapter (equation n 5.4) the total in-cylinder mass is known and so the temperature at IVC is known too:

$$T_{IVC} = \frac{P_{IVC} V_{IVC}}{m_{tot} R} \tag{5.15}$$

The wall temperatures have been set to 450 K for the cylinder head, 475 K for the piston and 400 K for the crevices and liner region. The mixture composition is automatically determined by a libICE utility from an user input value of equivalence ratio and the ambient composition defined in table. Moreover, the flow field is set from the swirl ratio and the so called swirl profile, which defines the velocity profile in the plane orthogonal to the cylinder axis. The ambient composition has been determined in two different ways for the cases with and without EGR. For the operating conditions without external EGR it has been assumed from GT-Power simulation carried on by the industrial parter and it is reported in the table 5.4:

$Y_{O_2} = 0.225$
$Y_{CO_2} = 0.0031$
$Y_{H_2O} = 0.0012$
$Y_{N_2} = 0.77$

Table 5.4: ambient composition

For the cases with external EGR, it has been necessary to implement an iterative procedure to define the initial composition, since using the the GT-Power composition, the in-cylinder fuel mass differs from the experimental one.

Iterative cycle

As starting point the composition of exhaust gases ($bgas_0$) is computed from a complete combustion reaction carried on with fresh air and the fuel fraction corresponding to λ_H (using a constant pressure homogeneous reactor and assuming the fuel as Iso-Octane). The ambient composition considering the external EGR is then:

$$\begin{aligned} amb_k &= m_{air}(1 - \%EGR) + b_{gas,k-1}(\%EGR) \\ Y_{amb,i} &= Y_{i,air}(1 - \%EGR) + Y_{i,bgas}(\%EGR) \;\; i = H_2O, CO_2, O_2, N_2 \end{aligned} \tag{5.16}$$

The stoichiometric air/fuel ratio for the new mixture is computed:

$$\alpha_{st,k} = \frac{(n + m/4)[\sum_{i=1}^{N_s} \frac{Y_{i,amb}/W_i}{Y_{O_2,amb}/W_{O_2}} \cdot W_i]}{W_{fuel}} \tag{5.17}$$

defining the fuel as $C_n H_m$ and being W the molecular mass.

The next step is to define the in-cylinder mixture composition always with λ_H:

$$\begin{aligned} n_{fuel,k} &= 1 \\ n_{O_2} &= \lambda_H \cdot (m + \frac{n}{4}) \\ n_{i,k} &= \frac{Y_{i,amb}/W_i}{Y_{O_2,amb}/W_{O_2}} \cdot W_i \\ n_{tot,k} &= n_{fuel,k} + n_{O_2} + \sum_{i=1}^{N_s} n_{i,k} \\ x_{i,k} &= n_{i,k}/n_{tot,k} \end{aligned} \tag{5.18}$$

The complete combustion reaction is calculated using the mixture composition just determined. The new ambient composition with EGR is calculated $amb_k, Y_{amb,k+1,i}, \alpha_{st,k+1}$. The error is on the stoichiometric air fuel ratio on α_{st}:

$$err_{k+1} = |\frac{\alpha_{st,k+1} - \alpha_{st,k}}{\alpha_{st,k+1}}| \tag{5.19}$$

The cycle is stopped when $err < 5\%$. This procedure allows to have a simulate fuel mass equal to the experimental one.

5.2.3 Combustion Model and Table Generation

The combustion model used is Tabulated Well Mixed (TWM): each cell is considered as a homogeneous reactor with no interaction between chemistry and turbulence. The reference fuel used to represent commercial gasoline is Iso-Octane (IC_8H_{18}). The chemical mechanism used is Creck [31] that consists of 156 chemical species and 3465 reactions and it is suitable to represent gasoline like fuels. The input parameters chosen for the table generation are recalled in the table 5.5, they are a trade off between accuracy and computational time. A large number of equivalence ratios are useless for the single simulation being the mixture homogeneous but it is made to perform a large number of cases with the same table. The initial temperatures for homogeneous reactor calculations do not include fuel evaporation and mixing-line effect since no direct injection is present.

Pressure	20,40,50,60,70,80 90,100,110,120,130,140, 150
T [K]	400,450,500,550,600,650,700,750,800,850 900,950,1000,1050,1100,1150,1200,1250
ϕ	0,0.1,0.2,0.24,0.25,0.26,0.27 0.28,0.29,0.31,0.33,0.35,0.4,1e15

Table 5.5: Input parameters for table generation

5.3 Simulation Results

In this section the results of the simulations are presented; the cases analyzed are number five, eight,eleven and twelve of the table 5.2. These operating conditions have been chosen to consider different back-pressures and to evaluate the effects of EGR. The simulated thermodynamic conditions set at IVC for the cases without EGR are shown in the table 5.6:

Op. Point	λ	$T_{IVC}[K]$	$P_{IVC}[MPa]$
5	3.44	385	234000
6	3.28	385	234000
8	3.4	385	234000

Table 5.6: Simulated initial conditions

The relative air excess indexes have been slightly decreased respect to the experimental ones to increase a little the temperature at IVC since the start of HCCI combustion is widely influenced by it. The results represented in fig 5.4 show that the model can correctly predict the experimental results in all the analyzed conditions both in term of pressure trace and heat release rate.
In particular, the cool flames occurring around $-20CAD$ are overestimated by Creck chemical mechanism. This drawback is balanced by the prediction of the main injection; in this phase, the model correctly captures both the start of the main combustion and the peak of heat release rate. Also small variations of experimental cases apparent heat release rate at the end of the main combustion ($\sim 15\ CAD$) are well captured by the model.
The overestimation effect of cool flames apparent heat release rate affects also the evaluation of the cumulative ahrr between the cool flames and the main injection. The overestimation of the cumulative apparent heat relase at the end of combustion is the sum of two effects.
Firstly the experimental cases combustion efficiency is smaller than the simulations one (table 5.7). Combustion efficiency is defined as:

$$\eta_c = \frac{CO_2}{CO + CO_2} \tag{5.20}$$

This definition takes into account only the charge portion that actually reacts, therefore a second effect is added.

Op. Point	$\eta_{c,exp}[\%]$	$\eta_{c,sim}[\%]$
5	90.45	94.5
6	94.22	96.03
8	92.29	95.05

Table 5.7: Combustion Efficiency

The second effect, that is the most relevant, is that the charge portion that does not react at all is much larger in the experimental cases.

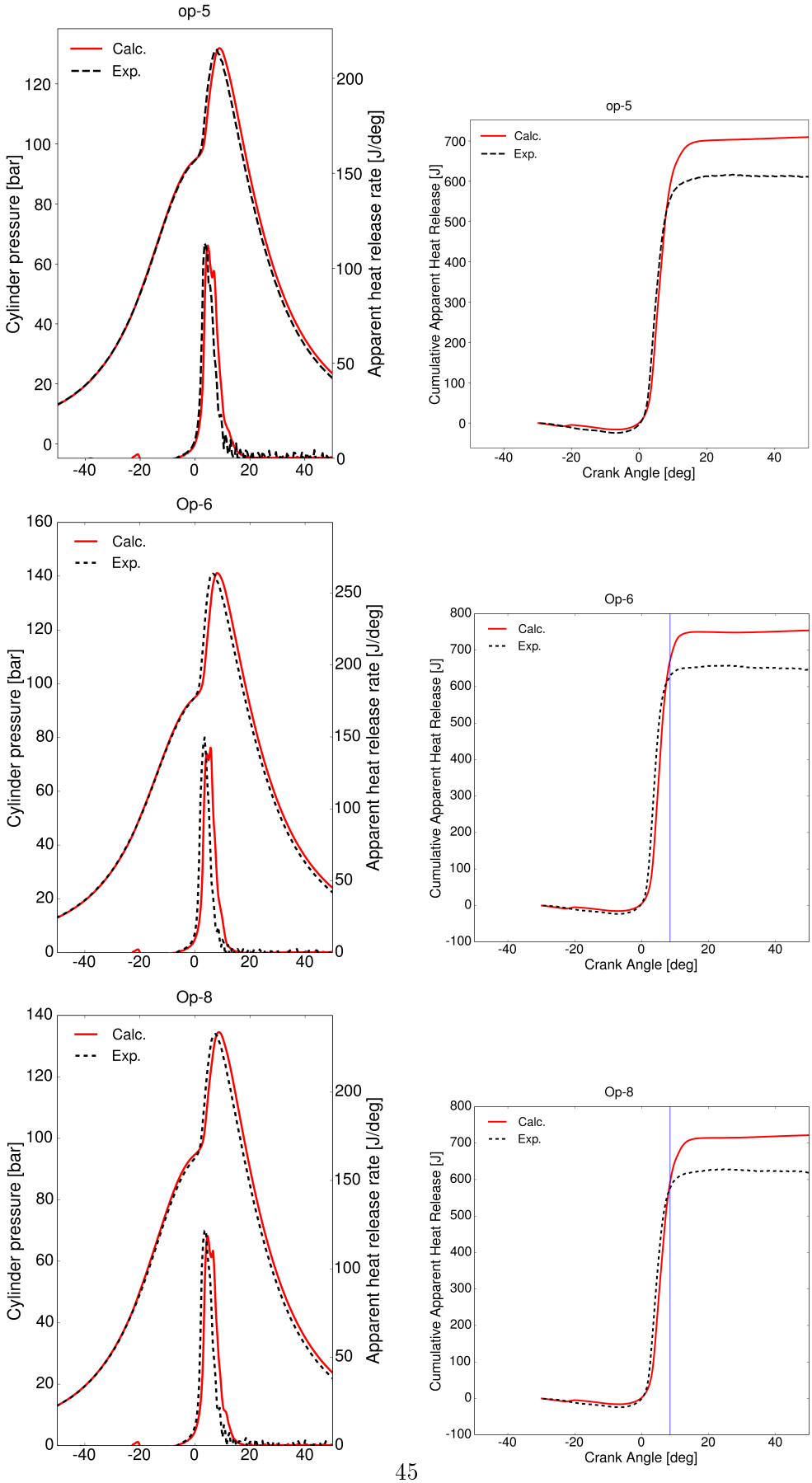

Figure 5.4: Comparison of pressure and roHR between simulation and experimental in HCCI cases

It can be noticed by the mass fraction of uHC at exhaust valve opening presented in the table 5.8, defined as:

$$Y_{uHC,dry} = Y_{IC_8H_{18},dry} + Y_{C_2H_2,dry} + Y_{CH_2O} \tag{5.21}$$

Op. Point	$uHC_{exp}[ppm]$	$uHC_{sim}[ppm]$
5	3067	130.4
6	2783	108.7
8	2867	127.5

Table 5.8: uHC emissions

This correlation is clearer considering that the ratio between the experimental mass fraction of uHC at EVO and the fuel mass fraction at IVC (assumed equal to the simulated one) is almost the reciprocal of the ratio between the experimental and simulated cumulative apparent heat release at EVC (table 5.9). Therefore, the overestimation is mainly due to a portion of the charge that does not react at all in the test bench engine.

Op. Point	$1 - \frac{Y_{uHC}}{Y_{IC8H18,IVC}}$	$\frac{cahrr_{EVO,exp}}{cahrr_{EVO,sim}}$
5	0.855	0.862
6	0.77	0.82
8	0.845	0.85

Table 5.9: uHC emission

A graphical post-processing has been carried on in the next section to understand the reasons of these results. As regards the cases with external EGR the ambient composition is evaluated with the iterative process previously described. The ambient compositions of the operating conditions analyzed are presented in the table 5.10:

Op. Point	% EGR	Y_{O_2}	Y_{CO_2}	Y_{H_2O}	Y_{N_2}
11	18	0.21	0.019	0.09	0.762
12	12	0.216	0.014	0.06	0.7635

Table 5.10: EGR operating points ambient composition

The simulated initial conditions at IVC are shown in the table 5.11:

Op. Point	λ	$T_{IVC}[K]$	$P_{IVC}[MPa]$
11	3.1	395	241000
12	3.22	390	241000

Table 5.11: EGR cases initial conditions

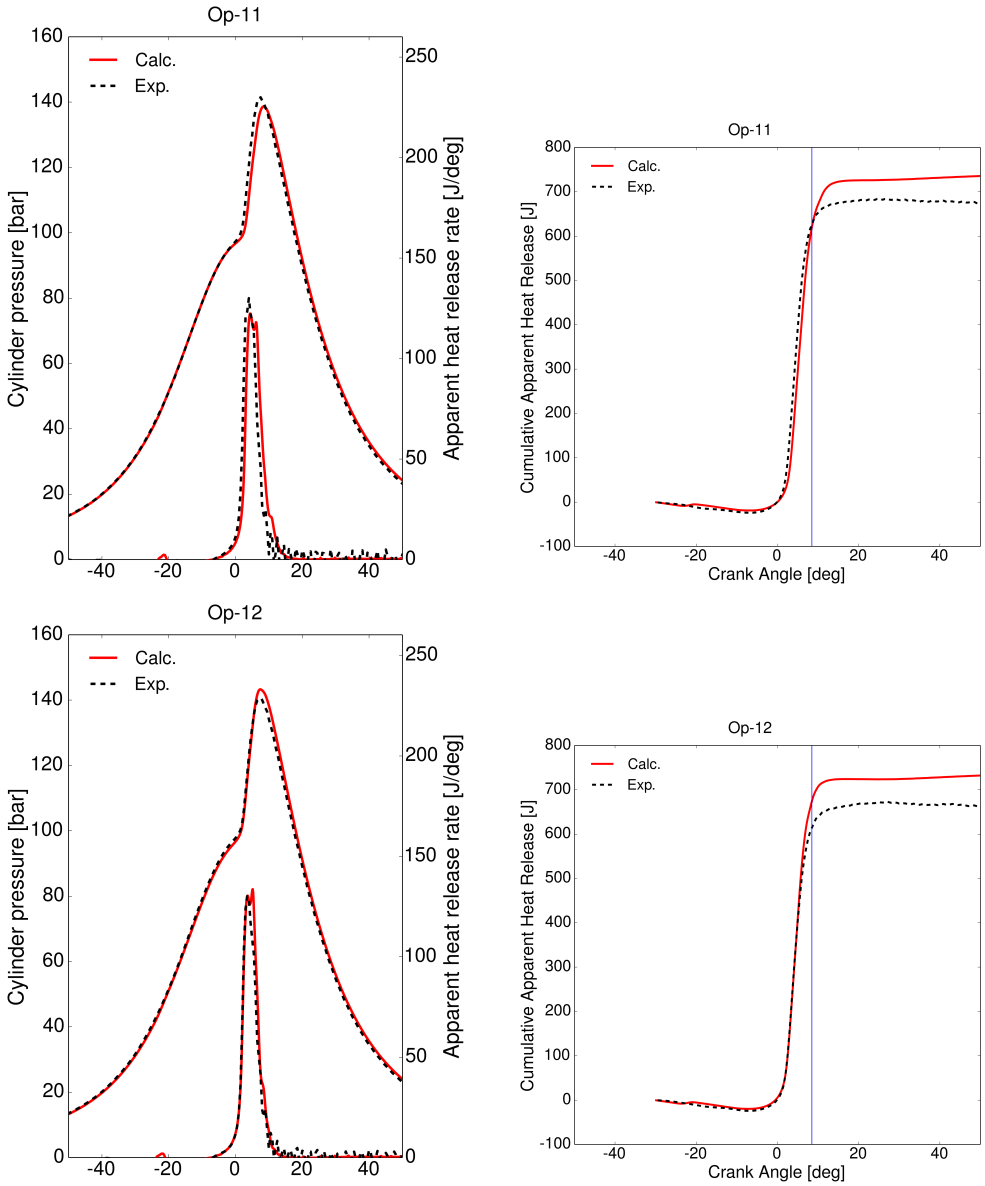

Figure 5.5: Comparison between simulation and experimental results cases with external EGR

The results in terms of pressure trace ,heat release rate and cumulative apparent heat release are presented in the figures 5.5. They show the same characteristics of the cases without EGR, therefore the analyses previously made are still valid.
In conclusion, the CFD simulations correctly predict the engine behavior in a wide range of operating conditions and they can be used to study the effect of the engine parameters like the piston head geometry. In conclusion to this section, the most important simulated performance and combustion parameters of these operating points have been tabulated in the table 5.12:

Op. Point	GIE [%]	GIMEP [Bar]	MFB10 [CAD]	MFB50 [CAD]	$\frac{dP}{dt}_{max}$	CD
5	44.42	8.18	2.2	6.1	1.69	9.15
6	45.2	8.76	2	5.35	2.2	7.4
8	44.66	8.34	2.15	5.9	1.82	8.6
11	44.25	8.46	2.05	5.65	1.89	8.2
12	44.36	8.44	1.35	4.7	2.11	7.3

Table 5.12: Performance and combustion parameters simulated HCCI operating conditions

The number after Mass Fraction Burned (MFB) stands for its percentage, for example MFB10 is the Crank angle degree where ten percent of the mass fraction is burned. It is a indicator of the combustion evolution. MFB10 is assumed as the start while MFB90 the end of combustion, therefore the Combustion Duration (CD) is calculated as (CD = MFB90-MFB10). Since in the cases with EGR the oxidizer (O_2) percentage in the ambient composition is lower, it has been necessary to increase the equivalence ratio compared to the cases without EGR to achieve similar GIMEP.
In the next section, a deeper analysis of the combustion process is performed.

5.3.1 Study on Combustion Process

The evolution of the combustion is well represented by the evolution of normalized progress variable. As explained in the section of the combustion model it represents the progress of combustion in a range between zero and one, where zero represent the initial condition and one the complete combustion. In the fig 5.10 is represented the evolution of this parameter between zero and 11 CAD of the operating point number five; the period chosen includes all the main combustion processes since 11 CAD is beyond MFB90 and therefore the combustion can be considered completed. Note that the color mapping scale is logarithmic to highlight the first stage of combustion and the points where combustion is not complete.
The first characteristic to notice is that the cool flames do not produce a significant increase of the progress variable. The main combustion starts in the center of the piston bowl, that is the region further away from the walls and so it is characterized by the higher unburned gases temperature, as illustrated in the fig 5.6 .
The heat released by the combustion in the piston bowl area ignites the rest of the

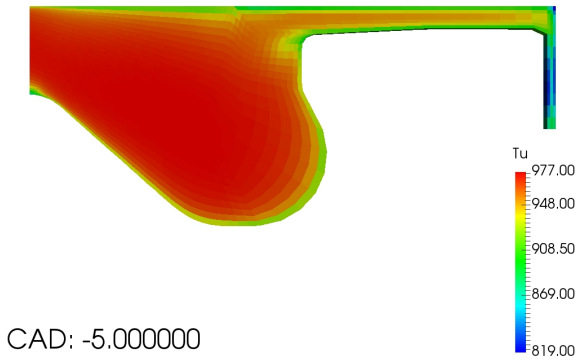

Figure 5.6: Unburned Charge Temperature -5 CAD

combustion chamber. Regarding the CO emissions, they are mainly concentrated in the squish region near the cylinder wall, where the combustion is not complete (fig 5.7). The reason is that this region has a very large surface volume ration and a small height, therefore it is characterized by a large heat exchange with the walls and large thermal boundary layer. This entails lower unburned gas temperature that hinders the combustion promoting CO and uHC emissions. This behavior was already understood by Vressner [12] and it can explain the higher pollutant emission of the experimental cases respect to the simulations. It is plausible to assume that experimentally the in-cylinder temperature at IVC is not homogeneous but it is stratified due to the presence of a sack of internal EGR at the bottom of the piston bowl. The difference of temperature between the bowl and the squish area is more pronounced and the combustion has more difficulties to penetrate in the squish region.

The crevices are also responsible for uHC emissions since they are characterized by an elevate heat exchange with the walls that does not allow to ignite the mixture. These results show that the diesel combustion chamber geometry is not ideal for

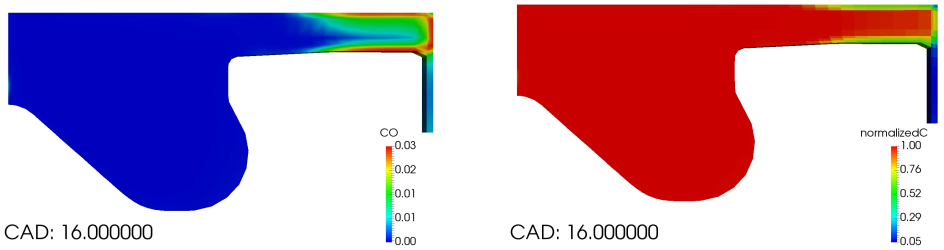

(a) *CO mass fraction at 16 CAD* (b) *Normalized Progress Variable at 16 CAD*

Figure 5.7: Uncomplete combustion region

premixed combustion.

5.3.2 Combustion Turbulence interaction

As suggested by Vressner [12] (section 3.1.2) an important role on HCCI combustion is played by the interaction between combustion and turbulence. For this reason,this effect is deeply discussed in this section.
When combustion starts in the piston bowl, the increase of temperature and the consequent expansion of the burning gaseous charge causes a motion of the unburned charge from the piston bowl to the squish volume. The small squish height leads to an increase of the flow velocity and turbulence. This behavior is represented in the figures 5.8. The color map is the map of normalized progress variable and the

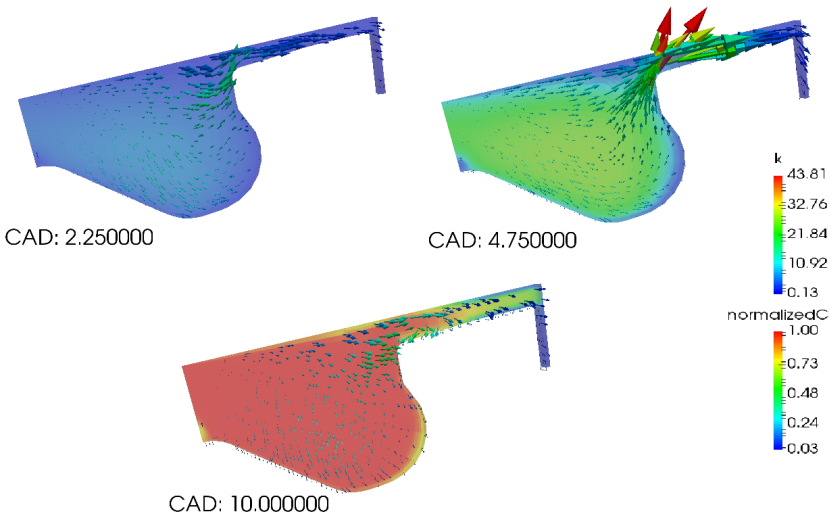

Figure 5.8: Combustion turbulence interaction

vectors represent the velocity field.

The dimension of the vectors is scaled according to the magnitude of the velocity while the color represents the magnitude of the turbulence kinetic energy. This process causes the second peak of the turbulent kinetic energy average between MFB10 and MFB90 (fig 5.9).

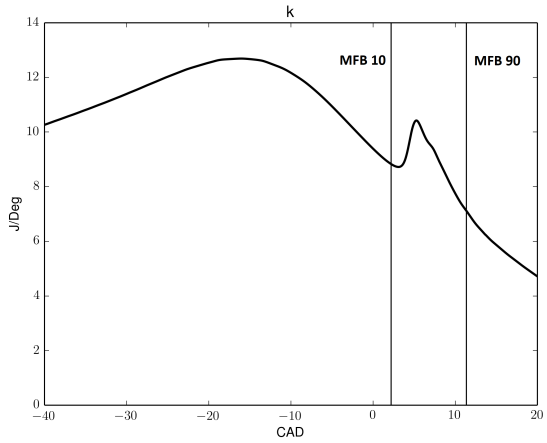

Figure 5.9: Avarage turbulence kinetic energy evolution

In the next chapter starting from the achieved conclusions and previous works, the piston head influence will be discussed and new geometries proposed.

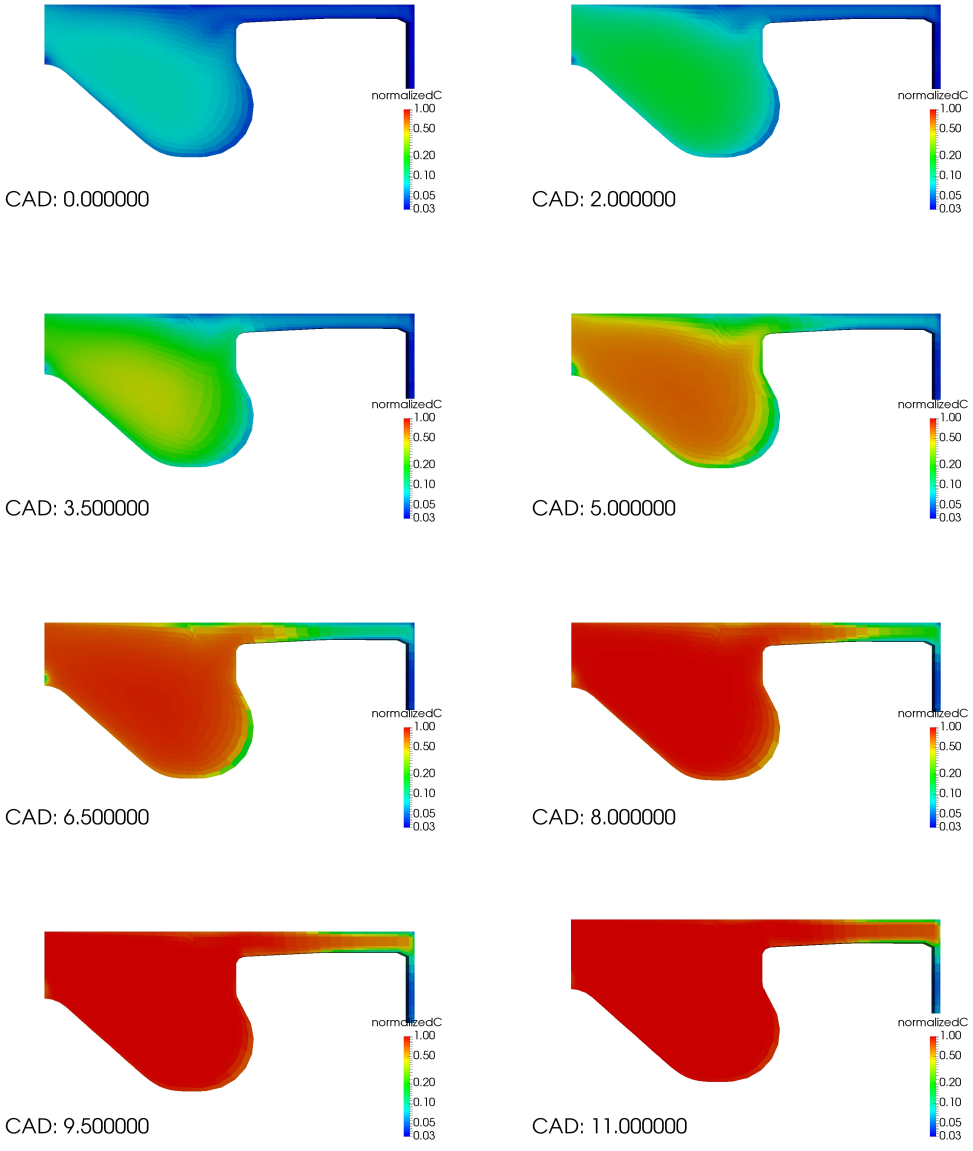

Figure 5.10: Normalized progress value evolution

Chapter 6

HCCI Piston Design

In this chapter different piston geometries are studied to understand which parameters have the greatest influence on the combustion process and a new piston design is proposed based on the achieved conclusions. The volume of the combustion chamber at TDC has been kept constant for all the proposed geometries to preserve the original compression ratio.

6.1 Square Bowl

The square bowl is the first analyzed piston head. In the previous study [12], this type of geometry allowed to have slower combustion keeping the same thermal efficiency with respect to a flat piston. This allows to have a smaller $\frac{dP}{dt}_{max}$ and therefore the possibility to increase the load. In this chapter a comparison between this geometry and the original diesel one has been conducted. The quotes have been scaled respect to the ones proposed in the literature according to the variation of the bore and to keep the compression ratio equal to the original engine. Also the squish height has been kept equal to the Diesel one (fig 6.1). It is important to notice that the two

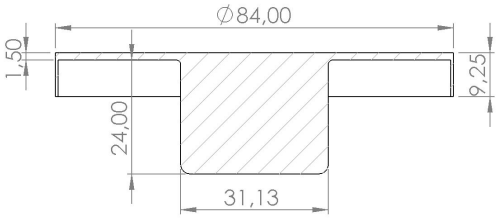

Figure 6.1: Square bowl piston quotes

geometries have different squish ratio, defined as:

$$S_r = \frac{A_s}{\pi * b^2/4} \tag{6.1}$$

In particular the square combustion chamber has a larger squish ratio than the original one (table 6.1) :

	$S_r\%$
Square Bowl	82.5
Diesel Bowl	73.2

Table 6.1: Squish Ratio

6.1.1 Mesh

Since this geometry is not axis-symmetric, it has been necessary to simulate a quarter of the cylinder. The mesh is made of 164700 cells (fig 6.2). A Cartesian mesh has been adopted since a direct injection is not foreseen for this study.

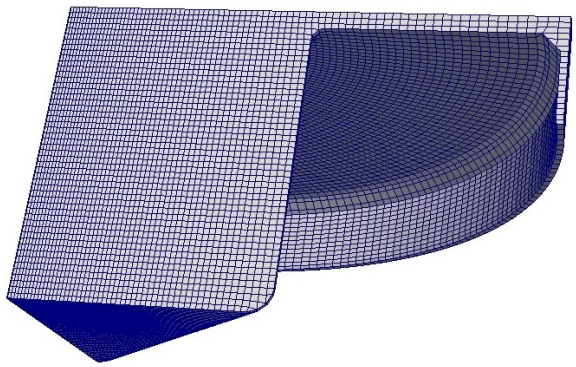

Figure 6.2: Square bowl piston mesh

6.1.2 Simulation Results

The simulations performed are based on the operating point number five, which initial conditions are recalled in the table 6.2:

Op. Point	λ	$T_{IVC}[K]$	$P_{IVC}[MPa]$
5	3.44	385	234000

Table 6.2: Initial Condition operating point five

The results of this case show that the square piston can decrease the pick of heat release rate compared to the original one, while the ignition timing is kept constant. As a consequence also the peak of pressure and pressure rise rate are decreased. The reasons for this behavior are found in the higher combustion generated turbulence for the square bowl (fig 6.3) and in the larger squish volume, where the combustion rate is lower as consequence of a larger heat exchange with the walls.
This geometry has although two drawbacks. Firstly the heat exchange is bigger because it is characterized by a larger surface volume ratio; secondly, it shows higher CO emissions and lower combustion efficiency as a consequence of a larger squish

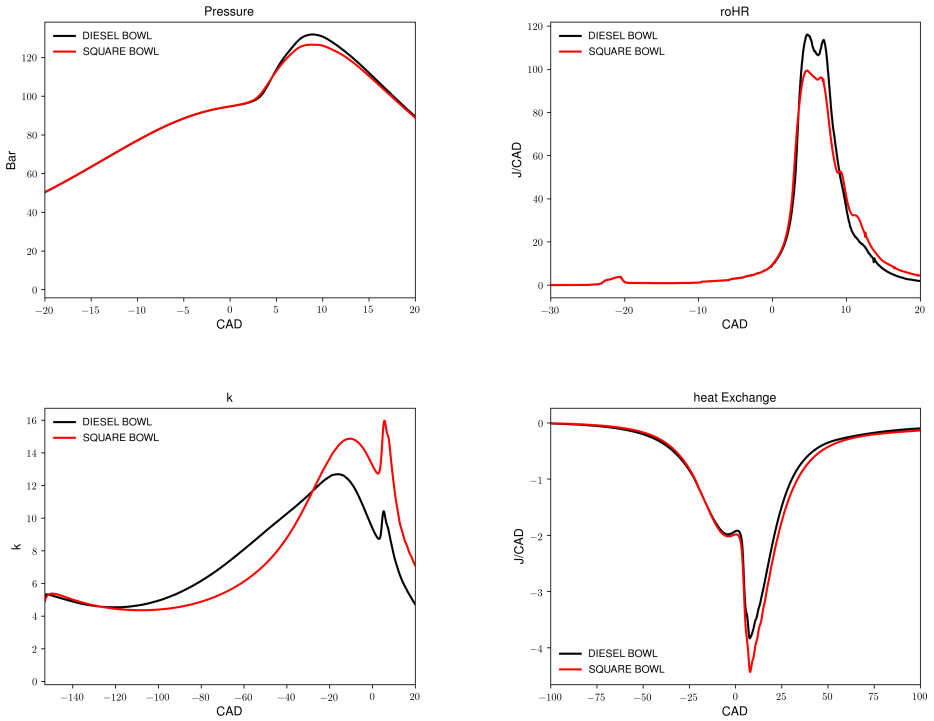

Figure 6.3: Square bowl piston results

volume. The sum of these effects leads to a decrease of GIE in the square bowl case, as shown in the table 6.3.

	Diesel Bowl	Square Bowl
GIE [%]	44.42	43.77
Tot. Heat E. [J]	-150	-164
MFB10 [CAD]	2.2	2.15
MFB50 [CAD]	6.1	6.35
$\frac{dP}{dt}_{max}$	1.69	1.4
CD [CAD]	9.15	11.25
η_c	94.49	93.71

Table 6.3: Comparison of Square and Diesel Bowl results

6.1.3 Influence of bowl geometry and Squish Ratio

Since in the previous analysis both bowl geometry and squish ratio vary, it is necessary to separate the two effects to understand their influence. For this reason, three new piston designs have been implemented. The first one is a new square bowl with the same squish ratio as the Diesel one; the bowl height has been decreased to keep the combustion chamber volume constant. Two piston heads characterized by a cylinder bowl with two different squish ratios have been also designed. The new pistons are shown in fig 6.4.

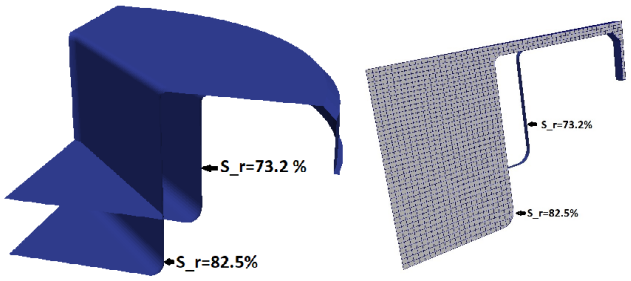

Figure 6.4: Further simulated piston bowls

The results (table 6.4) show that the engine behavior is very close for the different piston geometries when the squish ratio is kept constant and equal to the original diesel piston head. As a result the most effective parameter is the squish ratio. The reason is that this parameter controls the dimension of the squish volume, that is the most critical for the combustion propagation. The piston bowl geometry alone affects mainly the total heat exchange and the intensity of combustion generated turbulence since it influences the evolution of the flow field and the walls surface volume ratio. The square bowl shows a little earlier ignition that anticipates the combustion increasing a little the efficiency; the other differences are well inside the numerical error.

	Diesel Bowl	Square Bowl	Cylinedr Bowl
GIE [%]	44.42	45.11	44.53
Tot. Heat E. [J]	-150	-155.5	-154
MFB10 [CAD]	2.2	1.95	2.2
MFB50 [CAD]	6.1	5.75	6.15
$\frac{dP}{dt}_{max}$	1.69	1.75	1.66
CD [CAD]	9.15	9.4	10
η_c	94.49	95.3	95

Table 6.4: Results Different Bowl geometry squish ratio equal to 0.732

6.2 RCCI optimized Piston Design in HCCI simulations

The geometry proposed in this section is close to a flat piston geometry and it has been optimized for RCCI combustion; as a consequence, it will be probably more effective for TCRCI combustion since the presence of fuel stratification. However, it is interesting to understand its behavior in a pure HCCI case and with a homogeneous mixture. Due to its similarity with a flat piston, the expected behavior is a fast combustion with a large ignition region. The geometrical quotes have been modified with respect to the reference one [20] to keep the volume equal to the original diesel combustion chamber (fig. 6.5).

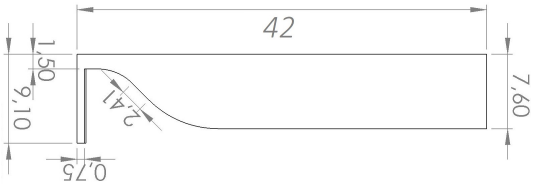

Figure 6.5: RCCI optimized piston quotes

6.2.1 Mesh

The mesh is pure Cartesian utility and covers a sector of 5° (fig. 6.6).

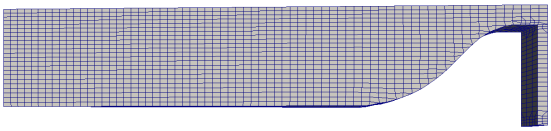

Figure 6.6: RCCI optimized piston mesh

6.2.2 Simulation Results

This first analysis has been carried on the basis of the operating point number five. The main ignition starts around 1 CAD in a large portion of the combustion chamber and rapidly spreads all over.
The combustion is very quick since almost all the mixture ignites simultaneously as shown in the figure 6.7, as a consequence the peaks of heat release rate and pressure rate are much larger in comparison to the case with a diesel piston (fig. 6.8). This behavior limits the potentiality at high load operating points. The positive effect of this geometry is that the CO emissions are much smaller since the combustion efficiency is high all over the cylinder.
This new geometry shows a significant increase of the Gross indicated efficiency (table 6.5). The reasons are the faster combustion that closes the cycle to the ideal Otto and the much smaller total heat exchange due to the much smaller wall surfaces

	Diesel Bowl	Square Bowl
GIE [%]	44.42	46.37
Tot. Heat E. [J]	-150	-135.8
MFB10 [CAD]	2.2	1.7
MFB50 [CAD]	6.1	4.95
$\frac{dP}{dt}_{max}$	1.69	3.02
CD [CAD]	9.15	5.7
η_c	94.49	95.6

Table 6.5: Comparison results Diesel and Optimized RCCI Bowl

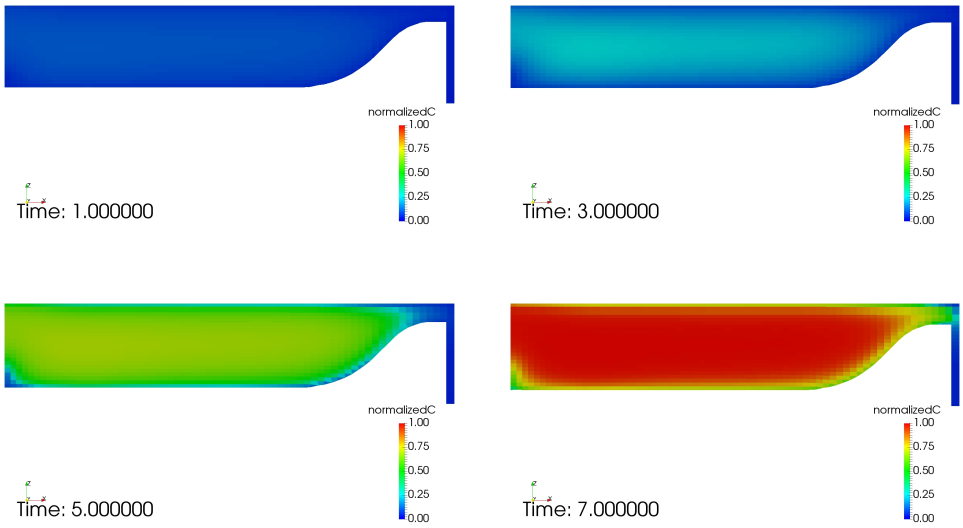

Figure 6.7: Evolution of normalized progress Value for RCCI piston bowl

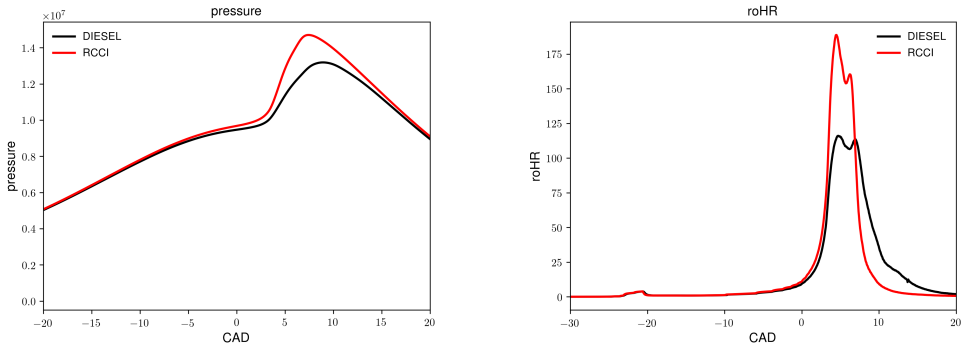

Figure 6.8: Results of RCCI CC simulations

6.3 Optimized HCCI Design

The effects of the squish volume have been understood from the previous sections:

- The presence of a combustion generated turbulence slows down the combustion respect to a flat piston, the larger is the squish ratio the larger will be the combustion duration.
- An increase of CO and uHC emissions as consequence of the presence of a volume characterized by a small height and a large surface volume ratio where the combustion efficiency is low.

A possible optimized solution for this type of combustion has been proposed in this chapter (fig 6.9). The idea behind is to preserve the combustion generated turbu-

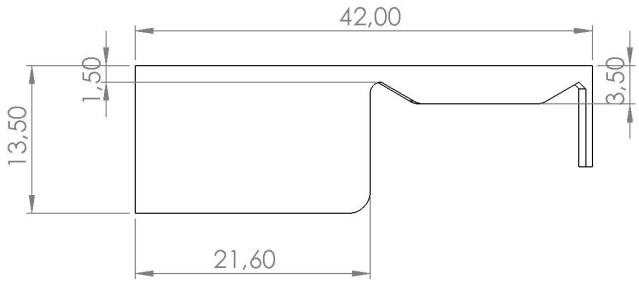

Figure 6.9: HCCI optimized piston

lence keeping a restriction at the end of the piston bowl, which height is equal to the squish height of the previous geometries. The squish height is linearly increased till 3.5 mm after the restriction, in this way the ratio between the thermal boundary layer and the squish height significantly decreases and the average and maximum unburned temperature in this region increases. This is made to enhance the combustion efficiency of the squish volume and to decrease pollutant emissions. The effect of this design on the unburned charge temperature in the squish volume is illustrated in fig 6.10, which represents the comparison between the evolution of Unburned gas temperature along with the squish height for the HCCI Optimized piston and the original Diesel one. The effect of the presence of a second volume almost separated

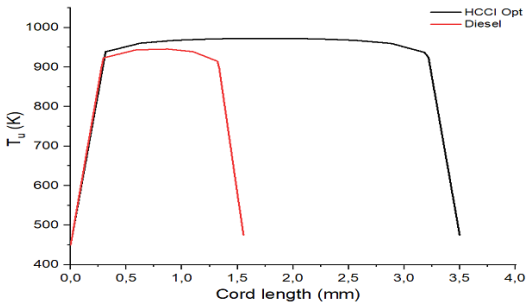

Figure 6.10: Tu evolution along squish height

from the bowl generates a sort of post-combustion that starts after the main one in the expansion stroke as shown by the evolution of the normalized progress variable

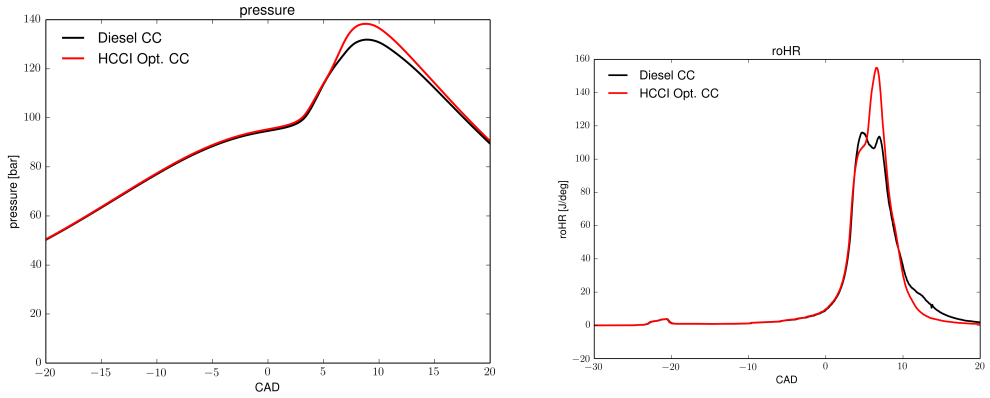

Figure 6.11: Results of HCCI piston bowl

in fig 6.12. The benefits of this behavior compared to Diesel piston bowl are multiple (the results shown in table 6.6 are based on op. point n. 5); firstly the combustion efficiency in the squish volume increases and as consequence, the CO emissions are reduced by 20%. Secondly, the increase of the maximum rate of pressure rise is limited to 11% even if the increase of the peak of roHR is 33% (fig. 6.11). The reason of this behavior is that the peak of the rate of heat release occurs concurrently with the post combustion, which is delayed in the expansion stroke.

	Diesel Bowl	HCCI optimized piston
GIE [%]	44.42	45.5
Tot. Heat E. [J]	-150	-149.5
MFB10 [CAD]	2.2	2.15
MFB50 [CAD]	6.1	6.05
$\frac{dP}{dt}_{max}$	1.69	3.02
CD [CAD]	9.15	7.25
η_c	94.49	95.6

Table 6.6: Comparison results of operating point n.5 between Diesel and Optimized HCCI piston

From the point of view of the turbulence generated combustion, this design adds to the effect of the fresh gas flow in the squish volume consequent to the start of combustion in the main chamber an opposite effect consequent to the secondary ignition; the sum of them leads to a much larger turbulence production.

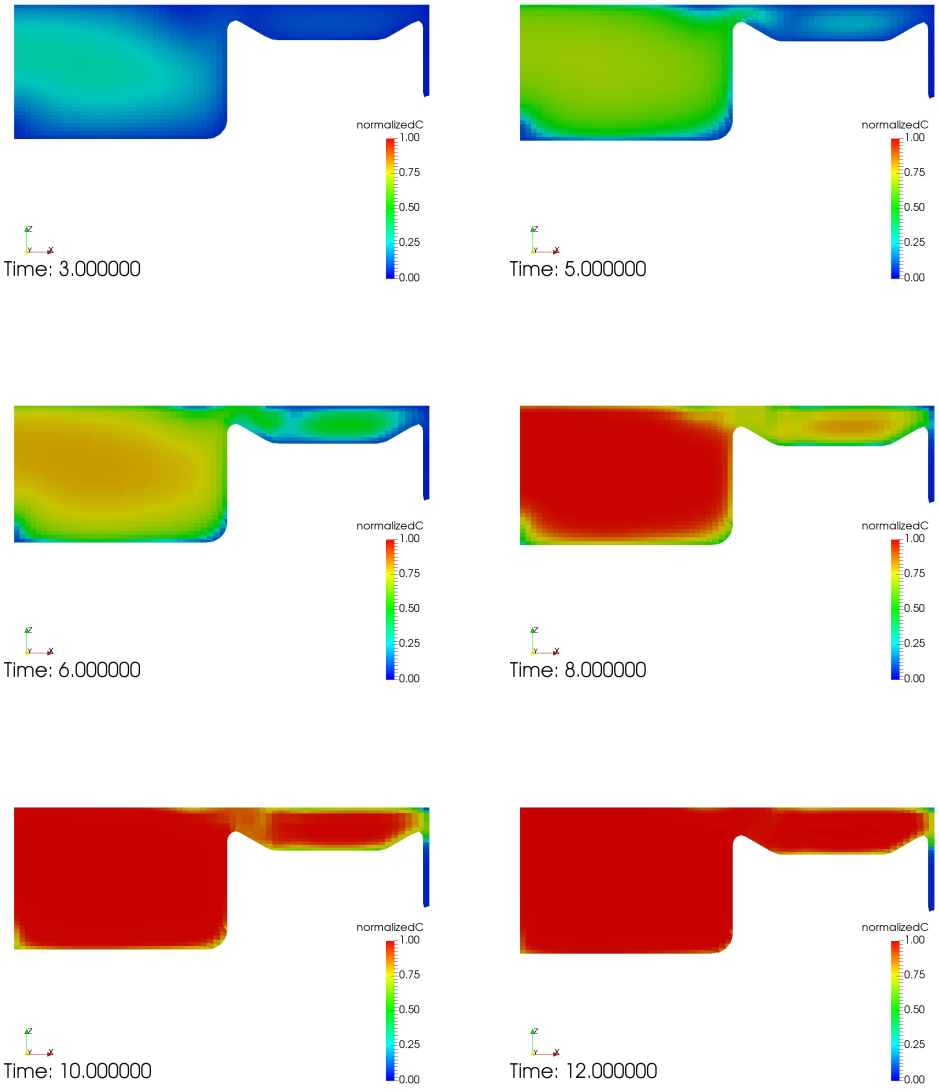

Figure 6.12: Evolution of normalized progress value in HCCI optimized piston

6.4 Different piston designs behavior at different operating conditions

The results achieved in the previous sections have been deducted for a single operating point. As consequence, it is necessary to extend the analysis to different values of equivalence ratio, temperature and pressure at IVC to understand the piston geometry influence on the engine behavior in a wider range of operating conditions. It has been decided to limit the analysis to three designs: original Diesel Geometry, optimized HCCI piston and optimized RCCI piston. The choice has been made to consider geometries that limit the CO emissions and optimize the Gross indicated efficiency, the geometries with larger squish ratio have been neglected for this reason. The results of this analysis have been summarized by three engine parameters:

1. $\frac{dP}{dt}_{max}$: this index is taken in consideration to understand the propensity of the geometry to operate at high loads, since it is correlated to the knock tendency.

2. GIE: this parameter is important to understand the work that is possible to achieve given the same fuel mass.

3. CO emissions: as already explained the most critical pollutants in HCCI combustion are CO and uHC since the combustion efficiency tend to be smaller than conventional compression ignition combustion. Only CO is considered in this study since the trends of CO and uHC are similar.

The starting point of this analysis is the operating point number 5, from this base one initial condition at a time has been changed till the range summarized in the table 6.7 has been covered:

λ	3 ,3.22,3.44,3.85,4
$P_{IVC}[Bar]$	1.94,2.34,2.74
$T_{IVC}[K]$	380,385,390

Table 6.7: Initial conditions variation

6.4.1 Variation of equivalence Ratio

The variation of the equivalence ratio has been made keeping constant the pressure and temperature at IVC. This parameter affects the engine load since it defines the fuel mass. λ has been varied from 3 to 4, the bottom value has been chosen since both RCCI and HCCI optimized piston exceed the threshold of $\frac{dP}{dt}_{max}$; the top one has been chosen equal to 4 to avoid misfiring. The optimized HCCI and RCCI geometries show benefits in terms of CO emissions and GIE with respect to the Diesel one, especially in the leaner operating points; the reason is that the combustion efficiency inside the squish volume drops leaning the mixture. This effect can be noticed looking at Diesel bowl heat release rate evolution to vary the value of λ (fig 6.13); in the richer condition, the shape is almost equal to the one of HCCI optimized geometry (fig 6.11), this suggests that the mixture is reactive enough to have an effective combustion also in the squish volume. The drop of combustion efficiency in the Diesel combustion chamber for the leanest mixtures causes relevant CO and

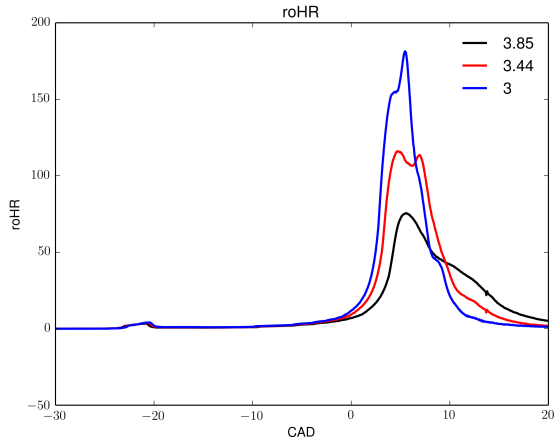

Figure 6.13: Variation of roHR with lambda

uHC emissions. It is interesting to notice how the GIE for the HCCI Optimized bowl tends to stabilize at 45.5 % decreasing the relative excess of air index. A band of $\frac{dP}{dt}_{max}$ between 3.6 and 7 $\frac{MPa}{ms}$ has been considered as a possible intermediate knock condition since the threshold value is not unique. The combustion in RCCI cases is always stepper, while HCCI and DIESEL piston bowls have almost the same values of $\frac{dP}{dt}_{max}$ for λ between 3.44 and 4; for richer mixture, the steepness of HCCI optimized piston combustion tend to be higher. Nevertheless high load limits for these two pistons are similar.The results are summarized in the figure 6.14.

6.4.2 Variation of Initial Temperature

The temperature variation has a double effect; firstly the in-cylinder mass decreases when the temperature increases, secondly the ignition delay decreases and the start of combustion is anticipated when the temperature increases, as shown in the equation 1.2. These two effects conflicts from the point of view of the rate of pressure rise. For all the piston designs there is almost a linear correlation between T_{IVC} and $\frac{dP}{dt}_{max}$; the RCCI Piston bowl has always a higher value of this parameter also in this case. The emissions of CO tend to become closer between the different geometries increasing the temperature firstly because combustion is anticipated and therefore the maximum in-cylinder temperature is higher, secondly because the charge temperature in the squish region is higher. This affects also the evolution of the GIE (fig 6.14). The results are summarized in the figure 6.14.

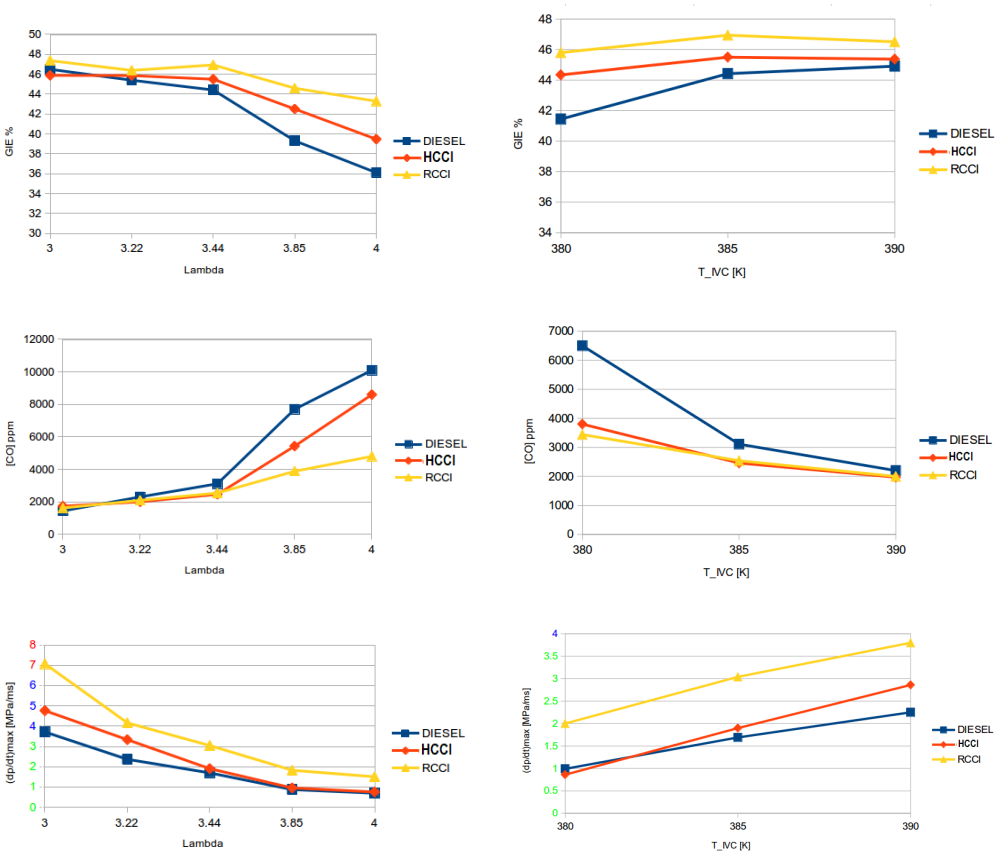

Figure 6.14: Comparison of different Piston Bowl at different equivalence ratio value and IVC temperature

6.4.3 Variation of Initial Pressure

The in-cylinder mass increases with the initial pressure and the ignition delay is anticipated since the different chemical species are physically closer. Both effects cause an increase of the peak of the pressure raise rate. A sort of anomaly for CO emissions at the lower inlet pressure is that the HCCI optimized piston shows higher emissions than Diesel one, even if the GIE is higher, the reason is that a portion of the charge in squish volume of the Diesel combustion chamber does not react at all. This has been deduced from the values of mass fractions of iso-octane at EVO that are 472 ppm for Diesel combustion chamber and 253 ppm for HCCI Optimized combustion chamber. The results are summarized in the figure 6.15.

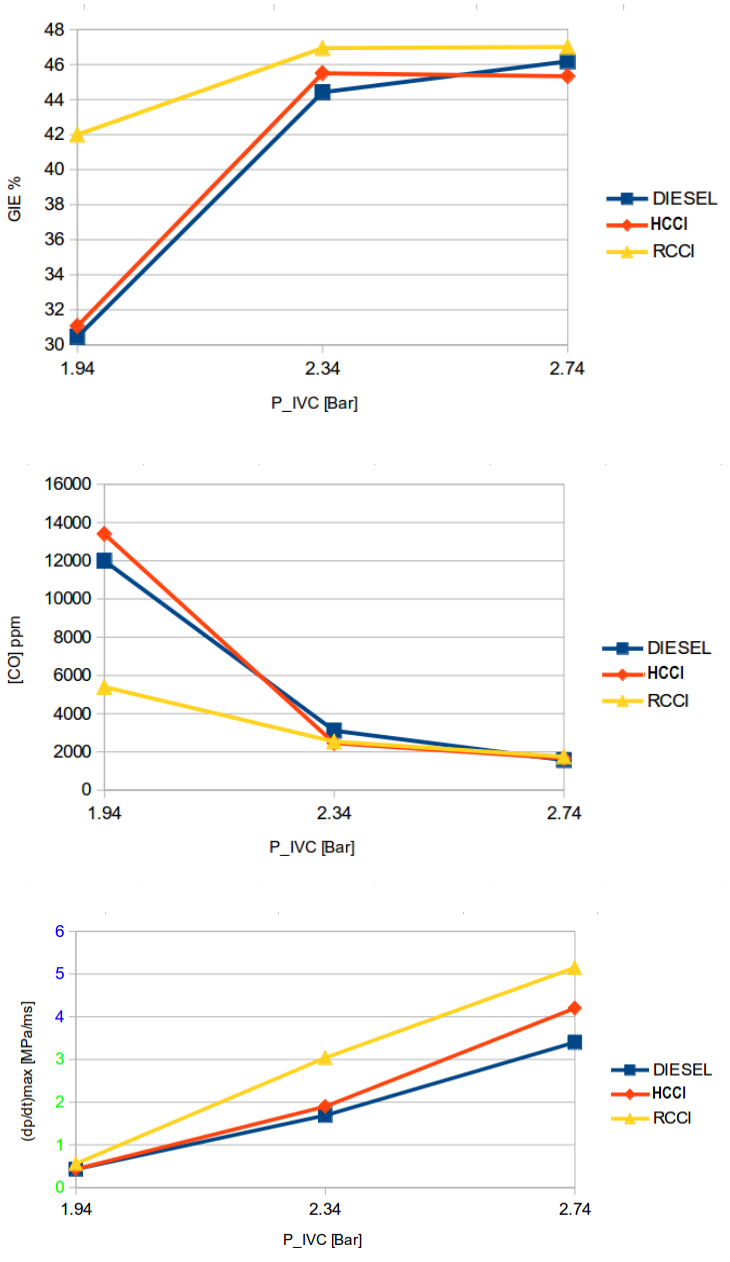

Figure 6.15: Comparison of different Piston Bowl at different IVC pressure

Conclusions

Some clear conclusions can be made considering all the points analyzed in the previous section. RCCI Piston bowl well behaves at low loads and always have the highest GIE, since the combustion is always faster and the heat exchange always smaller. However, the high values of the peak of pressure rate limit its high load operations potential. The absence of a squish area helps to contain the emission of CO. Diesel Bowl geometry is largely limited at low loads, initial temperatures and pressures since the combustion efficiency in the squish volume is very low. The values of CO emissions and GIE are similar to the other geometries at high loads, where the charge is more reactive. It shows the largest possibility to extend the operations forwad high loads, since the maximum rate of pressure rise is the lowest between all the geometries. HCCI optimized piston is intermediate between the two other configurations since it shows good behavior both at low and high loads, thanks to the so-called post-combustion.

Chapter 7

TCRCI combustion simulations

The TCRCI combustion mode is studied in this chapter. Three different operating conditions provided by the industrial partner have been simulated to validated the CFD model and a graphical post-processing has been conduced to describe the combustion process.

7.1 Direct injection

The physics behind the injection changes with the injection temperature since with phase change the passage from an incompressible to a compressible flow happens.

7.1.1 Gaseous Injection

Since the final boiling point of gasoline is 488 K and the critical point of iso-octane is 539 K, the direct injected fuel in the TCRCI case is normally in supercritical condition at the exit of injector. The Lagrangian injection model used in liquid injection can not be used for this reason, since it models the interaction of liquid fuel droplets. In the supercritical region, the fuel behavior is far from the concept of ideal gas, nevertheless the previous simulations performed by the ICE group show that the difference in jet penetration between real and ideal gas are limited, as a consequence, the ideal gas model is used in this work for the sake of simplicity. Depending on the injection pressure and temperature, the jet can be fully expanded, chocked or under-expanded and the mass flow rate is upper bounded by the choked mass flow rate. The injection pressure is high enough to have always an under-expanded jet and a chocked mass flow rate in the operating points discussed in this work.
The chocked mass flow rate for an ideal gas is defined as:

$$\dot{m}_c = C \cdot \frac{\pi d_{nozzle}^2}{4} \rho_{01} a_{01} [2/(k+1)]^{(k+1)/2(k-1)} \propto \frac{p_{01}}{\sqrt{T_{01}}} \tag{7.1}$$

Where k is the heat capacity ratio, C the discharge coefficient, a_{01} the sound speed of the gaseous fuel, p_{01}, T_{01} the injection pressure and temperature and p_2 the in cylinder pressure.
The actual steady state mass flow rate can be defined as:

$$\dot{m} = C \cdot \frac{\pi d_{nozzle}^2}{4} \rho_{01} \Phi_f(p_2/p_{01}) \tag{7.2}$$

Where Φ_f is a function of the pressure ratio. The jet is fully expanded till $\dot{m} < \dot{m}_c$, when this threshold is overcome, the jet is under-expanded and the mass flow rate is equal to the chocked one. It is possible to see that the choked mass flow rate is directly proportional to the injection pressure and inversely proportional to the square root of the injection temperature. Therefore it could be useful to increase the injection pressure with the injection temperature to keep the injection duration almost constant.

7.1.2 Liquid Injection

The injection is in the liquid phase when the injection temperature is below the critical value. For this condition, the Lagrangian approach has been used to describe the evolution of the spray, which is represented by a finite number of liquid fuel droplets with the same physical properties [32]; the breakup model implemented in FOAM package is the Kelvin-Helmotz-Rayleigh-Taylor. The purpose of the breakup model is to reduce the liquid droplets characteristic size due to aerodynamic forces. Given the value of injected pressure p_1 and in-cylinder pressure p_2 the steady-state mass flow rate can be estimated as:

$$\dot{m} = C \cdot \frac{\pi d_{nozzle}^2}{4} \sqrt{2\rho_{fuel}(p_1 - p_2)} \tag{7.3}$$

It is interesting to notice that the liquid mass flow rate is quite larger with respect to the gaseous one, given the same injection pressure, therefore the injection duration for liquid fuel is shorter.

7.2 Simulation pre-processing

7.2.1 Mesh

The mesh configuration is the same as HCCI cases except for the sector angle that has been set to 60 degrees (fig 7.1), the reason is that the injector is characterized by six holes and thus the minimum sector angle possible to have a cyclic symmetry of the direct injection process is 1/6 of the combustion chamber. The injection cell-set is composed by 8 cells and it is enough refined to correctly predict the jet penetration.

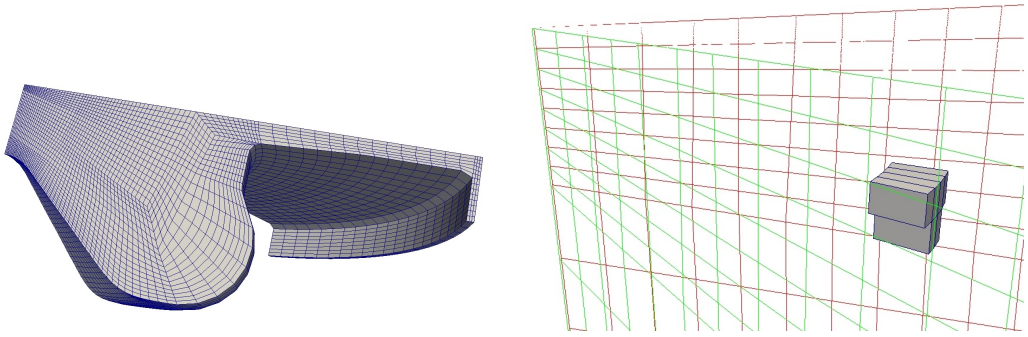

Figure 7.1: TCRCI Mesh and injection cell-set

7.2.2 Initial conditions

Three different operating points with different fuel mass, external egr, percentage of port and direct fuel injected, SOI and load have been simulated to validate the numerical model. The experimental parameters provided by the company are summarized in the table 7.1:

	Low Load	Medium Load	High Load
GIMEP [bar]	4.4	6.86	13
$m_{fuel,tot}$ [mg]	13.5	19	35
$PFI\%$	29.6	76.3	85.7
SOI [CAD]	-30	-32	-40
$t_{inj}[\mu s]$	455	431	409
$T_{DI}[^{\circ}]$	390	365	360
P_{DI} [bar]	300	300	300
$EGR_{ext}\%$	0	0	22
λ	5.1	4.15	2.17
P_{IVC} [bar]	2.3	2.4	3.2
T_{IVC} [K]	378	380	370

Table 7.1: Initial experimental condition TCRCI

The values of the IVC temperature and ambient composition, shown in the table 7.2, derive from GT-Power zero-dimensional simulations, the value of λ is provided by Horiba exhaust gas analyzer . The ambient composition of low and medium cases are slightly different since there is a small difference in the calculated internal EGR.

	Low Load	Medium Load	High Load
Y_{O_2}	0.2293	0.2263	0.203
Y_{CO_2}	0.0024	0.0032	0.0219
Y_{H_2O}	0.0009	0.0012	0.0083
Y_{N_2}	0.7672	0.7693	0.7668

Table 7.2: Ambient composition

Some adjustments have been made from this starting point to match the experimental results. The reason is that LTC engines are very sensitive to initial conditions, especially in terms of start of combustion and peak of heat release rate and so small variations of initial temperature (that is not a measured parameter but it has been taken from previous simulations) lead to a big divergence of pressure trace and evolution of roHR. The final conditions simulated are provided in the table 7.3:

	Low Load	Medium Load	High Load
GIMEP [bar]	4.63	6.6	11.7
$m_{fuel,tot}$ [mg]	12.78	16.89	31.1
$PFI\%$	27.9	73.9	84.2
SOI [CAD]	-30	-32	-40
$t_{inj}[\mu s]$	455	431	409
$T_{DI}[^{\circ}]$	390	365	360
P_{DI} [bar]	300	300	390
$EGR_{ext}\%$	0	0	22
λ	4.77	3.92	2.6
P_{IVC} [bar]	2.1	2.3	3.1
T_{IVC} [K]	378	380	378

Table 7.3: Initial simulated condition TCRCI

7.2.3 Injection profile

The injection profile has not been provided by the industrial company and thus a reference one has been adopted. Since the injection temperature is above the critical one the virtual injector model is used. The injection pressure is high enough to always have a steady-state chocked mass flow rate and the injection profile has been scaled according to the injected fuel mass (fig.7.2). It has been necessary to increase

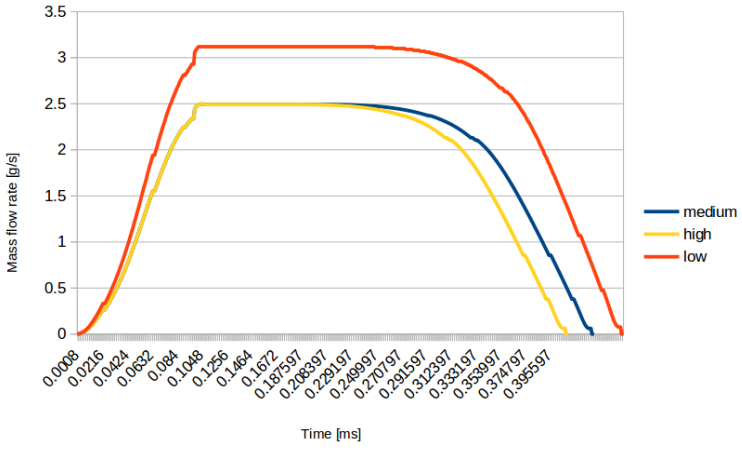

Figure 7.2: Different injection profiles

the mass flow rate in the low case to guarantee a correct jet penetration, therefore the intrinsic assumption made is to increase the injection pressure to 390bar. Otherwise

the injection velocity would have been too small and a portion of the fuel mass would have been injected in the wrong direction distorting the simulation results.

7.3 Combustion Model and Table Generation

The simulation set up used for these conditions is the same used in HCCI simulations (section 5.2.3), the table parameters have been refined for each case to have a trade-off between accuracy and computational time. Since the mixture in these cases is stratified, the equivalence ratios must range from 0 to 3.5 to correctly predict the start and the evolution of the combustion, the reaction rates for higher equivalence ratios are set to 0 to avoid a fstep combustion.

7.4 Simulation Results

The simulation results (fig. 7.3) show a significant overestimation of the cool flames intensity. This is mainly referable to the modeled behavior of Iso-Octane in that thermodynamical conditions by the Creck kinetic mechanism, the accuracy can be improved changing the fuel composition or using a different reaction mechanism like LLNL [33]. The LLNL mechanism has been tried; however, it requires a much larger adjustment of initial conditions to give slightly better results. This model also shows a smaller overestimation of the main peak of heat release rate. The final effect is an overestimation of the cumulative apparent heat release rate for the low and medium load case, this does not occur for the high load since it has been necessary to decrease a little the simulated in-cylinder mass respect to the experimental value to match the start of the combustion. The described results are adequate since the experimental injection profile is unknown and a certain level of uncertainty subsists for the values of the directly injected fuel mass and temperature. They can be improved by progresses in the understanding of the behavior of the heated fuel inside the injector. This topic is the subject of study by the industrial partner, so it will be possible to have more precise parameters in the future. The main performance parameters of the simulated conditions are presented in the table 7.4:

	Low Load	Medium Load	High Load
GIMEP [bar]	4.63	6.6	11.7
GIE [%]	39.57	42.66	41.1
$\frac{dP}{dt}_{max}$ [MPa/ms]	1.59	2.04	1.73

Table 7.4: Simulated performance parameters TCRCI cases

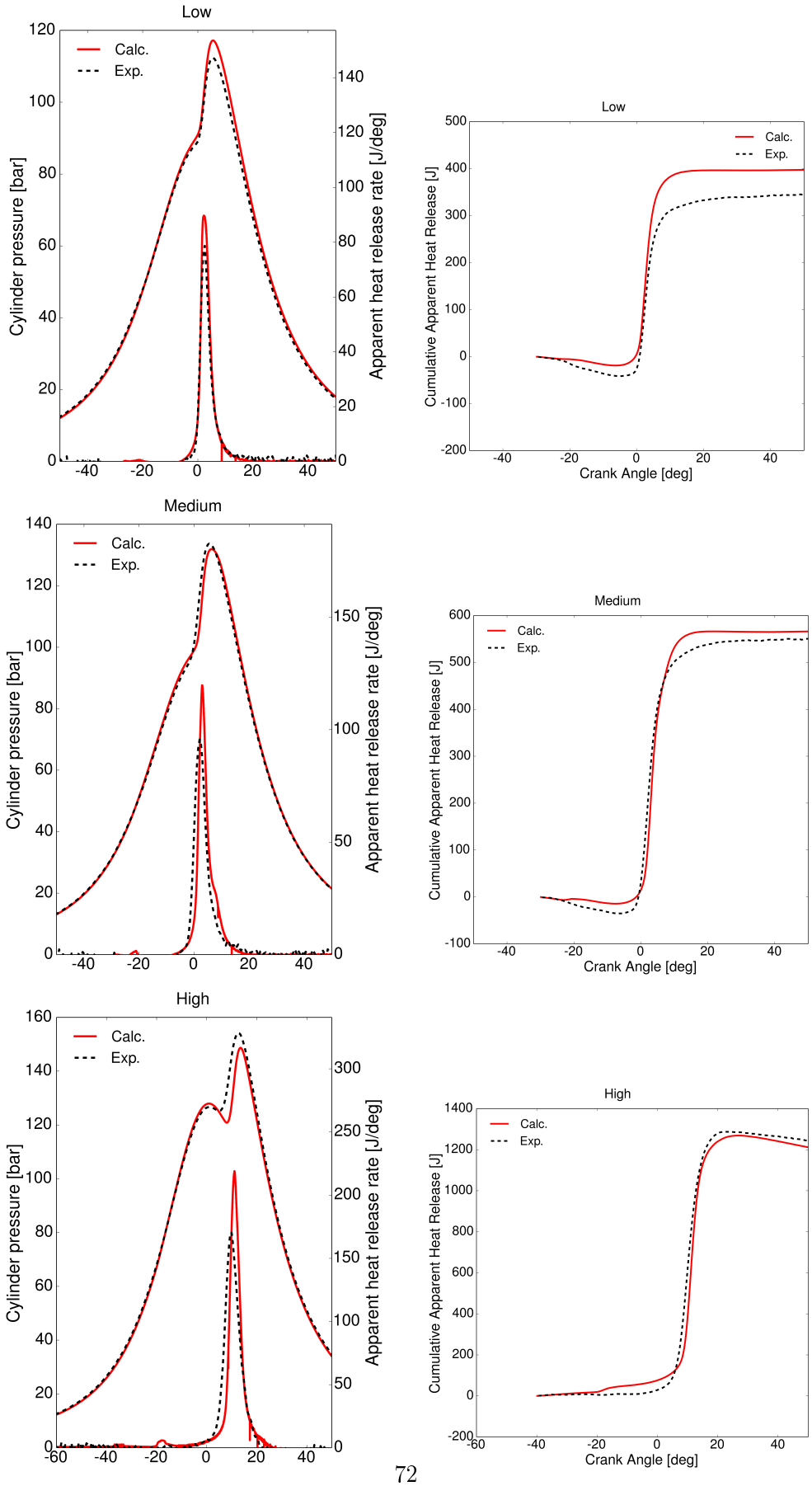

Figure 7.3: Comparison between simulation and experimental TCRCI simulations

7.4.1 Combustion Process

To understand the differences between this type of combustion and the HCCI one, a deeper study on the combustion process has been proposed based on the medium load case. The first interesting effect to notice is that the in-cylinder temperature at the start of injection is 492°, hence the direct injected fuel still cools the mixture. The main effect of the direct injection is to create a richer region inside the piston bowl as it is possible to understand in fig 7.4, this region is also characterized by a higher temperature thanks to the smaller influence of heat exchange with the walls. The region located at the bottom of the bowl is the first to ignite since the ignition

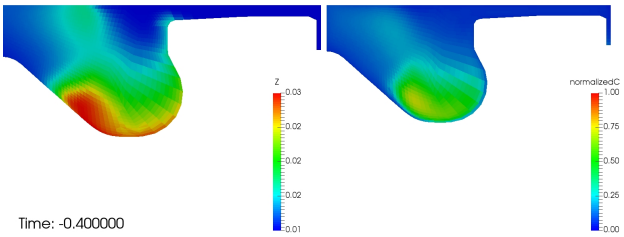

Figure 7.4: Effect of mixture stratification on combustion

delay decreases when the mixture is richer and warmer. The progress variable of the cells involved in the start of combustion increases and it diffuses through the surrounding regions firing up the rest of the mixture (fig 7.5). This behavior is typical of non-homogeneous combustion [24] and can be easily understood looking at the mixture fraction-temperature map evolution during the combustion; the first cells that are subjected to a temperature increase are the ones characterized by a richer mixture, when combustion proceeds also the cells with a leaner mixture increase their temperature.

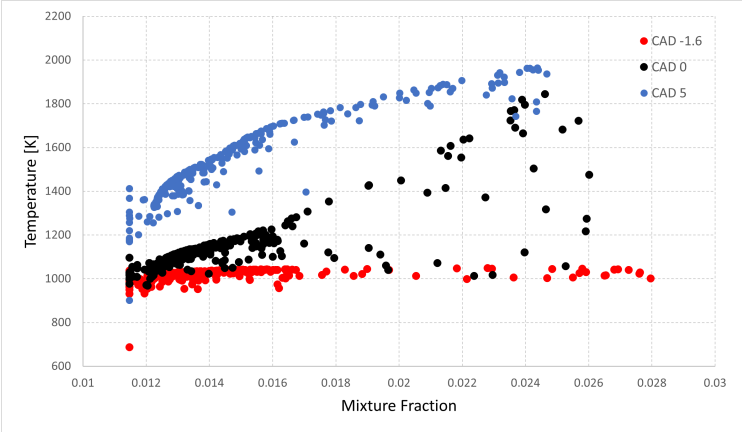

Figure 7.5: Z-T distribution of medium load case

Chapter 8

Influence of Injection Parameters on TCRCI Combustion

The focus of this chapter is put on the influence of the injection strategy on the combustion process. The parameters analyzed are:

- Differences between gaseous and liquid injection
- temperature of supercritical direct Injection
- SOI
- PFI/DI ratio
- Split Injection

All these studies have been carried out on the bases of the medium load operating condition.

8.1 Direct Injected Fuel Temperature

The difference between liquid and gaseous injections and the influence of injection temperature in the supercritical injection are treated separately.

8.1.1 Differences between liquid and gaseous Injection

The first important effect of the increase of injection temperature is that the phase of the injected fuel changes from liquid to gaseous. As consequence, the fuel mass flow rate changes significantly keeping constant the injection pressure. The steady-state liquid mass flow rate is 5.8 g/s considering a liquid injection at 108°. This value is more than two times bigger than the gaseous mass flow rate and, as a consequence, the injection duration is reduced to 180 μs. The injection velocity is much larger in the gaseous injection, as it is possible to see in the fig 8.1. The supercritical injection is largely sub-expanded since the Mach number is close to 3.1 (the sound speed of iso-octane at 640 K is 249.9 m/s). The turbulence generated by gaseous jet penetration is larger respect to the liquid one since the jet is faster.

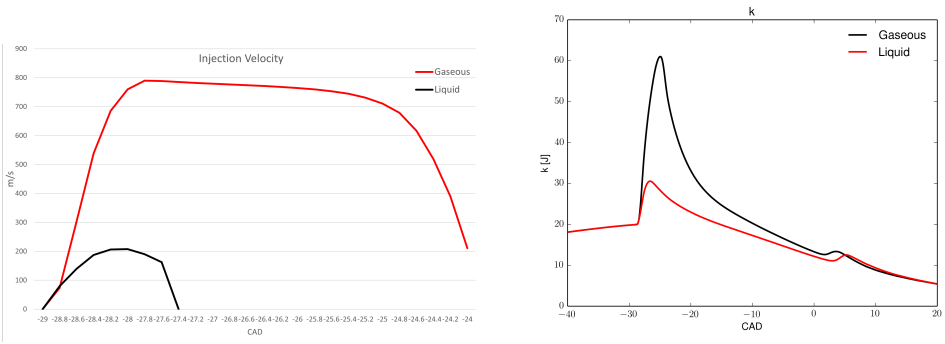

Figure 8.1: Comparison between injection velocity and turbulence evolution of liquid and gaseous state

The second important effect is the mixture cooling consequent to the interaction with the injected fuel; the liquid fuel has an higher cooling potential since it is colder and evaporates inside the cylinder. This effect is well represented by the average unburned mixture temperature during the injection(fig 8.2). The temperature difference at the

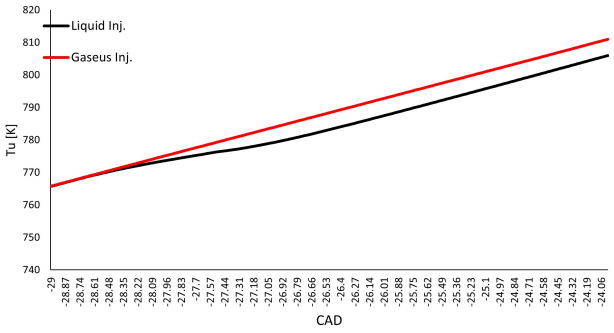

Figure 8.2: Tu evolution during injection

end of the injection is 5 K and it is responsible for the early combustion phasing in the supercritical case. Finally a region of richer mixture near the piston bowl wall is present in the liquid case, since the liquid spray tends to mix less with the mixture being in a different phase for a certain amount of time. All the observations previously made can be easily understood looking at the map of mixture fraction to unburned gas temperature just before the main ignition at -1.9 CAD (fig 8.3). It is possible to see that the maximum mixture fraction is higher for liquid injection and the temperature of the gaseous case are globally higher.

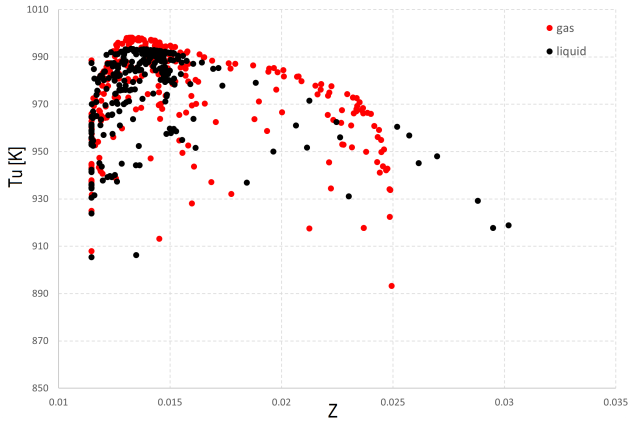

Figure 8.3: Z-Tu map comparison between liquid and gaseous injection at -1.9 CAD

These differences result in an earlier combustion and a higher peak of apparent heat release for the hot injection, as shown in the figures 8.4. Therefore the efficiency is approximately 2 % higher and the peak of pressure rise is higher (table 8.1).

	Gaseous Inj	Liquid Inj
GIE [%]	42.67	40.84
Tot. Heat E. [J]	-122	-114
MFB10 [CAD]	0.63	1.65
MFB50 [CAD]	4.11	5.55
$\frac{dP}{dt}_{max}$	2.04	1.77
CD [CAD]	10.13	12.15

Table 8.1: Comparison of results between Square and Diesel Bowl

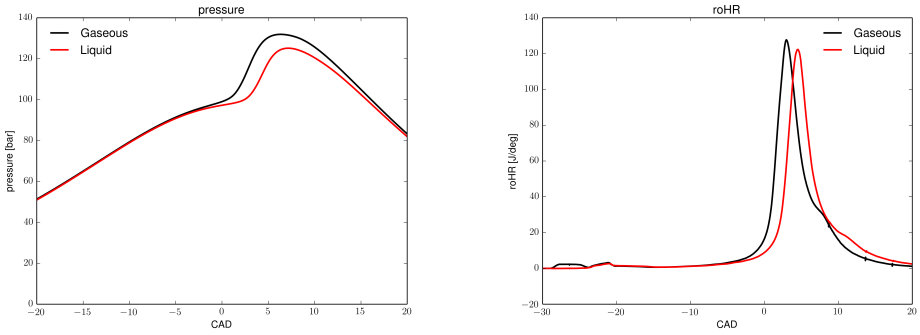

Figure 8.4: Pressure and RoHR comparison liquid and gaseous injection

8.1.2 Effect of fuel temperature in gaseous state

Three different temperatures have been analyzed (367,467°,567°) to study the effect of gaseous fuel temperature variation on the combustion. Keeping the injection pressure

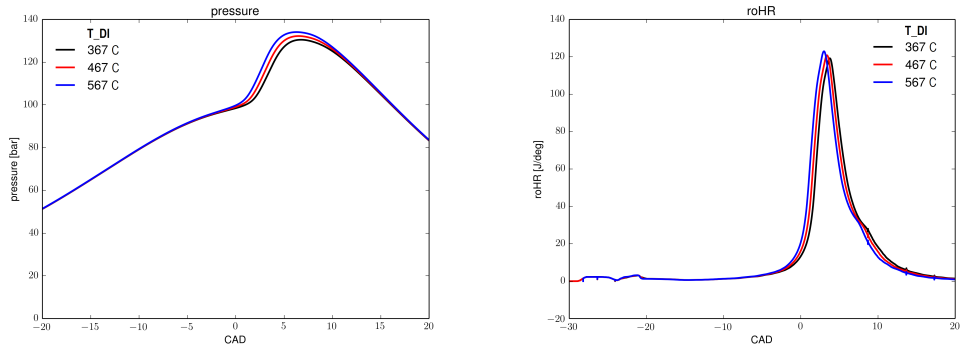

Figure 8.5: Pressure and roHR comparison between different gaseous injection temperatures

constant, the chocked mass flow rate decreases with an increase of the temperature. The mass flow rate has been kept constant to isolate the effect of the temperature and hence the injection pressure has been ideally increased. The influence on mixture temperature is negligible, as shown in the table 8.2. This suggests that the highest contribution in mixture cooling is played by the fuel evaporation.

Direct Fuel T. [°]	367	467	567
T_u [-23 CAD] [K]	820.46	821.6	823

Table 8.2: Unburned Charge temperature variation

The main consequence of the different mixture thermal level is a small variation in combustion timing, as shown in fig 8.5.
Simulation results are summarized in fig. 8.6 for what concerns the dependency of the GIE on the injected fuel temperature.

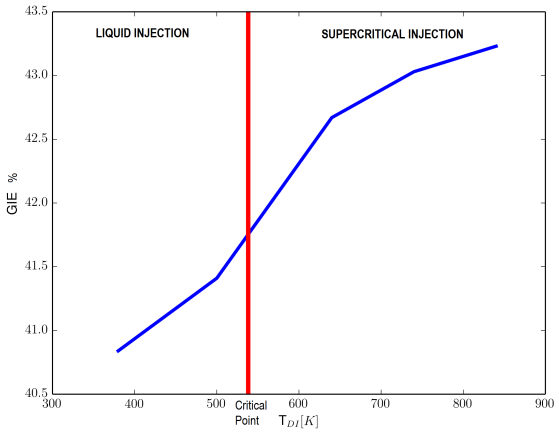

Figure 8.6: GIE vary to DI Fuel temperatures

The most relevant efficiency increase is across the phase change while the influence of the temperature in the supercritical region is limited. This result is interesting since

it is possible to achieve a good efficiency without excessively increase the fuel temperature. Therefore the injector design is technically easier and the energy necessary to heat the fuel limited.

8.2 PFI Fraction sweep

The partition between PFI and DI fuel fraction is one of the most effective parameter to control the combustion process since it affects the level of stratification of the mixture and the global reactivity. Three different operating points based on the medium load are analyzed to study how the combustion is influenced and the PFI/DI ratios considered are 64, 74 and 84 %. Looking at the fig 8.7 it is clear how the mixture homogeneity increases with the PFI fuel percentage, being the premixed mixture richer and the maximum mixture fraction smaller. As a consequence, combustion starts

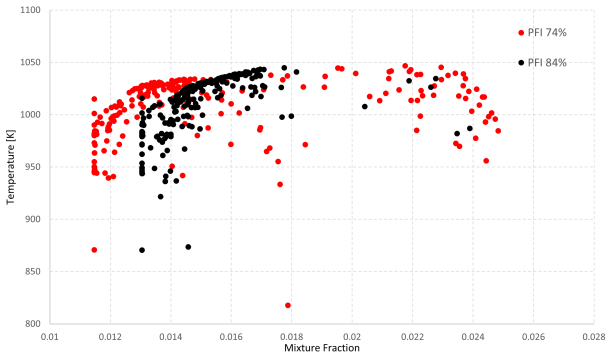

Figure 8.7: Z-T map comparison between PFI percentage equal to 74 and 84 at -1.6 CAD

earlier and the peak of pressure and heat release rate increase with the decrease of PFI/DI ratio (fig. 8.8). At the same time, the presence of a richer region and the earlier ignition increase the maximum temperature, promoting NO_x formation. In the context of ignition control, it is useful to increase the DI fuel fraction at the low loads, where the mixture is less reactive.
The summary of the performance parameters is presented in table 8.3:

$PFI\%$	64	74	84
GIE [%]	42.91	42.67	42.94
Tot. Heat E. [J]	-126	-122	-118
MFB10 [CAD]	-0.105	0.635	0.985
MFB50 [CAD]	2.875	4.11	5.1
$\frac{dP}{dt}_{max}$	2.42	2.04	1.55
CD [CAD]	9.55	10.13	10.5

Table 8.3: Results of variation of PFI Fraction

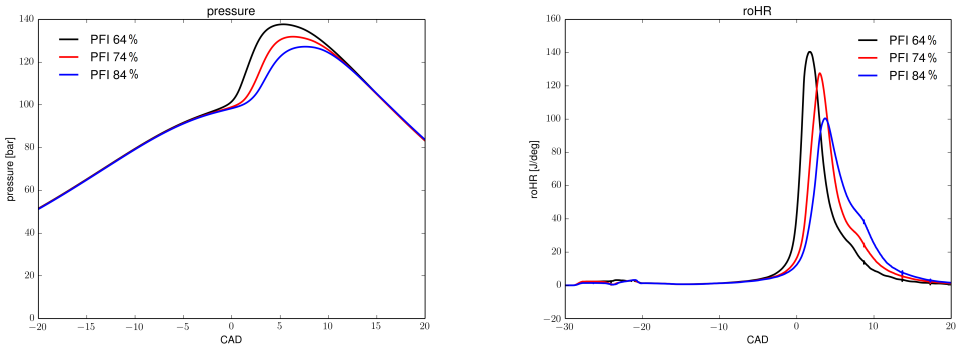

Figure 8.8: Pressure and roHR comparison between different PFI fractions

8.3 SOI sweep

The start of injection affects the evolution of the mixture distribution inside the cylinder. The SOIs considered are -40,-32 and -28 CAD; the more the injection is anticipated the lower the in-cylinder pressure is and the higher the injection velocity and the generated turbulence will be. The effect of the different stratification levels can be noticed looking at the comparison between the mixture fraction at -1.8 CAD between the cases at -40 and -28 CAD (fig 8.9). The earlier injection is more homogeneous while the latter one shows a rich core that helps to ignite the mixture and therefore the combustion starts earlier, as it is possible to notice in fig 8.10. The

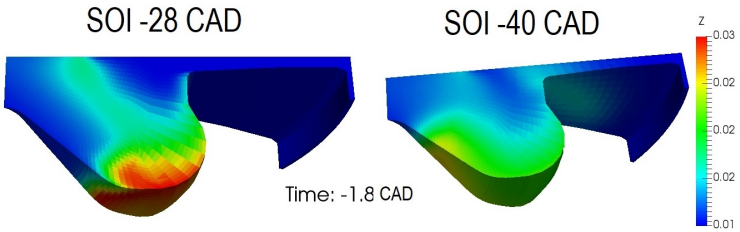

Figure 8.9: Mixture fraction comparison at -1.8 CAD

differences are limited between the cases at -32 and -28 CAD since the structure of the mixture is closer. The higher efficiency of the cases with delayed injection, shown in the table 8.4, is due to the earlier combustion.

SOI [CAD]	-28	-32	-40
GIE [%]	42.75	42.67	42.59
Tot. Heat E. [J]	-123.4	-122	-119.8
MFB10 [CAD]	0.415	0.635	0.985
MFB50 [CAD]	3.83	4.11	5.1
$\frac{dP}{dt}_{max}$	2.00	2.04	1.55
CD [CAD]	9.99	10.13	10.7

Table 8.4: Results of variation of PFI Fraction

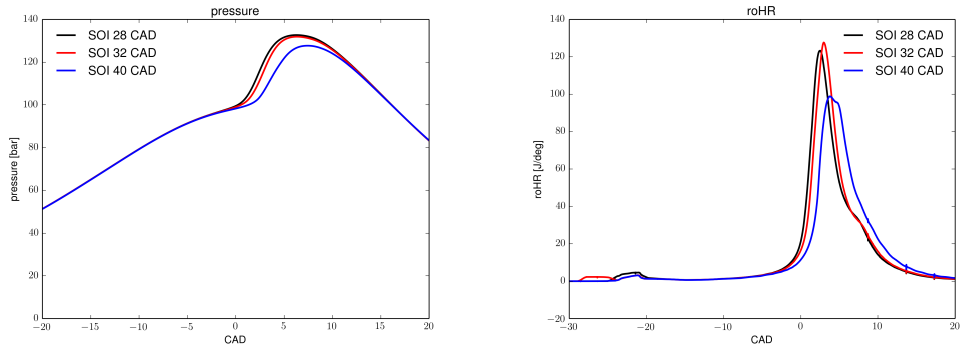

Figure 8.10: Pressure and roHR comparison SOI sweep

8.4 Split Injection

The last injection strategy investigated is to split the injection in two separate events. The idea behind is to increase the combustion efficiency in the squish region thanks to an early injection that locally increases the mixture fraction. The injection strategy used is composed by two injections with the same fuel mass, the other initial conditions are the same of the medium load case. The SOI1 is at -63 CAD, while the SOI2 is at -32 CAD. This strategy is responsible for the presence of two separate rich regions. The first one is located in the squish volume and it is caused by the pilot injection, the second one is located in the piston bowl (fig 8.11). The roHR shows

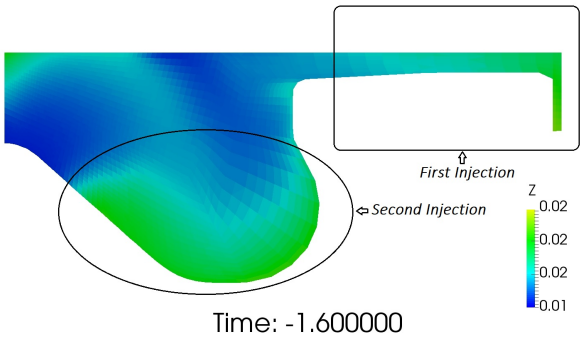

Figure 8.11: Split Injection mixture fraction at -1.6 CAD

a much smaller peak than the single injection strategy since the mixture inside the bowl is leaner (fig 8.12); the presence of richer mixture in the squish region and the increase of temperature subsequent to the start of combustion inside the bowl which promotes a more exothermic combustion in the squish region, which results in the second peak of heat release rate.

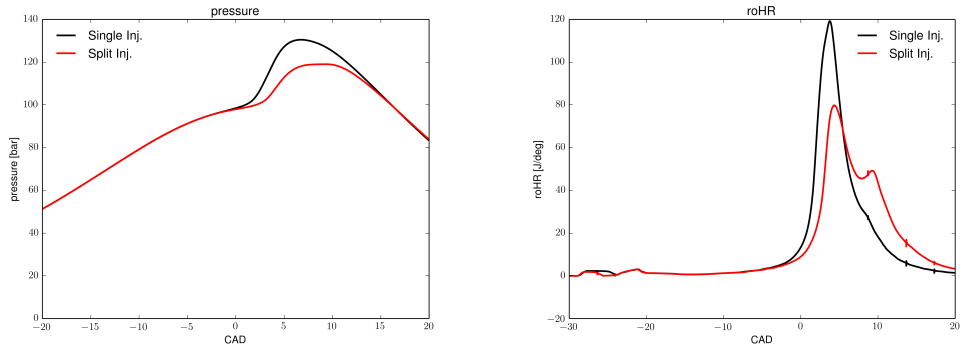

Figure 8.12: Pressure and roHR comparison split injection

From the performance parameter point of view (table 8.5), the peak of pressure raise is smaller and the combustion is longer, the efficiency decrease is limited because the longer combustion is partially balanced by the lower heat exchange with the walls.

	Single Injection	Split Injection
GIE [%]	42.67	42.57
Tot. Heat E. [J]	-122	-119
MFB10 [CAD]	0.63	1.4
MFB50 [CAD]	4.11	6.39
$\frac{dP}{dt}_{max}$	2.04	1.17
CD [CAD]	10.13	12.48

Table 8.5: Results of single and split injection

Chapter 9

Piston Geometry effect on TCRCI combustion

The different piston geometries studied in the chapter 6.4 are applied to TCRCI combustion mode in this last chapter; this is necessary to understand the interaction between the jet and the combustion chamber geometry. In all LTC engines, the injection is anticipated with respect to CCI combustion therefore the mixing requirements are completely different. The mixing requirements of TCRCI are close to those of RCCI combustion and for this reason the optimization of the piston geometry shown in the dedicated section is promising. It is also interesting to understand how the optimized HCCI piston behaves with this different combustion technology. The operating points considered are the ones of the TCRCI model validation (low, medium and high cases)

9.1 Comparison between Diesel and RCCI piston

The results of the comparison between the Diesel and RCCI piston performed at the three different load levels are presented in this section. Unlike the Diesel piston, which tends to concentrate the direct injected fuel inside the bowl, the RCCI piston promotes the mixing processes being almost a flat surface. Therefore the mixture fraction distribution tends to be more homogeneous as shown for the medium load case in fig 9.1.

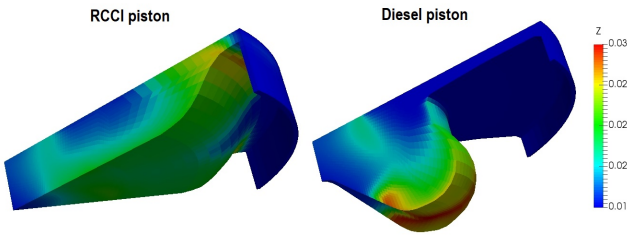

Figure 9.1: Comparison of mixture fraction distribution at medium load for RCCI and Diesel pistons

As a consequence, the combustion ignition tends to be delayed for the RCCI piston. This property has been balanced by a small increase of the temperature at IVC, as shown in the table 9.1:

		Diesel Piston	RCCI Piston
Low Load	$T_{IVC}[K]$	378	382
	$P_{IVC}[Pa]$	210000	212000
Medium Load	$T_{IVC}[K]$	380	381
	$P_{IVC}[Pa]$	230000	230600
High Load	$T_{IVC}[K]$	378	379
	$P_{IVC}[Pa]$	309400	310218

Table 9.1: Variation of Initial Condition for piston comparison

The initial pressure is proportionally increased to keep the in-cylinder mass constant. The results of the three considered operating points (fig 9.2) show that the ignition delay is always larger for RCCI piston and the peaks of heat release rate are comparable to the Diesel piston bowl ones. Therefore, also the peaks of the rate of pressure rise are smaller. The benefits of this geometry are relevant in the medium and high load; for the low load case, the effect of the temperature at Inlet Valve Closing on the charge reactivity is limited since the fraction of port injected fuel is 27.9%. For this reason it is necessary to take action on the injection strategy to anticipate the ignition.

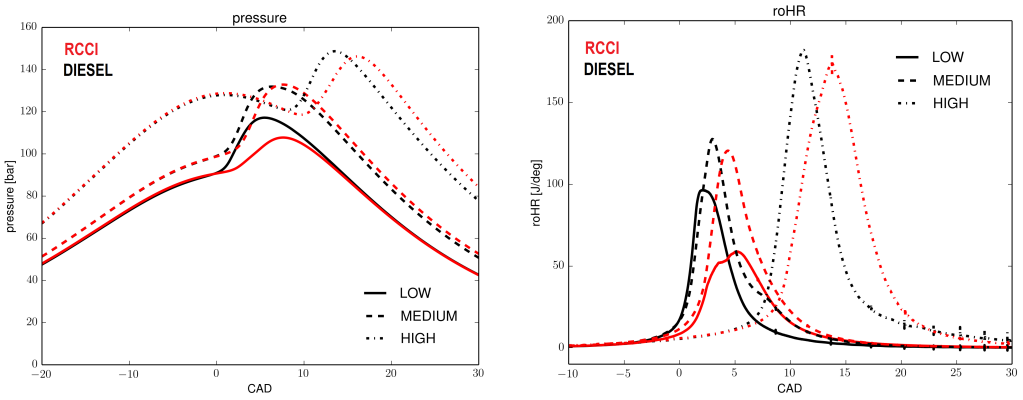

Figure 9.2: Comparison of TCRCI cases for RCCI and Diesel pistons

The results summarized in the table 9.2 show the benefits of the RCCI piston geometry, the delayed combustion and the smaller walls surfaces decrease the total heat exchange with the walls, increasing the Gross Indicated Efficiency. At the same time, the smaller peaks of pressure rise allow to extent the operating conditions toward higher loads.

		Diesel Piston	RCCI Piston
Low Load	GIE %	39.57	37
	$\frac{dP}{dt}_{max}[MPa/ms]$	1.59	0.68
	Heat Exchange $[J]$	-106.3	-109.1
Medium Load	GIE %	42.67	46.81
	$\frac{dP}{dt}_{max}[MPa/ms]$	2.04	1.89
	Heat Exchange $[J]$	-122.27	-116.2
High Load	GIE %	41.11	46.71
	$\frac{dP}{dt}_{max}[MPa/ms]$	1.74	1.34
	Heat Exchange $[J]$	-146.2	-127.6

Table 9.2: Performance parameters of Diesel and RCCI piston comparison

9.2 Comparison between HCCI and Diesel optimized piston

The mixture stratification inside the HCCI and Diesel optimized combustion chambers is close since the piston bowl dimensions are comparable. Nevertheless richer regions are present in the HCCI piston since the cylinder piston bowl is not optimized for promoting the mixing processes (fig 9.3). Therefore the start of combustion is slightly anticipated. The heat release rate is characterized by two peaks (fig 9.4),

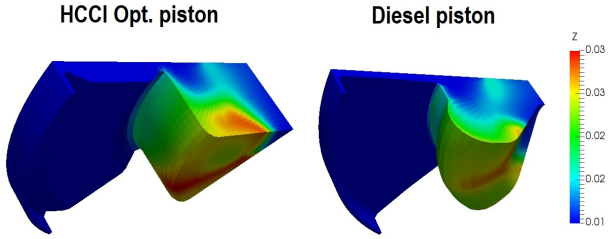

Figure 9.3: Comparison of mixture fraction distribution at medium load for HCCI and Diesel pistons

the first one corresponds to the start of combustion in the piston bowl, the second one is caused by the speed up of combustion of the leaner premixed charge in the squish volume. At the end of the compression stroke the temperature in the squish volume is high enough to promote pre-combustion reactions, when the temperature and the pressure inside this region further increase, as a consequence of the combustion in the piston bowl, the combustion reactions speed up until the completion of the combustion; this process causes the second peak of heat release rate.

This type of combustion can be achieved also for Diesel combustion chamber with the use of a split injection, as shown in the previous chapter. The low load case is characterized by a single peak of roHR since the portion of port injected fuel is only 27.9 %, therefore the mixture in the squish volume is too lean to start the pre-combustion reactions.

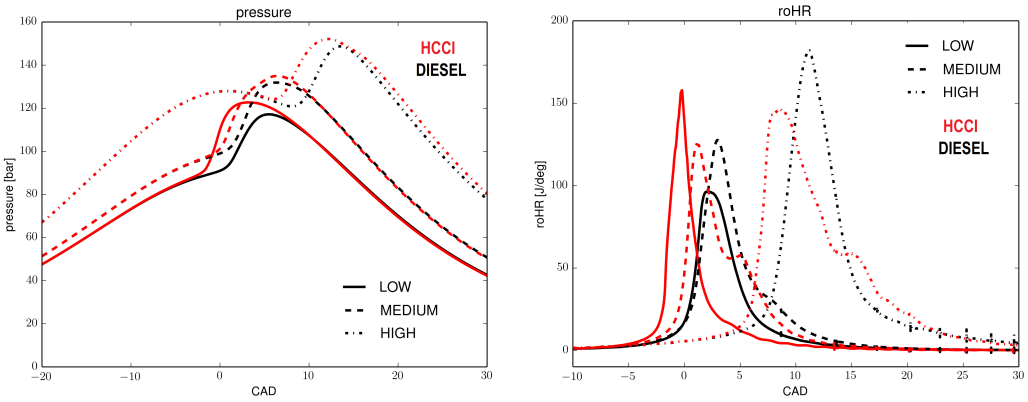

Figure 9.4: Comparison of TCRCI cases for HCCI and Diesel pistons

The only relevant improvement in the Gross indicated efficiency occurs for the high load case, the other ones show worst efficiencies since the total heat exchange is higher for the HCCI optimized piston bowl, as shown in the table 9.3. Furthermore this geometry shows higher peak of pressure rise rate.

		Diesel Piston	RCCI Piston
Low Load	GIE %	39.57	38.96
	$\frac{dP}{dt}_{max}[MPa/ms]$	1.59	2.76
	Heat Exchange $[J]$	-106.3	-112.36
Medium Load	GIE %	42.67	42.00
	$\frac{dP}{dt}_{max}[MPa/ms]$	2.04	2.14
	Heat Exchange $[J]$	-122.27	-124.76
High Load	GIE %	41.11	43.81
	$\frac{dP}{dt}_{max}[MPa/ms]$	1.74	1.57
	Heat Exchange $[J]$	-146.2	-158.0

Table 9.3: Performance parameters of Diesel and HCCI piston comparison

Conclusions and future development

This work has been focused on HCCI and TCRCI combustion modes. The CFD model for HCCI combustion has been first validated through a set of experimental conditions, it is proved capable of correctly capture the combustion process. The influence of the piston head geometry has been studied comparing a set of geometries found in literature. It has been understood that the most important parameter is the squish ratio, since it affects the combustion duration and the pollutant emissions. A new piston bowl optimized for HCCI combustion has been developed based on the achieved results, it allows to increase the combustion efficiency in the squish volume. This geometry has been compared to a Diesel and RCCI piston head on a large number of operating conditions to deeply understand its behavior; it is able to ensure a better combustion efficiency than the Diesel bowl and, in parallel, it shows a slower combustion than RCCI piston, allowing higher load operations.
The second part of this work has been focused on TCRCI combustion. The CFD model based on the developed virtual gaseous injector has been validated on a set of experimental operating conditions characterized by different loads. It is able to capture the combustion process even if it shows an overestimation of the apparent heat release rate.
The effects of the injection parameters have been also analyzed, this type of combustion is promising from the engine control point of view since it shows a larger sensibility to the simulated injection strategies. The combustion shows a large improvement in terms of GIE when the fuel is injected at supercritical conditions compared to liquid injection. On the contrary, the effects of the variation of direct injected fuel temperature in super-critical conditions are limited.
This type of combustion is also influenced by the start of injection and by the partition between Port Injected Fuel and Direct Injected fuel. Both parameters affect the combustion timing since they influence the stratification level of the mixture.
The possibility of a split injection has been also considered, it helps to reduce the peak of pressure rise keeping almost constant the Gross Indicated Efficiency.
Finally the three piston geometries considered in the HCCI sections have been applied to TCRCI combustion. The effect of the fuel stratification and the smaller surface walls area allow RCCI geometry to show a higher GIE and a smaller peak of pressure rise respect to the Diesel piston bowl. As a consequence this geometry is the most promising for this technology. The HCCI optimized piston geometry shows a similar combustion evolution respect to the Diesel bowl and its benefits in

terms of combustion efficiency are limited.
Besides, the effect of an increase of combustion efficiency in the squish region can be achieved also by the conventional Diesel bowl by the use of a split injection.

Future development

A more structured analysis of the effects of the following parameters on TCRCI combustion is necessary:

- Key piston parameter
- Injector geometry
- Injection Parameters
- Split Injection
- Air management

A part of this work will be carried out by the thesis author during a stage period in CMT-Motores Térmicos in Valencia. An optimization of the TCRCI combustion system will be performed by the use of an advanced optimization methodology combining an evolutive system (PSO) plus machine learning (ML).

Bibliography

[1] Norbert Peters. *Combustion Theory*. RWTH Aachen University, 2010.

[2] Giancarlo Ferrari. *Motori a combustione interna*. Bologna: Società Editrice Esculapio, 2016.

[3] *Research in an optical engine*. 2009. URL: https://rkdmb.home.xs4all.nl/rkd/engine/engine.html.

[4] Ali Keskin. "The pollutant emissions from diesel-engine vehicles and exhaust aftertreatment systems". In: (2015).

[5] *Nitrogen oxides (NOx) emissions*. 2010. URL: https://www.eea.europa.eu/data-and-maps/indicators/eea-32-nitrogen-oxides-nox-emissions-1.

[6] Laarnie Mueller et al. "Morphological and Elemental Classification of Freshly Emitted Soot Particles and Atmospheric Ultrafine Particles using the TEM/EDS". In: *Aerosol Science and Technology* 44 (Feb. 2010), pp. 202–215. DOI: 10.1080/02786820903518907.

[7] M. Krishnamoorthi et al. "A review on low temperature combustion engines: Performance, combustion and emission characteristics". In: *Renewable and Sustainable Energy Reviews* (2019). ISSN: 1364-0321. DOI: https://doi.org/10.1016/j.rser.2019.109404.

[8] *Low Temperature Combustion*. 2011. URL: https://dieselnet.com/tech/engine_ltc.php.

[9] J. A. Eng. "Characterization of Pressure Wave Oscillation in HCCI Combustion". In: *SAE TECHNICAL PAPER SERIES* (2002).

[10] Wai K. Cheng Morgan M. Andreae. "On HCCI Engine Knock". In: (2007). DOI: 10.4271/2007-01-1858.

[11] Hassan Aljaberi, Abdul Aziz Hairuddin, and Nuraini Abdul Aziz. "The use of different types of piston in an HCCI engine: A review". In: *International Journal of Automotive and Mechanical Engineering* 14 (June 2017). DOI: 10.15282/ijame.14.2.2017.17.0346.

[12] Anders Hultqvist Andreas Vressner and Bengt Johansson. "Study on Combustion Chamber Geometry Effects in an HCCI Engine using High-Speed Cycle-Resolved Chemiluminescence Imaging". In: (2007).

[13] John E. Dec, Magnus Sjöberg, and Wontae Hwang. "Isolating the Effects of EGR on HCCI Heat-Release Rates and NOX Emissions". In: *SAE Int. J. Engines* (). DOI: 10.4271/2009-01-2665.

[14] Jan-Ola Olsson et al. "Compression Ratio Influence on Maximum Load of a Natural Gas Fueled HCCI Engine". In: *SAE International* (2002). DOI: 10.4271/2002-01-0111.

[15] Dong-bo Yang et al. "Experimental study of fuel stratification for HCCI high load extension". In: *Applied Energy* 88.9 (2011). ISSN: 0306-2619. DOI: https://doi.org/10.1016/j.apenergy.2011.03.004.

[16] N.P. Komninos. "The effect of thermal stratification on HCCI combustion: A numerical investigation". In: *Applied Energy* 139 (Feb. 2015), pp. 291–302. DOI: 10.1016/j.apenergy.2014.10.089.

[17] Ganesh Duraisamy Rolf D. Reitz. "Review of high efficiency and clean reactivity controlled compression ignition (RCCI) combustion in internal combustion engines". In: *Progress in Energy and Combustion Science* 3 (2014).

[18] S L Kokjohn. "Fuel reactivity controlled compression ignition (RCCI): a pathway to controlled high-efficiency clean combustion". In: (2010). DOI: 10.1177/1468087411401548.

[19] Derek Splitter et al. "Effect of Compression Ratio and Piston Geometry on RCCI Load Limits and Efficiency". In: *SAE International* (2012).

[20] Reed Hanson et al. "Piston Bowl Optimization for RCCI Combustion in a Light-Duty Multi-Cylinder Engine". In: *SAE International* (2012).

[21] Reed M. Hanson et al. "An Experimental Investigation of Fuel Reactivity Controlled PCCI Combustion in a Heavy-Duty Engine". In: *SAE International* (2010).

[22] Reed Hanson et al. "Fuel Effects on Reactivity Controlled Compression Ignition (RCCI) Combustion at Low Load". In: *SAE International paper* (2011).

[23] Filippo Gazzola. "EVALUATION OF THE POTENTIALS OF TEMPERATURE CONTROLLED REACTIVITY COMPRESSION IGNITION COMBUSTION FOR EFFICIENCY INCREASE IN CI ENGINES". In: 3 (2018).

[24] T. Lucchini et al. "Modeling non-premixed combustion using tabulated kinetics and different flame structure assumptions". In: *SAE International* (2017).

[25] W. Malalasekera H. K. Versteeg. *An Introduction to Computational Fluid Dynamics*. Harlow: Pearson Prentice Hall, 2007.

[26] Hakan Nilsson. *A Thorough Description Of How Wall Functions Are Implemented In OpenFOAM*. URL: http://www.tfd.chalmers.se/~hani/kurser/OS_CFD_2016.

[27] Francesco C. Pesce Mirko Baratta Andrea E. Catania. "Multidimensional Modeling of Natural Gas Jet and Mixture Formation in Direct Injection Spark Ignition Engines—Development and Validation of a Virtual Injector Model". In: *Journal of Fluids Engineering* (2011).

[28] Nicola Rapetto Mirko Baratta. "Fluid-dynamic and numerical aspects in the simulation of direct CNG injection in spark-ignition engines". In: *ScienceDirect* (2014).

[29] K. Glover N. Collings. "IC engine exhaust gas analysis". In: (2016).

[30] Tommaso Lucchini et al. "Automatic Mesh Generation for CFD Simulations of Direct-Injection Engines". In: *SAE International* (2015).

[31] E. Ranzi et al. "Reduced kinetic schemes of complex reaction systems: Fossil and biomass-derived transportation fuels". In: *International Journal of Chemical Kinetics* (2014).

[32] Nordin P A Niklas. "Complex Chemistry Modeling of Diesel Spray Combustion". In: ().

[33] M. Mehl et al. "Chemical kinetic modeling of component mixtures relevant to gasoline". In: *4th European Combustion Meeting* 4 (2009).